uOttawa

L'Université canadienne
Canada's university

FACULTÉ DES ÉTUDES SUPÉRIEURES ET POSTOCTORALES

uOttawa

L'Université canadienne
Canada's university

FACULTY OF GRADUATE AND POSDOCTORAL STUDIES

Zhu Fu

AUTEUR DE LA THÈSE / AUTHOR OF THESIS

M.A.Sc. (Civil Engineering)

GRADE / DEGREE

Department of Civil Engineering

FACULTÉ, ÉCOLE, DÉPARTEMENT / FACULTY, SCHOOL, DEPARTMENT

Numerical Simulation of a Centrifuge test related to the interaction between an ice feature and an offshore pipeline

TITRE DE LA THÈSE / TITLE OF THESIS

Dr. Erman Evgin

DIRECTEUR (DIRECTRICE) DE LA THÈSE / THESIS SUPERVISOR

CO-DIRECTEUR (CO-DIRECTRICE) DE LA THÈSE / THESIS CO-SUPERVISOR

EXAMINATEURS (EXAMINATRICES) DE LA THÈSE / THESIS EXAMINERS

Dr. Sai Vanapalli

Dr. Siva Sivathavalan

Gary W. Slater

Le Doyen de la Faculté des études supérieures et postdoctorales / Dean of the Faculty of Graduate and Postdoctoral Studies

NUMERICAL SIMULATION OF A CENTRIFUGE TEST RELATED TO THE INTERACTION BETWEEN AN ICE FEATURE AND AN OFFSHORE PIPELINE

Zhu FU, B.Eng.

A Thesis

Submitted to the School of Graduate Studies and Research

under the supervision of

Dr. Erman Evgin

in partial fulfillment of the requirements for the degree of

Master in Applied Science in Civil Engineering

Department of Civil Engineering
University of Ottawa
Ottawa, Ontario
Canada

August 2007

The Master in Applied Science in Civil Engineering is a joint program between Carleton University and the University of Ottawa, which is administered by the Ottawa-Carleton Institute for Civil Engineering

Your file Votre référence
ISBN: 978-0-494-49202-4
Our file Notre référence
ISBN: 978-0-494-49202-4

ABSTRACT

Ice features present one of the major obstacles to offshore development in the Arctic and Atlantic regions of Canada. Ice features have been observed to interact with the see floor creating scour features (Clark et al., 1986). In particular, when an ice feature is driven by environmental forces into the shallow water, ice scouring of the seabed may cause a danger to bottom installations such as submarine pipelines.

In the present study, the ice-scour event in a centrifuge test is simulated by using PLAXIS and ADINA finite element programs. The centrifuge test data reported by (Lach et al., 1993; Yang and Poorooshasb, 1997) and the input data in their numerical study are utilized in the present work. In numerical analysis, geometric and material nonlinearities are considered. Two dimensional and three dimensional finite element models are used to calculate the stresses and deformations in the seabed soils, the deflections of the pipe, and the stresses acting on the pipe. In order to establish the validity of the finite element calculations, the experimental results and the numerical results are compared. The importance of using interface elements between the soil and the ice feature is also investigated.

The FE predictions are reasonably close to the centrifuge test data. The displacements of the pipe in 3-D model are smaller than those predicted by 2-D model due to the three dimensional effects. Bending and torsion of the pipe along its long axis can only be calculated in 3-D FE analysis. Using the interface elements in the numerical analysis helps to obtain a better agreement between the calculated and measured values. In addition, convergence problems are reduced.

ACKNOWLEDGMENTS

The author wishes to express his sincere thanks to his supervisor, Dr. Erman Evgin, for his continuous encouragement, general advice, and financial support throughout the research program. I benefited significantly from the graduate courses offered by Drs. V. Garga, T. Law, S. Sivathayalan, S.K. Vanapalli, and B. Wang. I also thank Dr. S. Tavoularis for permitting me to use the FE program ADINA.

The author would like to thank his parents and sisters, for their encouragement and financial support. Finally, it is the author's wife, Xin Lu, whose encouragement and patience made this M.A.Sc. study successful.

TABLE OF CONTENTS

LIST OF TABLES

LIST OF FIGURES

CHAPTER 1
INTRODUCTION

1.1 Statement of Problem

Ice features present one of the major obstacles to offshore development in the Arctic and Atlantic regions (Surkvo et al., 2000). In particular, when an ice feature is driven by environmental forces into the shallow water, the ice will scour the seabed. The scours can be several meters deep (Blasco et al., 1998). Ice scouring may create problems to bottom installations such as submarine pipelines. In average, the scouring force can be 10 MN (similar to the pullover force by ship anchors) and sometimes much more (Woodworth-Lynas, 1998). Below the base of the ice feature, the seabed soil is heavily deformed. A pipeline buried below the base of the ice feature should be strong enough to withstand large forces and deformations derived from the ice scouring (Palmer , 1990).

Palmer (1997) idealized the deformed seabed soil into three zones: namely, an uppermost zone (Zone 1) in which the ice passes through the soil, an intermediate zone (Zone 2) in which the soil is deformed plastically and the lowest zone (Zone 3) in which deformations of the soil are elastic as shown in Figure1.

A pipeline buried in Zone1 will contact the keel of the ice feature directly. Most of the scour force will be transferred directly to the pipeline. Scour force on the order of 200 MN might be expected (Woodworth-Lynas, 1996) in a large ice scouring. This is about 20 times greater than the pullover force by a dragging ship anchor that is known to damage pipelines severely (Paulin, 1997). Therefore, a pipeline will be destroyed in Zone1.

A pipeline buried in Zone 2 will be dragged forward and pushed downwards by the moving soil (Palmer, 1990). Nixon et al. (1996) pointed out that due to the relative movements between the dragged soil below the scour and non-moving soil outside the scour, a pipe will be subjected to bending and stretching. In some cases, although the pipe is severely bent, it could withstand large deformations without failing (Palmer, 1990). Thus the pipeline buried in some depth within Zone 2 might be safe.

When a pipeline is buried in Zone 3, the soil around the pipe would not move significantly. A pipeline will be safe in this zone. However, trenching a pipeline into Zone 3 is beyond the reach of most conventional trenching equipment.

Due to the fact that the cost increases rapidly with increasing trenching depth, the geotechnical study should be conducted to identify the minimum safe depth in Zone 2 below which pipeline deformations are acceptably small. That is what most numerical studies reported in the literature focus on.

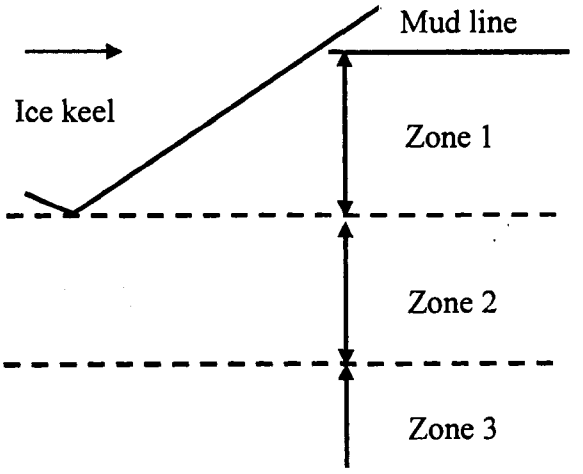

Figure 1.1 Three deformation zones during ice-scouring (modified from Palmer 1997)

1.2 Research Objectives

The main objectives of this thesis are as follows:

1. To identify the most important factors and, subsequently, to explore their influence on the simulation of the behaviour of a pipeline buried in Zone 2.

2. To determine the deformations in the seabed soil, the components of the scour force, and displacements of the pipe using the finite element method.

1.3 Scope of Research

In order to achieve the above objectives, the following tasks are undertaken in this research:

1. Simulate an ice-scouring event in a centrifuge test using a 2-D finite element program.

2. Using the same centrifuge test data, analyze the interaction between the ice feature and seabed with a pipeline using both 2-D and 3-D finite element programs.

The 2-D analysis is conducted using PLAXIS and ADINA finite element programs. The 3-D calculations are performed using ADINA only.

1.4 Outline of Thesis

The thesis is organized in the following way:

Chapter 2 presents a literature review on the experimental and field investigations of ice-scouring phenomena.

Chapter 3 describes the soil models used in the analysis, i.e., Mohr-Coulomb Model and Soft-Soil Model.

Chapter 4 describes the literature review in numerical simulations of interaction between ice features and seabed soils.

Chapter 5 presents the 2-D FE model using PLAXIS and ADINA programs to model the interaction between an ice feature and seabed soil deposits with a pipeline.

Chapter 6 describes a 3-D FE model using ADINA program to model the interaction between an ice feature and seabed soil deposits with a pipeline.

Chapter 7 presents the conclusions of the present research, and provides recommendations for future research.

CHAPTER 2
ICE FEATURE-SEABED- PIPELINE INTERACTION LITERATURE REVIEW

To explore the ice feature-seabed-pipeline interaction, field observations, laboratory tests and numerical studies are conducted by various researchers. Based on the field data, simulations of ice scouring are carried out by experimental and numerical techniques. It is also necessary to have adequate knowledge of the characteristics of ice features and soil properties in ice scour events. Other essential information includes the number of icebergs passing through the given area annually, their mass, shape, and velocities.

2.1 Characteristics of Ice Features

Some of the ice in the oceans is present in the form of icebergs and ice ridges (Croasdale, 1985). An iceberg is a large fresh water ice that has broken off from glaciers and is floating in open water with 87 percent of its mass below the water surface (Croasdale et al., 2001). An ice ridge is formed by broken ice blocks held together by re-freezing at the contact points. Water present in the voids also freezes with time and increases the strength of the ridge. Figure 2.1 shows a typical first-year Arctic pressure ridge. Its total thickness is about 10m, most of which is under the water line. An iceberg or an ice ridge could cause an ice-scouring event when it is drifting toward shallow water. In North America, the distribution of ice- scouring occurrences is shown in Figure 2.2. In Canadian east coast, most of scouring activities are caused by icebergs originated from Greenland ice cap. While in the Arctic Ocean, in particular, the southern Beaufort Sea, ice ridges or

ice island fragments are involved in the ice-scouring event. Some of these areas also have potential offshore hydrocarbon production reserves such as the Grand Banks of Newfoundland and the Beaufort Sea (Lewis and Blasco, 1990).

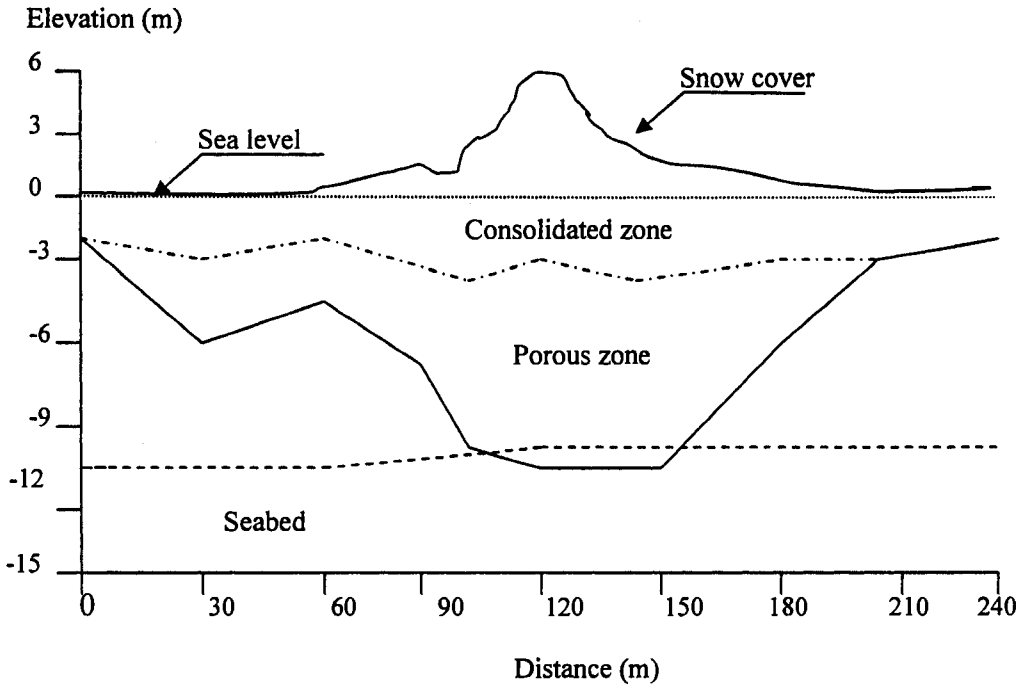

Figure 2.1 Typical first-year ice ridge (Croasdale, 1985)

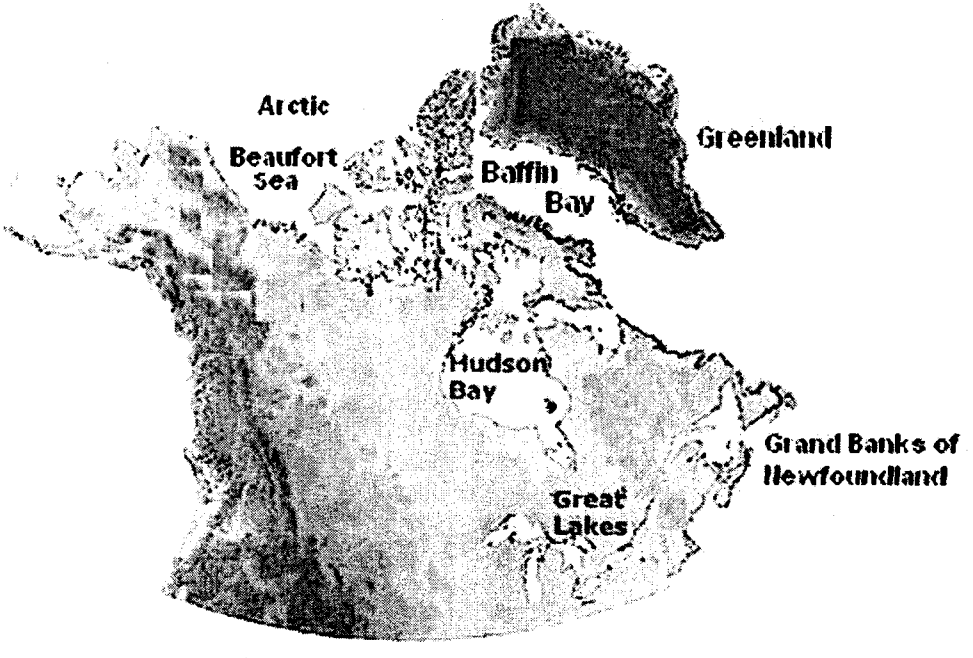

Figure 2.2 Ice scouring regions in North America (www. ice-glaces.ec.gc.ca)

2.1.1 Iceberg Size

According to the Classification of International Ice Patrol (IIP) (1980), there are six size categories of icebergs as shown in Table 2.1.

Table 2.1 Iceberg size categories

Type	Height (meter)	Length (meter)	Approx. Mass (tons)
Growler	1	6	200
Bergy bit	1-5	6-20	200-700
Small Iceberg	6-15	21-60	7000-200,000
Medium Iceberg	16-45	61-122	200,000-2.5M
Large Iceberg	46-77	123-213	>2.5 M
Very Large Iceberg	≥78	≥214	>>2.5 M

2.1.2 Iceberg Flux

The number of icebergs for a specified area gradually decreases with increasing distance from their source which is generally a glacier. For example, in West Greenland area, in an average year, about 3000 icebergs pass through Hudson Strait, 1000 get across the Strait of Belle Isle, and 400 survive to reach the Grand Banks of Newfoundland (Ebbesmeyer and Helseth, 1980). Figure 2.3 illustrates the mean annual number of icebergs observed at different latitudes. Iceberg flux in a given area is one of the key elements for estimating the probability of impact between an iceberg and seabed with a pipeline. As a result of global warming, glaciers melt at an increasing rate and iceberg activity increases. Data compiled by the International Ice Patrol shows that the yearly iceberg flux increases from 27 in1966 to a maximum of 2100 in 1984 at Grand Banks (Mobile Oil Canada Ltd., 1985).

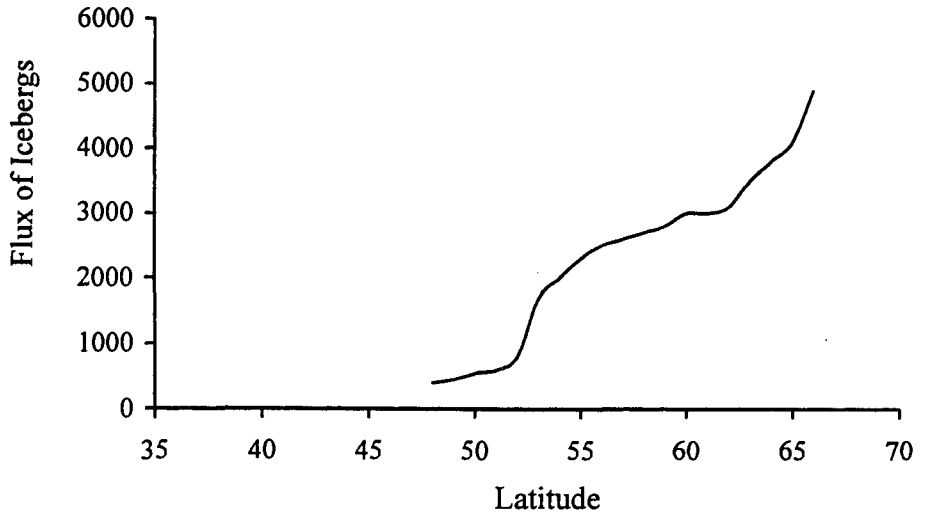

Figure 2.3 Mean annual iceberg flux (1980) of west coast Greenland (from Arunachalam, et al., 1985)

Normally, drift velocities of icebergs are less than 1.5 m/sec while their movement is largely controlled by that of the water around them as shown in Table 2.2.

Table 2.2 Iceberg drift speed (modified from Nordco Limited, 1984)

Site	Years	Average speed (m/sec)	Max speed (m/sec)
Labrador Site	1971	0.17	--
Labrador Site	1976	0.21-0.39	1.69
Grand Banks	1959	1.25	--
Grand Banks	1980	--	1.30
Baffin Bay	1978	0.09-0.04	--

2.2 Seabed Soil

The shallow seismic profiling and borehole data show that the Beaufort shelf is blanketed with a thin layer of recent marine clays or silty clays. The following deposit is interbedded with sand, silts and clay. In water depths of 15 to 40 m the seafloor is remoulded by ice scouring activities (Crooks et al., 1986). On the eastern Canadian continental shelves,

very dense granular soils are dominant in water depth between100 m and 110 m, and hard silty sand deposits are observed at greater depth. (Sonnichsen and King, 2001)

2.3 Process of Ice Scouring

The ice feature-seabed interaction is a complex phenomenon. During scouring, the driving force generated by environmental forces, such as wind, wave and currents, pushes the huge mass of a scouring ice feature forward as shown in Figure 2.4. The soil will undergo deformation. If a pipeline is situated in a zone of large soil deformation below the scouring iceberg, it will be displaced by the soil movements. These movements may result in damage to the pipeline. Therefore, the performance of the marine pipelines can be determined if the magnitude of the soil deformation can be assessed. During ice scouring, the ice feature has sufficient strength to bear the force derived from the ice-soil interaction (Kovac and Mellor, 1974). In numerical simulations, the ice-feature has been treated as a rigid body, which cannot be destroyed while scouring the seabed.

The field evidence shows that scours are uniform over long distances, often 10 km or more, and that the seabed is almost horizontal. Therefore, in the idealization of an ice scour process, the iceberg moves horizontally at a constant speed relative to the level seabed, in which the iceberg is partially embedded. This steady state scour model (Palmer et al., 1989) is used not only in the centrifuge test but also in the finite element analysis.

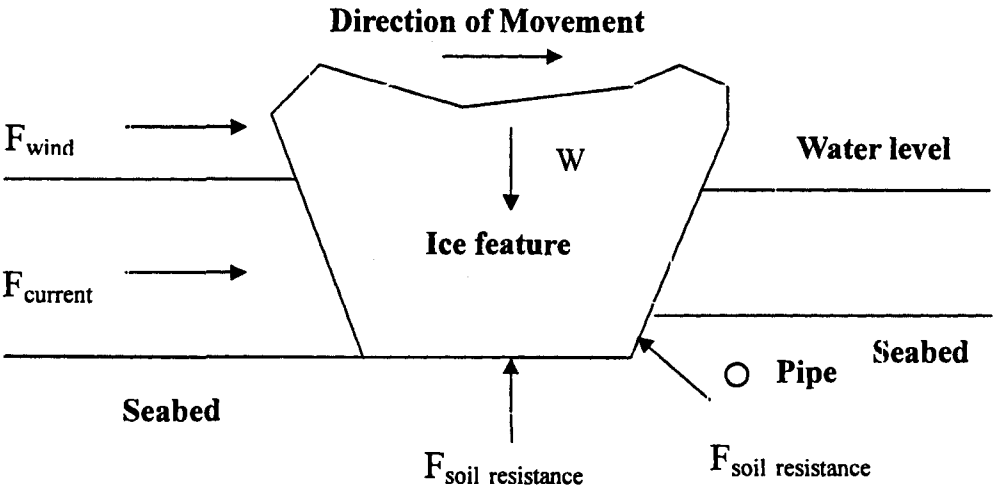

Figure 2.4 Schematics of ice scour event (modified from Yang and Poorooshasb, 1997)

2.3.1 Experimental Studies

Palmer et al. (2005) pointed out that there is no direct full-scale data on the soil deformations and on the forces involved in ice scouring events in nature. In addition, there is no certainty on the geometry of ice feature. Ice scour phenomenon is studied mostly by experimental methods. Therefore, the theoretical analysis should be equally valid in the response of a physical model and a full-scale event. There have been a number of laboratory studies to understand the mechanics of ice scouring, and to obtain information on the nature and effects of various factors in the ice scouring problems. Two types of tests are considered: (1) physical tests (the acceleration of gravity, g =9.81m/s^2) using rigid indenters in laboratory flumes filled with soil (Poorooshasb and Clark, 1990; Barker and Timco, 2003); (2) centrifuge tests (the acceleration in the vertical direction >> 1g) of scouring processes (Woodworth-Lynas et al., 1996; Paulin, 1997; Lach, et al., 1993). The first method can provide useful information on the ice-scouring process, but it is difficult to scale these results to the full-scale situation using conventional modeling laws (Barker and Timco, 2002, 2003). Centrifuge tests are costly and the models are small-scale, however; the full-scale situation can be achieved through the scaling laws. For example, if a centrifuge model is built to a scale of 1/N, the model should be subjected to an

acceleration of N times of gravitational acceleration; scale factors also exist for other quantities (Schofield, 1980) as shown in Table 2.3.

Table 2.3 Scale relationship between the model and prototype

Model (subscript: m)	Prototype (subscript: p)
Length	$L_m=(1/N)L_p$
Density	$\rho_m=\rho_p$
Stress	$\sigma_m=\sigma_p$
Strain	$\varepsilon_m=\varepsilon_p$
Velocity	$V_m=V_p$
Acceleration	$a_m=a_p$
Force	$F_m=(1/N)^2 F_P$
Displacement	$D_m=(1/N)D_P$
Mass	$F_m=(1/N)^3 F_P$

It should be noticed that the stress distribution between the real situation and the centrifuge model is identical. The force of the full-scale structure is scaled up directly. The centrifuge modeling has gained wide acceptance by geotechnical engineers.

In order to achieve an acceleration of N times of gravitational acceleration, the model is rotated about the central axis of the centrifuge. The angular velocity ω is set up to make centripetal acceleration $r\omega^2$ equal to $N \times g$ where g is the gravitational acceleration.

A series of 1:100 scale model tests at 100 g was performed on the beam centrifuge at the Geotechnical Centrifuge Center, University of Cambridge, England (Lach et al., 1993). Figure 2.5 shows a schematic vertical section through the 1:100 scale centrifuge model setup along the scour axis.

In these tests, Speswhite kaolin clay was used to represent the soils in the Beaufort Sea region where ice scouring occurs frequently. Ice feature was modeled by a piece of aluminum with specified geometry. The model pipe was placed below the keel of ice feature and perpendicular to the scour path. During 100 g centrifuge tests, the scour force, pore water pressure, deformation of the soil and deflection of pipe were measured.

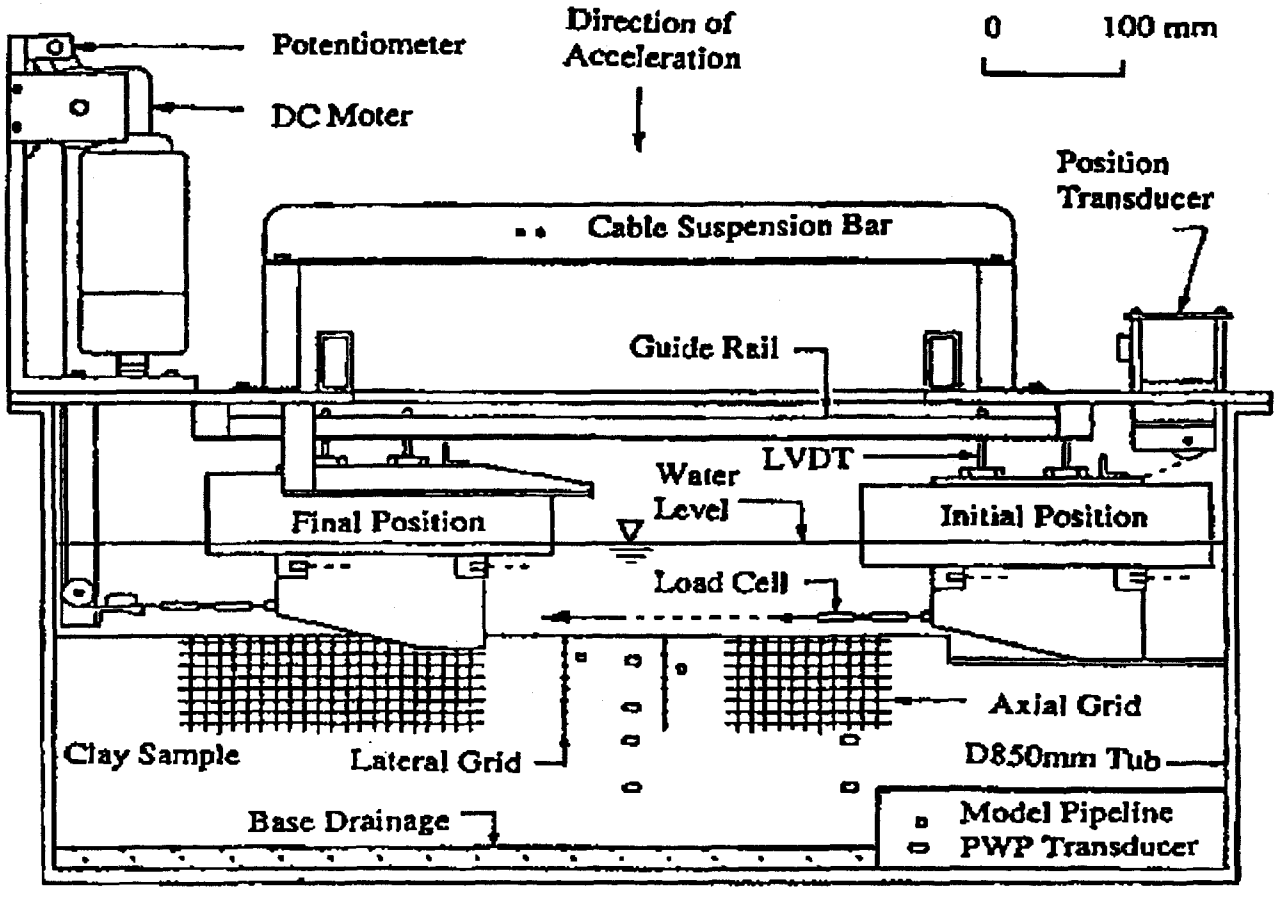

Figure 2.5 Centrifuge test setup: vertical section along scour axis (from Lach et al., 1993)

The model iceberg attack angle was 15° and the bottom contact length was 50 mm. The surface of the soil sample was topped with 100 mm high water (Lach et al., 1993). Centrifuge Test 02 showed that the model iceberg was raised up from its initial position to a constant depth after a brief period of scouring. There was a period of steady state at this constant depth, then, the model iceberg was lifted to another depth to continue with Test 04. The scour forces acting on the model iceberg-soil interface are shown in Figure 2.6 for Test 02. It was indicated that in the steady state the horizontal and vertical scour forces were relatively constant.

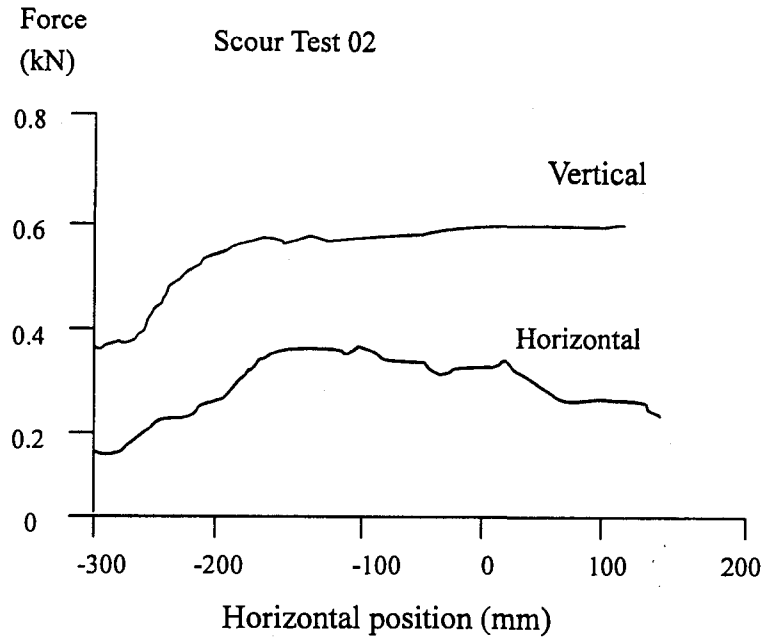

Figure 2.6 Scour forces data with movement of ice feature (from Lach et al., 1993)

There were three displacement components of soil deformation produced by the scouring events. The horizontal displacements were more significant than lateral and vertical displacements. Figure 2.7 shows the horizontal movement of the soil against the depth below the base of the iceberg for Test 02. It was noticed that most of the soil movement occurred within three times of the scour depth. As mentioned before, the soil deformation

will affect the performance of a pipeline.

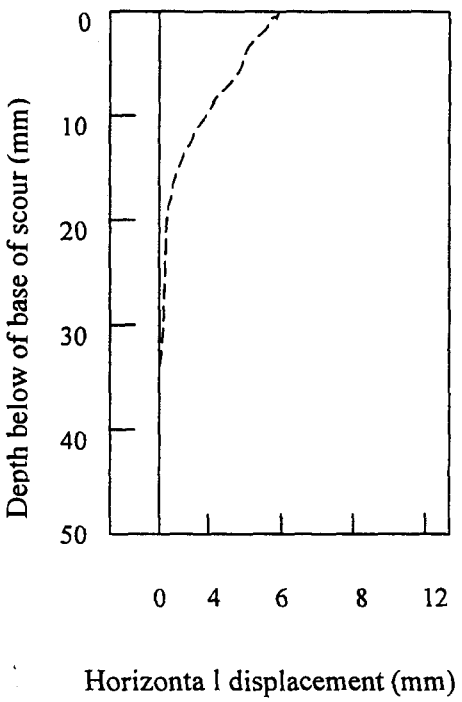

Figure 2.7 Horizontal displacements versus depth below the base of the ice feature (from Yang and Poorooshasb, 1997)

2.3.2 Numerical Method

Detailed information on the geometry of ice scours and subscour deformation is essential for making use of physical models of ice scouring (Woodworth-Lynas, 1998), but the published data-base is limited. Centrifuge tests provided most detailed and reliable data so far. Based on the experimental data, several numerical models are developed to predict some of the important aspects of scour process, the soil deformation and the soil-ice interaction forces.

Yang and Poorooshasb (1997) used finite element analysis program ANSYS (www.ansys.com) to simulate two centrifuge tests in two-dimensional finite element model. Plane strain was assumed and four–node solid elements were used. The

nonlinearity of soil behaviour was represented by Drucker-Prager model with plastic flow governed by the non-associated flow rule. Numerical results were close to the centrifuge model test data. Yang's model was a representation of ice scouring in steady-state conditions.

Lach and Clark (1996) adopted finite element code ABAQUS to analyze his own centrifuge tests. ABAQUS is a general purpose finite element program designed primarily to model the behavior of solids and structures under externally applied loading (www.simulia.com). Soil constitutive behaviour was described as the Modified Cam-Clay model.

Besides two-dimensional model of iceberg scouring, a three-dimensional simulation is also necessary due to the fact that most practical problems are in three-dimension. Figure 2.8 shows the calculated values of deflection of pipeline (Yang et al., 1993). It could be seen that the deflection appears uniform in the central portion which may be about one tenth of the scour width. However, beyond two times of scour width, there is zero deflection of the pipeline. There is a steep change in displacement of the pipe at the edge

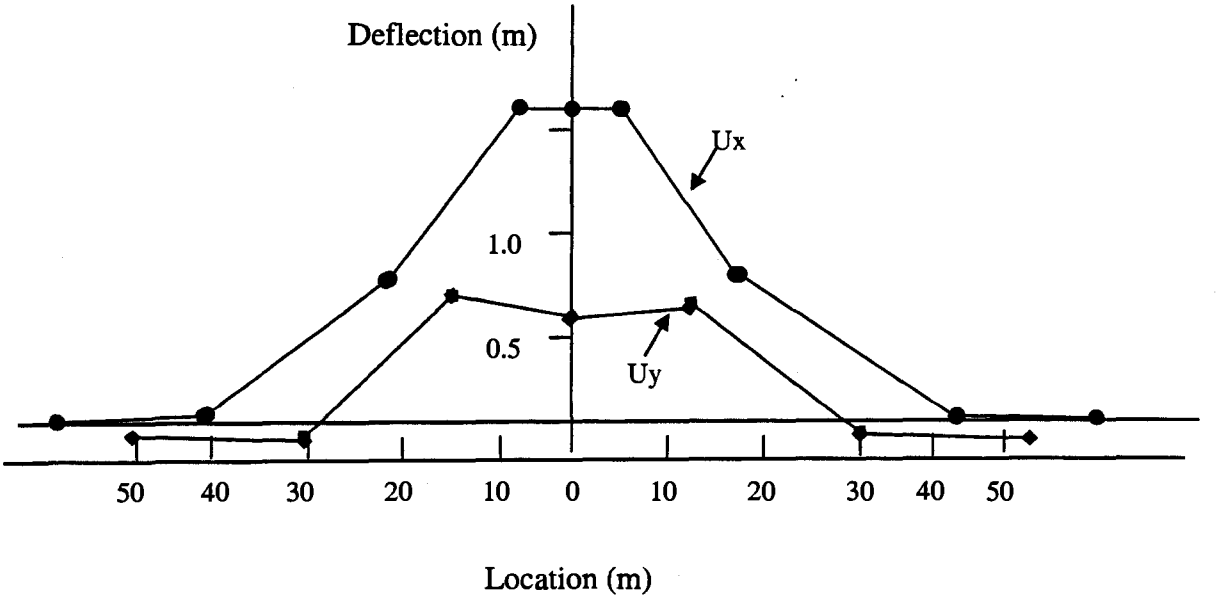

Figure 2.8 Horizontal (Ux) and vertical (Uy) deflections of the pipeline (modified from Yang et al., 1993)

2.4 Important Factors Influencing the Results of Numerical Analysis

Some of the influential factors have been identified during the literature review and some others are based on the experience gained during this study. Due to the elaborate works of many researchers, it seems that the ice scouring event can be simulated either by experimental or numerical methods. In order to represent reasonably the real life problems in engineering analysis, the following aspects need to be further considered in numerical analyses.

1) The two kinds of drainage conditions should be considered in the analysis, i.e., drained and undrained conditions.

2) The usefulness of interface elements in the analysis of ice feature-soil-pipeline interaction problem should be evaluated. Ice scouring should be modeled with and without interface elements.

3) Use different soil models to simulate the ice-scouring, such as Mohr-Coulomb model and Soft-Soil Model. There will be two possibilities of predicting scour forces: if the results are close to each other, two models will represent the same soil failure conditions; if they are different, this is because Young' Modulus (E) is constant in the stress-strain curve of Mohr-Coulomb model, however, E is variable for Soft-Soil Model.

4) A 3-D analysis is necessary for the calculation of the deflections of the pipe.

5) Large displacement analysis should be considered.

CHAPTER 3
CONSTITUTIVE MODELS USED IN THIS STUDY FOR SOIL BEHAVIOUR

Different soil models may be used to represent the behaviour of soil. The Mohr-Coulomb model and Soft-Soil model are used in this study. In order to explore the differences between these two models in the PLAXIS program, the behaviour of soil in consolidated drained triaxial tests (CD tests) and consolidated undrained triaxial tests (CU tests) is simulated. Numerical analysis provided the following relationships: (1) the axial strain and deviatoric stress (both CD tests and CU tests), (2) the axial strain and volumetric strain (CD tests), and (3) the axial strain and excess pore water pressure (CU tests).

3.1 Mohr-Coulomb Model

The Mohr-Coulomb model in PLAXIS is a linear elastic perfectly plastic model with non-associated flow rule. Deformation prior to yielding is assumed to be linear elastic governed by the elastic parameters, Young's modulus, E, and Poisson's Ratio, v. Other model parameters are friction angle, φ, cohesion, c, and dilatancy angle, ψ. This is the most frequently used model for soils in commercially available FE programs.

The yield surface of the Mohr-Coulomb Model is a hexagonal pyramid and it is expressed by six yield functions when formulated in terms of principal stresses (PLAXIS Manual, 2006)

$$f_{1a} = \frac{1}{2}(\sigma_2' - \sigma_3') + \frac{1}{2}(\sigma_2' + \sigma_3')\sin\varphi' - c'\cos\varphi' \leq 0 \quad (1)$$

$$f_{1b} = \frac{1}{2}(\sigma_3' - \sigma_2') + \frac{1}{2}(\sigma_2' + \sigma_3')\sin\varphi' - c'\cos\varphi' \leq 0 \quad (2)$$

$$f_{2a} = \frac{1}{2}(\sigma_3' - \sigma_1') + \frac{1}{2}(\sigma_3' + \sigma_1')\sin\varphi' - c'\cos\varphi' \leq 0 \quad (3)$$

$$f_{2b} = \frac{1}{2}(\sigma_1' - \sigma_3') + \frac{1}{2}(\sigma_1' + \sigma_3')\sin\varphi' - c'\cos\varphi' \leq 0 \quad (4)$$

$$f_{3a} = \frac{1}{2}(\sigma_1' - \sigma_2') + \frac{1}{2}(\sigma_1' + \sigma_2')\sin\varphi' - c'\cos\varphi' \leq 0 \quad (5)$$

$$f_{3b} = \frac{1}{2}(\sigma_2' - \sigma_1') + \frac{1}{2}(\sigma_1' + \sigma_2')\sin\varphi' - c'\cos\varphi' \leq 0 \quad (6)$$

Primed stress symbols indicate effective stresses. In addition to the yield functions, six plastic potential functions are defined for the Mohr-Coulomb Model. The parameter required for the plastic potential function is the dilatancy angle, ψ'.

$$g_{1a} = \frac{1}{2}(\sigma_2' - \sigma_3') + \frac{1}{2}(\sigma_2' + \sigma_3')\sin\psi' \quad (7)$$

$$g_{1b} = \frac{1}{2}(\sigma_3' - \sigma_2') + \frac{1}{2}(\sigma_2' + \sigma_3')\sin\psi' \quad (8)$$

$$g_{2a} = \frac{1}{2}(\sigma_3' - \sigma_1') + \frac{1}{2}(\sigma_3' + \sigma_1')\sin\psi' \quad (9)$$

$$g_{2b} = \frac{1}{2}(\sigma_1' - \sigma_3') + \frac{1}{2}(\sigma_1' + \sigma_3')\sin\psi' \quad (10)$$

$$g_{3a} = \frac{1}{2}(\sigma_1' - \sigma_2') + \frac{1}{2}(\sigma_1' + \sigma_2')\sin\psi' \quad (11)$$

$$g_{3b} = \frac{1}{2}(\sigma_2' - \sigma_1') + \frac{1}{2}(\sigma_1' + \sigma_2')\sin\psi' \quad (12)$$

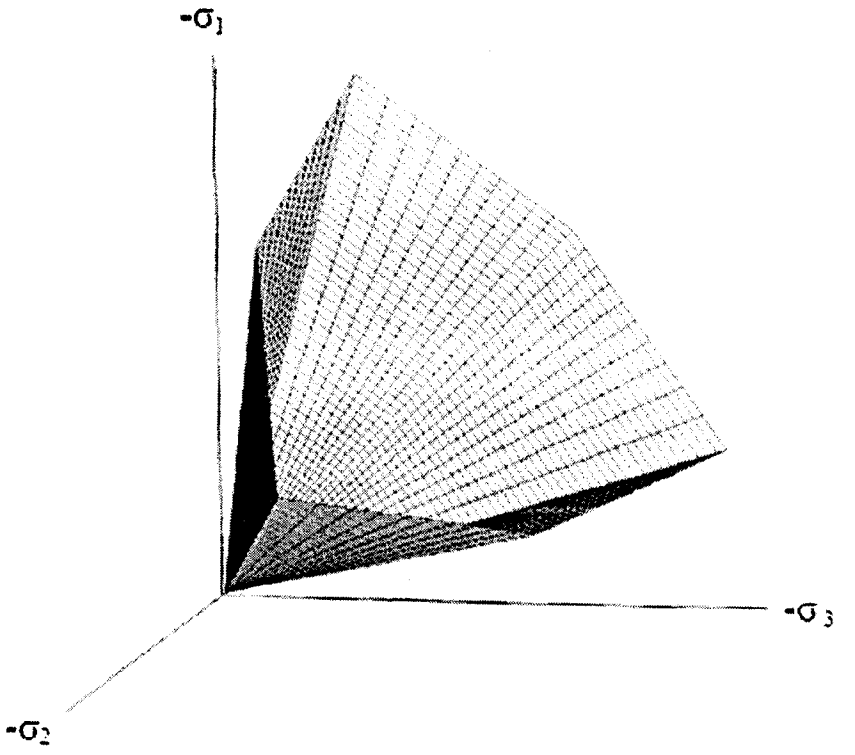

Figure 3.1 Mohr Coulomb yield surface in principal stress space (c=0) (PLAXIS Manual, 2006)

3.2 Soft-Soil Model

In PLAXIS, the behaviour of clay can be simulated by the Soft–Soil model. Its failure behaviour is represented by the Mohr-Coulomb failure criterion. However, there is a logarithmic relation between the volumetric strain, ε_v, and the mean effective stress, p', as shown in Figure 3.2, which can be formulated as:

$$\varepsilon_v - \varepsilon_v^0 = -\lambda^* \ln(\frac{p'}{p^0}) \quad \text{(virgin compression)} \tag{13}$$

where λ^* is modified compression index .

During isotropic unloading and reloading a different path is followed, which can be

formulated as:

$$\varepsilon_v - \varepsilon_v^0 = -\kappa^* \ln(\frac{p'}{p^0}) \qquad \text{(unloading and reloading)} \qquad (14)$$

where κ* is modified swelling index.

p^0 is initial mean effective stress.

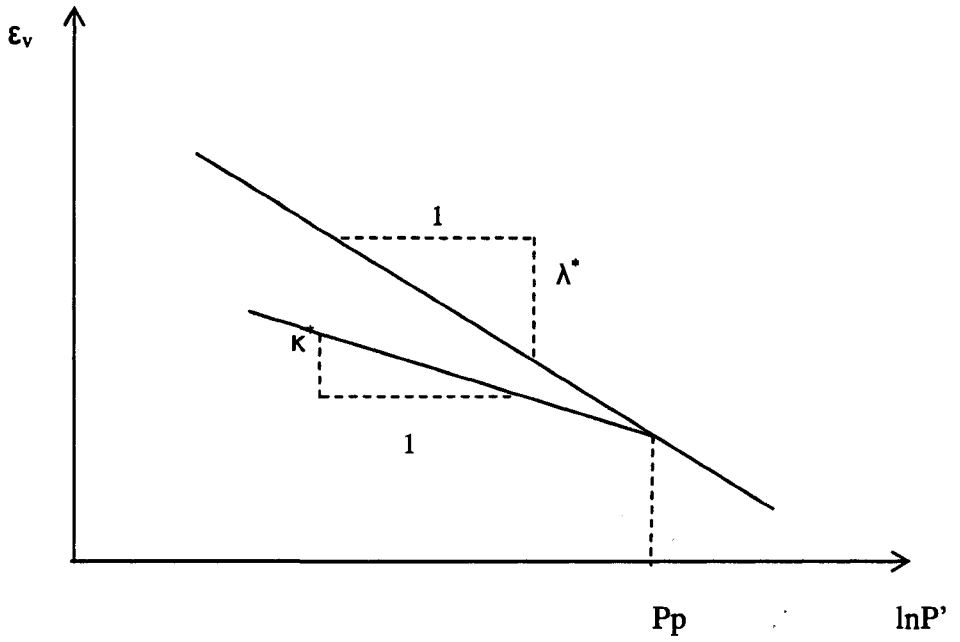

Figure 3.2 Logarithmic relation between volumetric strain and mean stress (PLAXIS Manual, 2006)

Note that the parameters λ* and κ * are different from the λ and κ as used in Cam-Clay model. The relationship between these parameters and Cam-Clay parameters are as follows:

Table 3.1 λ* and κ * relationship to Cam-Clay parameters

$\lambda^* = \frac{\lambda}{1+e}$	$\kappa^* = \frac{\kappa}{1+e}$

The basic parameters of Soft–Soil model are modified compression index, λ*, modified swelling index, κ *, cohesion, c, friction angle, φ, and dilatancy angle, ψ.

3.3 Soil Behaviour (in triaxial tests) Simulated by two Soil Models

The axisymmetric sample of a triaxial test is shown below. In numerical analysis, the dimensions of the sample are 35 mm * 150 mm * 1 radian. The vertical section of the sample and the boundary conditions are shown in Figure 3.3. The confining pressure is 50 kPa. The vertical displacement on top of the sample is specified by 7.5 mm increments up to a total of 30 mm. At the same time, the horizontal movement of the sample is kept free.

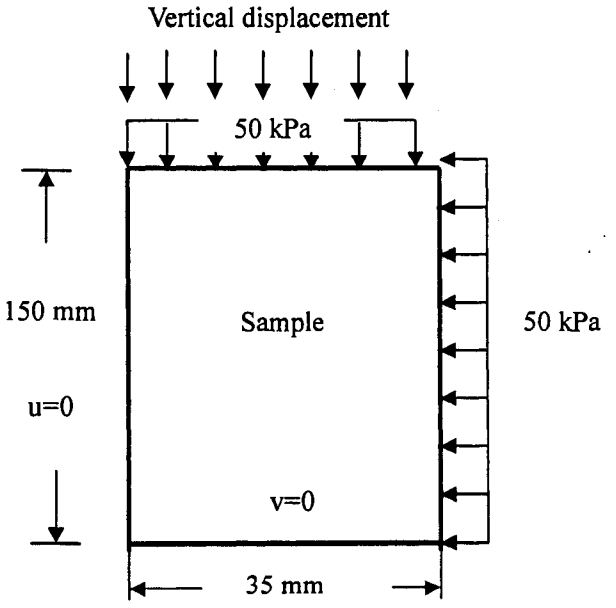

Figure 3.3 Schematic of finite element model
u: horizontal displacement, v: vertical displacement

Parameters of two soil models are presented in Table 3.2 and Table 3.3.

Table 3.2 Parameter of Mohr-Coulomb model for soil behaviour

Parameter	Name	Clay	Unit
Soil unit weight above phreatic level	γ_{unsat}	0.5 (a)	kN/m^3
Soil unit weight below phreatic level	γ_{sat}	0.6 (a)	kN/m^3
Horizontal permeability	K_x	1	m/day
Vertical permeability	K_y	1	m/day
Young's Modulus	E	5730	kN/m^2
Poisson's ratio	ν	0.3	--
Cohesion	c	5	kN/m^2
Friction angle	φ	23	°
Dilatancy angle	ψ	0	°

Note: E, ν, c, φ are taken from Yang and Poorooshasb (1997)

(a) A very small value is used for the unit weight of soil in the analysis to minimize the effect of gravity on the stress strain relation.

Table 3.3 Parameters of Soft-Soil model for soil behaviour

Parameter	Name	Clay	Unit	Note
Soil unit weight above phreatic level	γ_{unsat}	0.5 (a)	kN/m^3	
Soil unit weight below phreatic level	γ_{sat}	0.6 (a)	kN/m^3	
Horizontal permeability	K_x	1	m/day	
Vertical permeability	K_y	1	m/day	
Modified compression index	λ^*	0.15	--	λ =0.25 e=0.67
Modified swelling index	κ^*	0.024	--	κ=0.04 e=0.67
Poisson' ratio	ν	0.33	--	
Cohesion	c	5	kN/m^2	
Friction angle	φ	23	°	
Dilatancy angle	ψ	0	°	

Note: λ, κ are taken from Lach (1996)

(a) A very small value is used for the unit weight of soil in the analysis to minimize the effect of gravity on the stress strain relation.

3.3.1 Consolidated Drained Triaxial Test (CD test)

3.3.1.1 Strain and Stress

Figure 3.4 and Figure 3.5 present the relationship between the axial strain and deviatoric stress, (σ_1-σ_3) achieved by two models. According to Mohr-Coulomb model, the behaviour of soil is linear elastic until failure. On the other hand, stress-strain curve is nonlinear when Soft-Soil model is used. During unloading and reloading process, the stress-strain curve follows the same line as the primary loading line in the Mohr-Coulomb model, but in Soft-Soil model, the unloading reloading stress-strain curve follows a different slope than the nonlinear primary loading curve. Upon failure, however, both models show perfectly plastic behaviour.

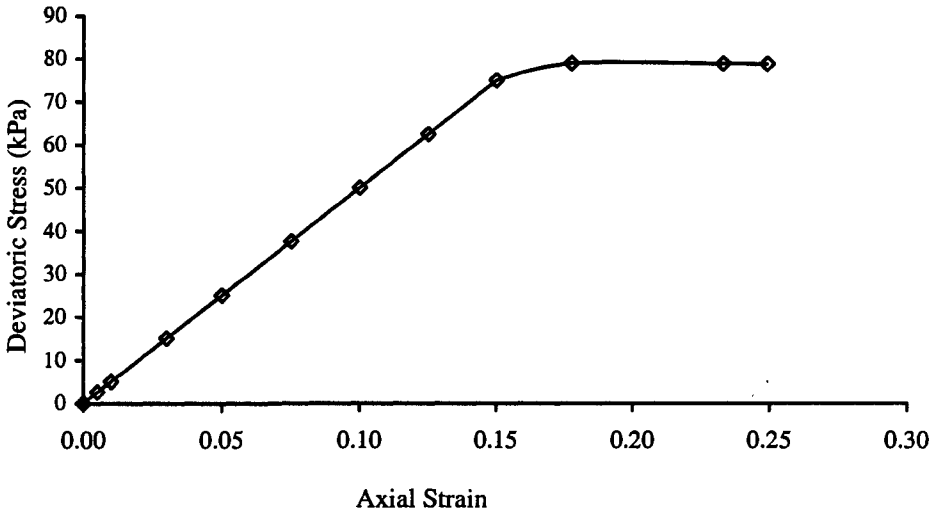

Figure 3.4 Simulation using Mohr-Coulomb model (CD test, σ_3 = 50 kPa)

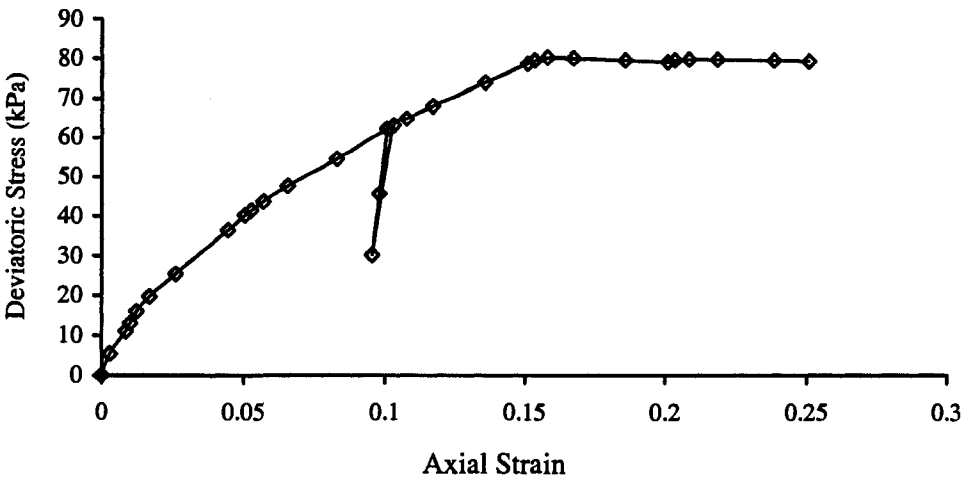

Figure 3.5 Simulation using Soft-Soil model (CD test, σ_3 = 50 kPa)

3.3.1.2 Axial Strain and Volumetric Strain

For CD tests, the volumetric strain achieved by Soft-Soil model is greater in comparison to the Mohr-Coulomb model as shown in Figure 3.6 and Figure 3.7.

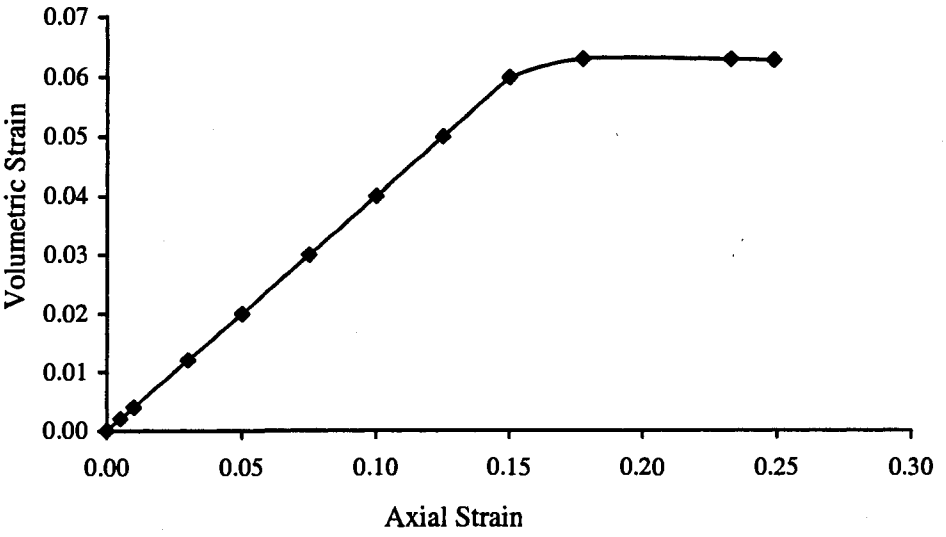

Figure 3.6 Simulation using Mohr-Coulomb model (CD test, σ_3 = 50 kPa)

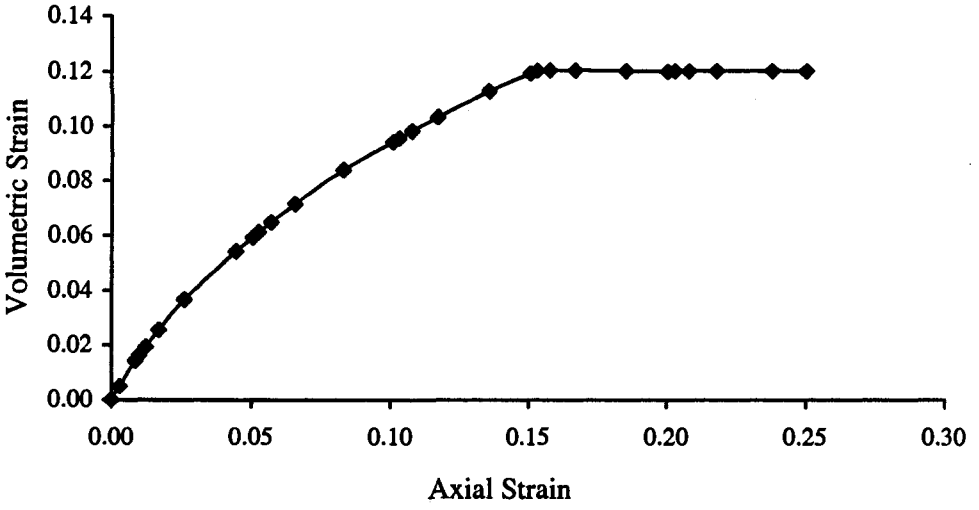

Figure 3.7 Simulation using Soft-Soil model (CD test, σ_3 = 50 kPa)

3.3.2 Consolidated Undrained Test (CU test)

3.3.2.1 Strain and Stress

The relationship between axial strain and deviatoric stress achieved by two soil models is illustrated in Figure 3.8 and Figure 3.9. Although the tendency of change of stress is quite the same in two models, the failure deviatoric stress from Mohr-Coulomb Model is greater than that in Soft-Soil model.

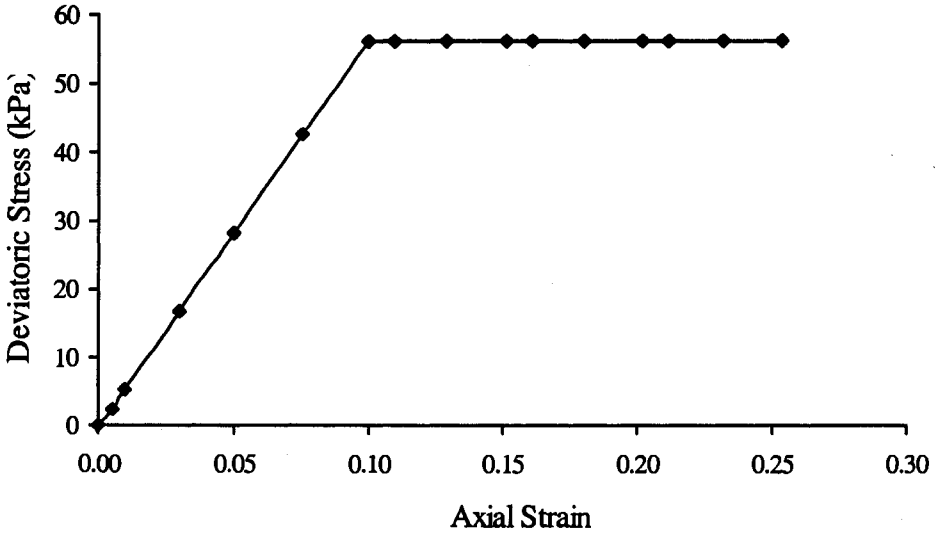

Figure 3.8 Simulation using Mohr-Coulomb model (CU test, σ_3 = 50 kPa)

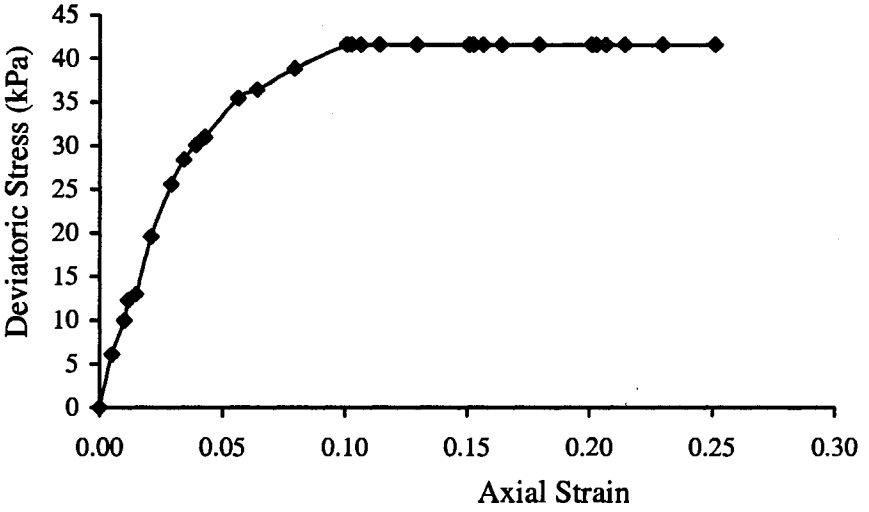

Figure 3.9 Simulation using Soft-Soil model (CU test, σ_3 = 50 kPa)

3.3.2.2 Axial Strain and Excess Pore Water Pressure

Figure 3.10 and Figure 3.11 show the relationship between axial strain and excess pore water pressure in the simulations of CU tests. It is noted that the excess pore water pressure calculated by the Soft- Soil Model is greater than that by Mohr-Coulomb Model.

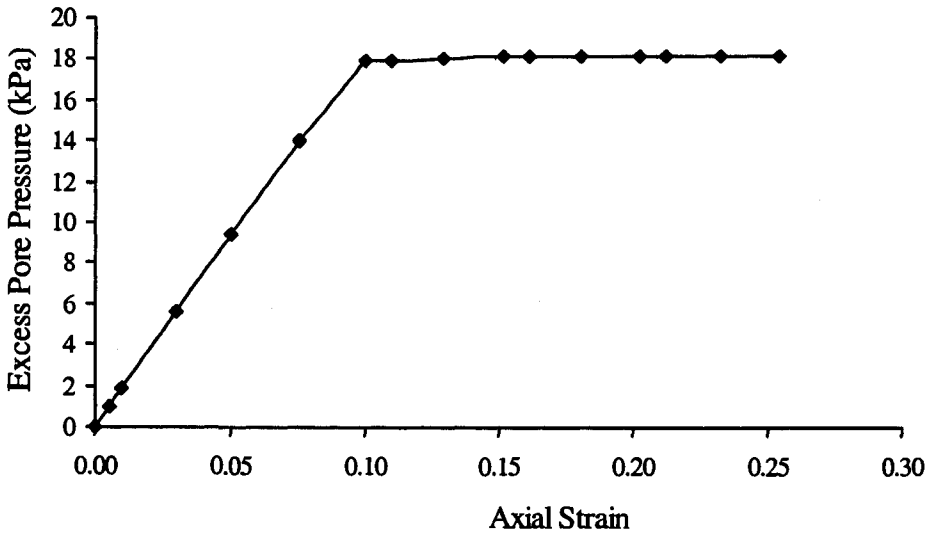

Figure 3.10 Simulation using Mohr-Coulomb model (CU test, σ_3 = 50 kPa)

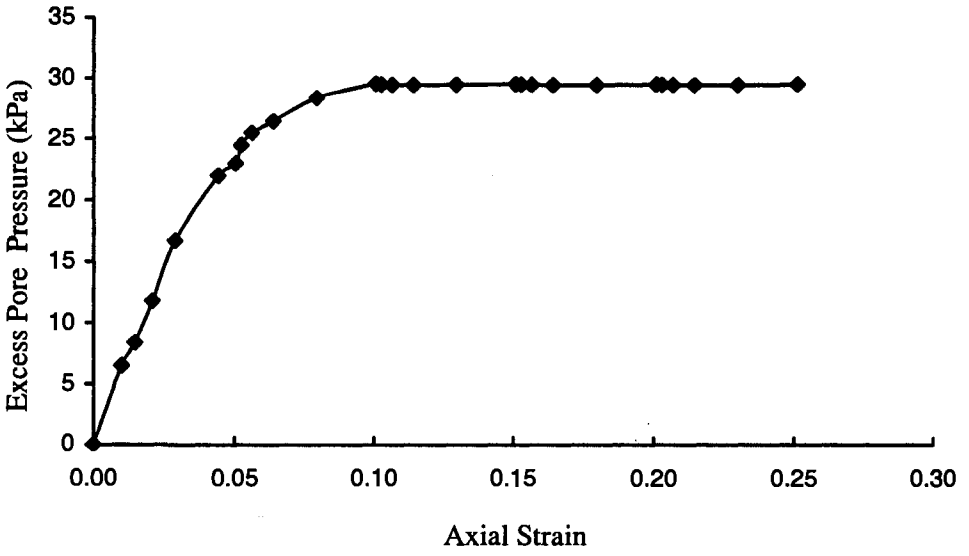

Figure 3.11 Simulation using Soft-Soil model (CU test, σ_3 = 50kPa)

At the same confining pressure (cell pressure), more excess pore water pressure is calculated by the Soft-Soil Model compared to Mohr-Coulomb Model. The soil fails at a lower deviatoric stress level when Soft-Soil Model is used because the effective confining pressure is less than that in the calculations using Mohr-Coulomb Model.

CHAPTER 4
DEVELOPMENTS IN NUMERICAL SIMULATIONS OF INTERACTION BETWEEN ICE FEATURES AND SEABED

Ice scouring is a complex engineering problem. Although experimental methods provide some information about ice scouring, the finite element method has been widely used for the analysis of the scour process, sub-scour soil deformations, and scour forces. The investigations by several researchers about ice-scouring events using numerical simulations in 2-D and 3-D are described in detail in this chapter.

4.1 Finite Element Modeling

The following nonlinearities are involved in the analysis of scouring events:

a) Geometric nonlinearity: Large deformation and strains are developed in the soil. Subscour deformation induces shear strains of the order of 0.5 (Woodworth-Lynas et al., 1996).

b) Material nonlinearity: Soil is a nonlinear elastic plastic material. It has been reported (Chari and Prasad, 1986) that the soil property is gradually altered during ice scouring.

Finite element method is capable of solving these forms of nonlinearity in the simulation of ice scouring. For example, the large displacement option is selected in the kinematic equations, the elastic-plastic constitutive models represented the material nonlinearity for

soil, and the interface elements are used between different material bodies in the finite element analysis. Moreover, this method is capable of accounting for changes in the geometry, layering in the soil deposit, and applied loads to represent the field conditions.

4.2 Two Dimensional Modeling

Centrifuge tests on ice scouring (Lach et al. 1993) have been conducted to investigate scour forces and soil deformations. Based on the centrifuge test data, Lach and Clark (1996) and Yang and Poorooshasb (1997) used different 2-D numerical models to simulate the interaction problem in these tests.

4.2.1 Yang's Numerical Model

Yang and Poorooshasb (1997) used the finite element analysis program ANSYS to simulate these centrifuge tests (Test 02 and 04). The simulations were performed using total stress analysis. A value close to 0.5 was used as Poisson ratio to reduce the volumetric strains to very small values. Under these conditions, soil behaviour was considered to be undrained. The undrained soil parameters were used as given in Table 4.1.

Table 4.1 Undrained soil parameters (Yang and Poorooshasb, 1997)

Unsaturated unit weight (N/mm^3)	γ_{unsate}	1.668E-5
Young's Modulus (N/mm^2)	E_u	5.73
Poisson's ratio	ν_u	0.49
Cohesion (N/mm^2)	c_u	0.02
Friction angle (°)	φ_u	0
Dilatancy angle (°)	ψ_u	0

The ice feature was not included in Yang's numerical model. The horizontal movement of

the ice feature was represented by specifying horizontal displacements at the nodes along the slope of the soil. There is no consideration of modeling the behaviour of interface between the ice feature and soil.

The numerical results showed that the soil moved forward and upward and a frontal mound was formed. The displacements in the soil mass were represented by displacement vectors as shown in Figure 4.1.

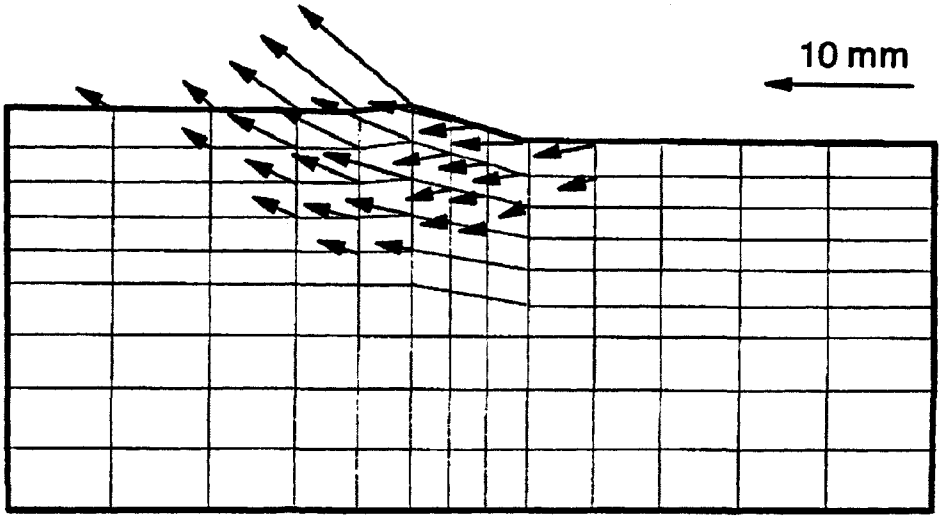

Figure 4.1 Soil displacement vectors corresponding to 7 mm horizontal movement of ice feature (from Yang and Poorooshasb, 1997)

4.2.2 Lach's Numerical Model

Lach and Clark (1996) performed numerical simulations of centrifuge tests using ABAQUS. The soil behaviour was represented by the Modified Cam-clay theory. The soil was assumed to be subjected to undrained loading conditions. The effects of pore water pressure were included in the numerical model. The soil parameters used are summarized in Table 4.2.

Table 4.2 Parameters for soil (Lach and Clark, 1996)

Compression index	λ	0.25
Swelling index	κ	0.04
Critical state stress ratio	M	0.90
Critical state reference specific volume	Γ	3.44
Poisson's ratio	ν	0.33

Due to large deformations and strains of soil during the ice-scouring, an updated Lagrangian formulation was used in this numerical model. During the incremental analysis, the geometry was updated to the state at the end of each increment.

The behaviour of the interface between the ice feature and soil was simulated in this numerical model. The effect of variation in the interface friction angle from 2.9 ° to 8.5 ° was investigated.

The numerical analysis showed that the total resultant force was the same for all interface friction angles. However, the horizontal and vertical force components were different when different interface friction angles were used. Force components predicted with low interface friction angle would be close to the measured values.

4.3 Three Dimensional (3-D) Numerical Model

In the 2-D numerical model, there is no lateral displacement of soil in the scour path. In order to reduce this restriction and make prediction of scouring effects more realistic, the 3-D numerical model is developed to study the ice-scouring process. In addition, 3-D analysis can help us to find the critical spot in the pipeline safety analysis when pipeline is deflected during the ice-scouring. Yang and Poorooshasb (1997) and Konuk et al. (2005, 2004) used different FE methods to set up their own 3-D numerical models. Yang's numerical model was based on the Lagrangian FE method. This method may cause

convergence problems and extreme mesh distortions when large deformations are involved. In order to overcome such a behavior, Konuk et al. (2005) adopted the Arbitrary-Lagrangian-Eulerian (ALE) FE method. The ALE method used a non-constant mass matrix; however, a constant mass matrix was used in the Lagrangian method.

4.3.1 Yang's 3-D Numerical Model

Yang and Poorooshasb (1997) conducted 3-D numerical analysis to investigate the ice scouring when the seabed contained a buried pipeline. 3-D beam elements were used to represent the pipeline. The analysis showed that the presence of pipe in the seabed did not affect the resultant forces, soil stresses, and soil displacements. Plastic strain contours are shown in Figure 4.2. The authors suggested that the problem of soil-pipeline interaction be treated in two steps: first obtain the soil deformation using a free field finite element analysis, then, design the pipeline based on information of the soil deformation.

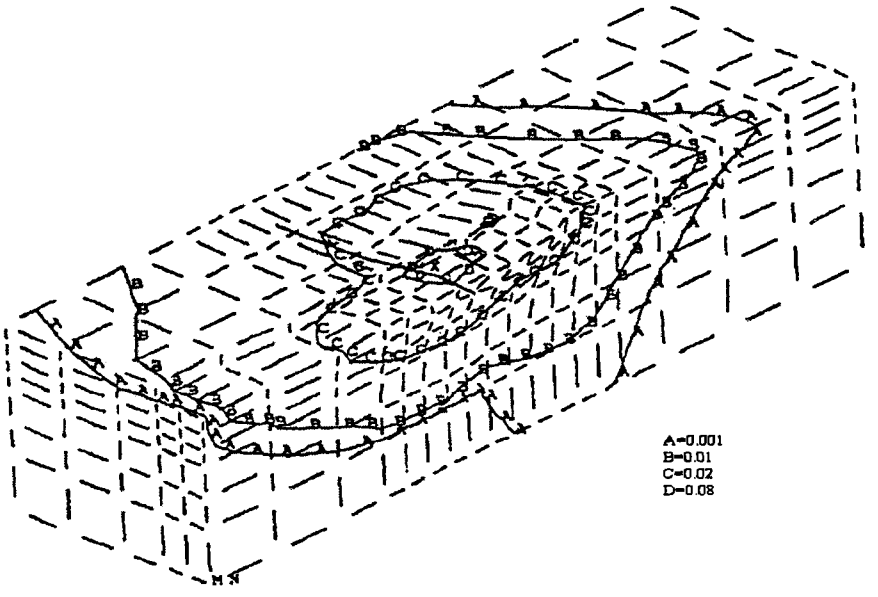

Figure 4.2 3-D plastic strain contours (from Yang and Poorooshasb, 1997)

4.3.2 Konuk's 3-D Numerical Model

Konuk et al. (2005) developed a 3-D numerical model of ice scour using LS-DYNA. The soil behaviour was represented by the CAP model (Simo et al., 1988) and eight–node solid elements were used in this model. The authors used ALE FE method in their numerical model. First, the Lagrangian FE analysis conducted, then, remapped the FE mesh, finally, used ALE approach to compute the strain, mass, and coordinates of the nodes of the new mesh.

The numerical analysis implied that the lower attack angles would cause more soil deformation (Table 4.3).

Table 4.3 Soil displacement at 1 m below the scour depth (from Konuk et al., 2005)

attack angle 45°	attack angle 30°	attack angle 15°
0.4 m	0.7 m	1.5 m

CHAPTER 5
2-D FE ANALYSIS USING PLAXIS AND ADINA

PLAXIS Version 8.0 is a special finite element package applied for the two-dimensional analysis of deformation and stability in various geotechnical problems around the world. It can simulate the non-linear, time-dependant and anisotropic behaviour of soils. In addition, PLAXIS can model the soil behaviour for undrained and drained conditions in geotechnical applications. It has interface elements which can be used in the simulation of interaction between a structure and soil.

ADINA Version 8.3 is a general purpose finite element program for two-dimensional and three-dimensional displacement and stress analysis. In particular, ADINA is suitable for large deformation problems.

The FE analysis of the present study makes use of the centrifuge tests of ice scouring, which were conducted by Lach and Clark (1996). Based on the centrifuge test data and the material model parameters provided by Lach et al. (1993) and Yang and Poorooshasb (1997), the ice-scour event is simulated in 2-D by using PLAXIS and ADINA finite element programs and the results are presented in this chapter.

5.1 Centrifuge Tests

A series of 1:100 scale model tests at 100 g was performed on the centrifuge (Lach et al., 1993). Centrifuge tests provided useful information on the seabed behaviour during ice scouring. First, a steady scour depth was imposed during the scouring. Second, the pore water pressure and the horizontal and vertical components of the scour forces were measured at a steady state. Finally, it was noticed (Lach et al., 1997) that most of the soil deformation took place within three times of the scour depth and the horizontal and vertical displacements were significant during ice scouring. Some additional information about this test is given in Chapter 2.

5.2 Finite Element Analysis Using PLAXIS

In the present numerical analysis of the centrifuge tests, the ice feature and the soil mass are dicretized as separate entities. The presence of interface between the ice and soil is modeled and the analysis is performed for undrained conditions.

For simplicity, a two-dimensional finite element model is established first to simulate the ice scour events. Plane strain conditions are assumed and 15-node solid elements are used for the seabed soil. It is assumed that the scour depth is known. Horizontal displacements are specified as the boundary conditions for the ice feature to plough seabed soil deposit.

5.2.1 Material Models

a) Material Model for Soil

- Mohr-Coulomb model

The behaviour of soil is simulated by the Mohr-Coulomb model. The basic parameters are Young's modulus, E, Poisson's ratio, v, cohesion, c, friction angle, φ, and dilatancy angle, ψ. The values of parameters used in this study are as follows:

Table 5.1 Parameters for soil using Mohr-Coulomb model

Unit weight (N/mm^3)	γ_{unsat}	1.668 E-5
Unit weight (N/mm^3)	γ_{sat}	1.958 E-5
Young's Modulus (N/mm^2)	E	5.73
Poisson's ratio	v	0.3
Cohesion (N/mm^2)	c	0.02
Friction angle (°)	φ	23
Dilatancy angle (°)	ψ	0

The values of model parameters are obtained from Yang and Poorooshasb (1997).

- Soft-Soil Model

The behaviour of soil is also expressed by Soft-Soil Model in a separate analysis. The basic parameters are modified compression index, λ^*, modified swelling index, κ^*, cohesion, c, friction angle, φ and dilatancy angle, ψ. The values of parameters used in this study are as follows:

Table 5.2 Parameters for soil using Soft–Soil model

λ^*	0.15
κ^*	0.024
c (N/mm^2)	0.05
φ (°)	23
ψ (°)	0

The values of model parameters are obtained from (Lach et al., 1993).

The difference in using these two kinds of soil models is shown in a later section entitled, "Detailed results of numerical analysis".

b) Material Model for the Ice Feature

The ice feature is modeled as a linear elastic material with a high elastic modulus value. The parameters used for the ice feature are shown in Table 5.3.

Table 5.3 Material parameters for ice

Unit weight (N/mm^3)	γ	9E-6
Young's Modulus (N/mm^2)	E	1000
Poisson's ratio	ν	0.3

c) Material Model for the Pipe

The pipe is assumed as a linear elastic material with a high elastic modulus value. The parameters used for the pipe are shown in Table 5.4.

Table 5.4 Material parameters for pipe

Unit weight (N/mm^3)	γ	2E-5
Young's Modulus (N/mm^2)	E	1000
Poisson's ratio	ν	0.3
Radius(mm)	r	3.175

5.2.2 Geometry of the 2-D Numerical Model

***a) Free field (no pipe* in the seabed)**

Centrifuge experiments and the publications by Lach et al (1993), Lach and Clark (1996), and Yang and Poorooshasb (1997) provided the necessary information for the geometrical and material model parameters for two-dimensional models. The vertical section along the symmetry axis of scour for two-dimensional finite element model (1 mm of thickness) is shown in Figure 5.1.

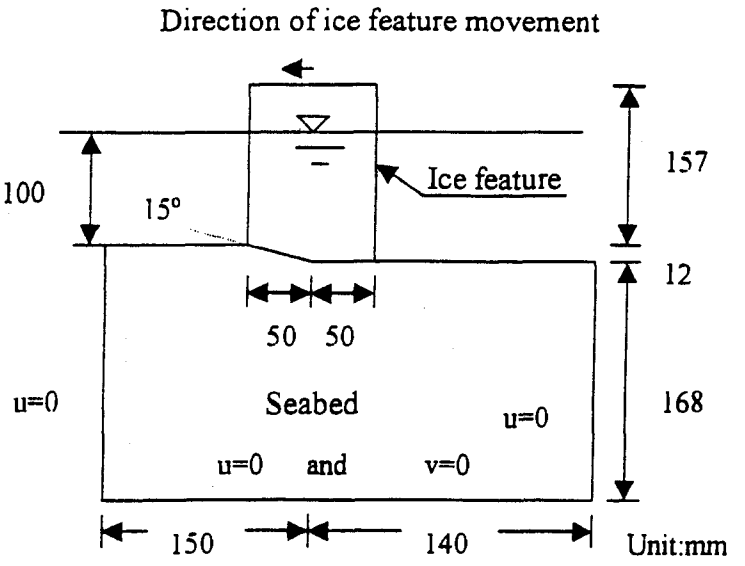

Figure 5.1 Schematics of solution region
u = horizontal displacement
v = vertical displacement

The solution region is 290 mm by 180 mm. The model iceberg attack angle is 15°, horizontal part of the bottom contact length is 50 mm, and scour depth is 12 mm. Boundary conditions were assumed such that the bottom surface of the seabed is fixed in both horizontal and vertical directions, no horizontal movement is allowed at the two vertical side surfaces of the seabed. In the finite element analysis, the vertical acceleration is chosen 100 times the acceleration of the earth's gravity.

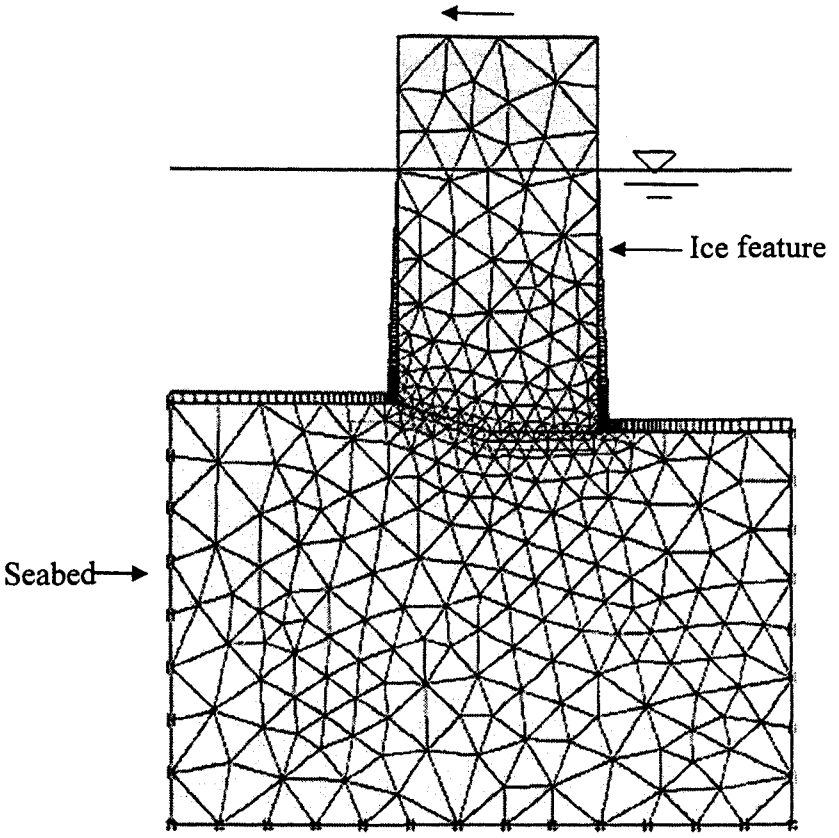

Figure 5.2 Finite element mesh

When the two components of the scour force, i.e. the horizontal and vertical forces arrived at constant values, the steady state of the ice scouring is reached. In the Yang's finite element analysis, the steady state is achieved after the model iceberg moved horizontally about 7 mm. In the present numerical study, the horizontal displacement of the iceberg is specified in increments. The analysis is continued up to a total of 8 mm horizontal displacement of the ice feature. At the same time, the ice feature is allowed to move freely in the vertical direction.

b) Seabed with pipe

In the numerical model, a pipe is placed at a location two times the scour depth under the keel of the ice feature as shown in Figure 5.3.

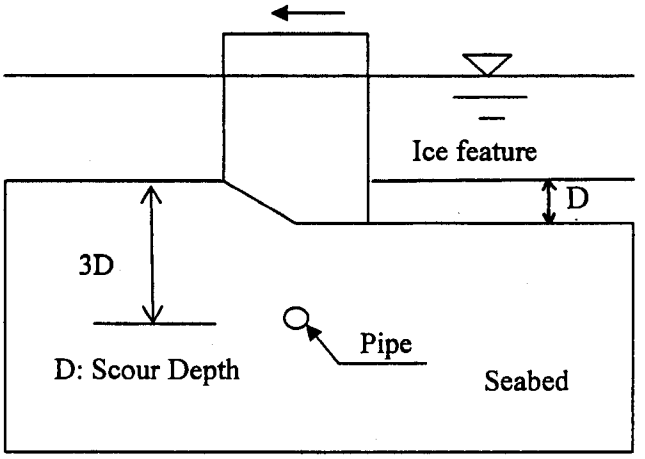

Figure 5.3 Schematics of the position of a pipe

c) Pipe with anchors

In 2-D numerical analysis, plane-strain conditions are assumed. However, in real life the ice feature is not infinitely long. The deformation of each pipe section due to this reason is different along its axis. The displacement of the pipe at the symmetry axis in 3-D analysis is less than that of the pipe in 2-D analysis due to the 3-D effects. In order to reduce the displacement of the pipe in 2-D analysis, an anchor is attached to the pipe as shown in Figure 5.4. For the stiffness of the anchor, three different values are used: 1E6 N/mm^2, 1E3 N/mm^2, and 10 N/mm^2. The displacements and the components of the force acting on the pipe are shown for different stiffness values in Table 5.5.

Table 5.5 Displacement and resistant force of an anchor

Stiffness	Force (N/mm)	Displacement (mm)
1000000N/mm^2	0.575	5.76E-7
1000 N/mm^2	0.096	9 E-5
10 N/mm^2	0.001	1E-4

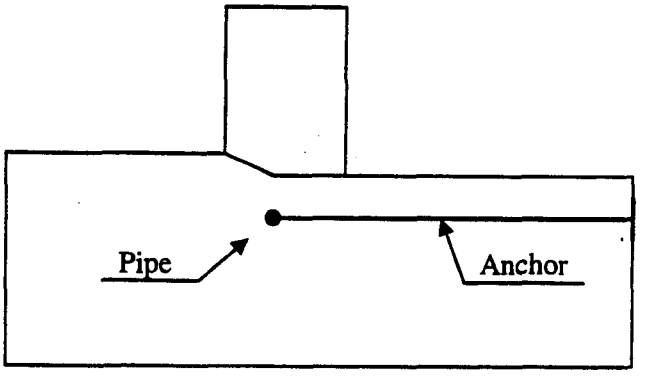

Figure 5.4 Pipe with anchor

It can be seen that in 2-D analysis when the stiffness of the anchor increases gradually, the anchor force increases. This suggests that, in 3-D analysis the soil pressure acting on the pipe becomes larger than that of 2-D analysis (no anchor) due to the three dimensional effects. The values of the anchor force obtained in 2-D analysis provide useful information about the soil pressure acting on the pipe during ice scouring.

d) Effect of interface elements in the FE analysis

In this study, interface elements are used between the ice feature and the seabed soil. Deformed meshes are shown in Figures 5.5 (without interface elements) and Figures 5.6 (with interface elements). It is noted that the elements between the ice feature and seabed are significantly distorted when no interface element is used. However, using interface elements reduces the amount of distortion and the interaction between soil and ice causes

less numerical problems. In a real life ice scouring event, failure takes place along the interface and the soil next to the ice feature starts slipping. The excess pore water pressure (P_{excess}), the horizontal scour force (F_X), and the vertical scour force (F_Y) with interface and without interface are shown in Table 5.6.

Table 5.6 Effect of interface elements on the P_{excess}, F_X, F_Y

Item	P_{excess} (kPa)	F_X (N/mm)	F_Y (N/mm)
Without interface	64.5	3.42	5.9
With interface(R=0.5)	62.1	3.26	5.94
Measured value	41	3.28	6.45
Note	At 59 mm depth below the base of ice feature	After 6.76mm horizontal movement of ice feature	

It is noted that values of P_{excess} and F_X with the interface case are close to the measured values. Therefore, the interface is considered in the analysis.

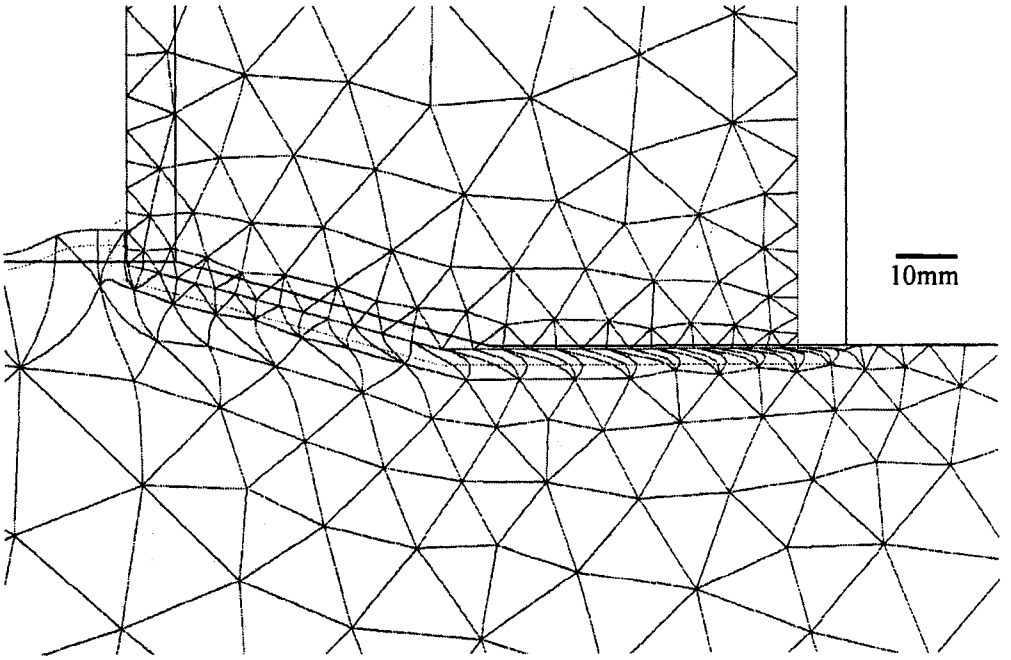

Figure 5.5 Deformed mesh without interface element

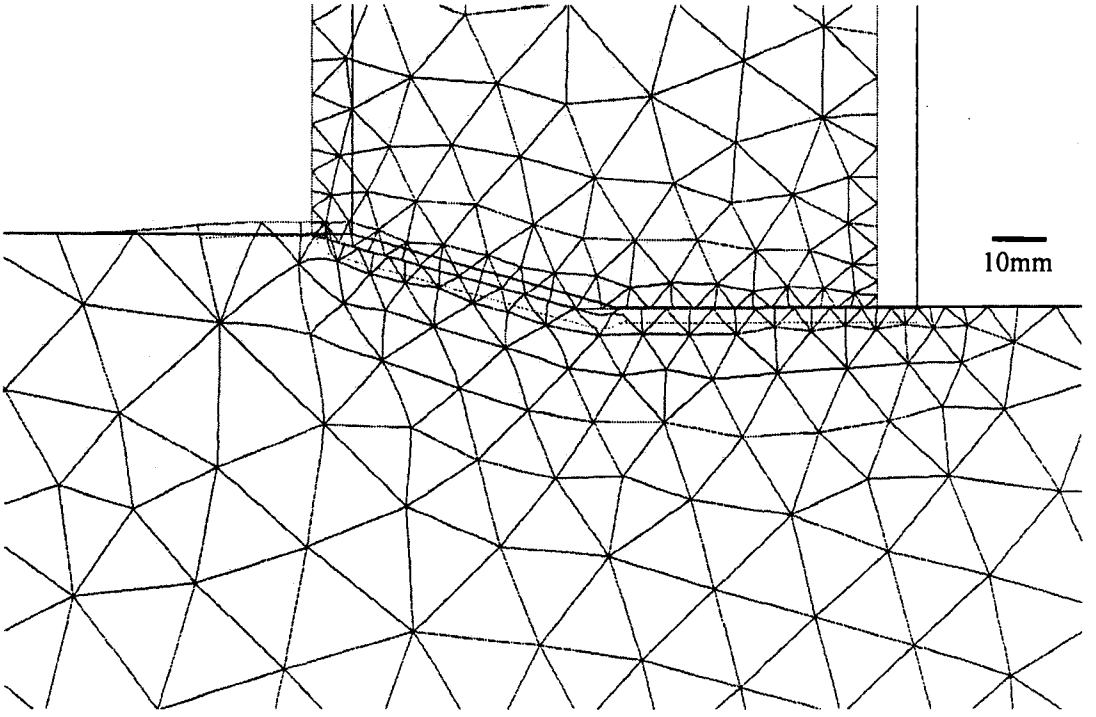

Figure 5.6 Deformed mesh with interface elements (R=0.5)

In order to determine the effect of the rigidity parameter, R, for interfaces, R is assigned values of 0.5, 0.6, 0.7, and 0.8. Comparing the scour force with the measured force, the rigidity of 0.7 is found appropriate in this study as shown in Figure 5.7.

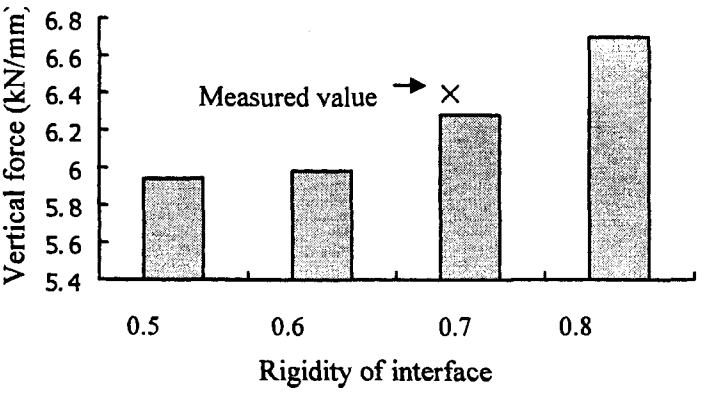

(a)

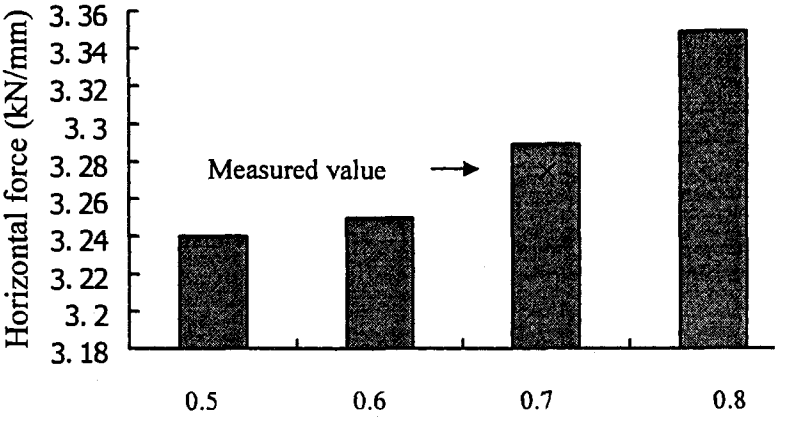

(b)

Figure 5.7 Scour force versus rigidity value of interface
a) vertical force versus rigidity value, b) horizontal force versus rigidity value

5.2.3 Undrained Analysis Using Total Stresses

Since ice-scouring happens quickly in centrifuge tests, the soil is considered undrained. The total stress parameters of soil model for undrained conditions are provided in Table 5.1.

The excess pore water pressure, Δp, is calculated by multiplying the changes in the

volumetric strain, $\Delta\varepsilon_v$, with the undrained bulk modulus, K_u.

$$\Delta p = K_u \Delta \varepsilon_v \tag{16}$$

$$K_u = \frac{E_u}{3(1-2\nu_u)} \tag{17}$$

In undrained conditions, no volumetric strains are allowed to take place. However, this condition requires an infinitely large bulk modulus. At the same time, the bulk modulus can be assigned only a very large value (but not infinitely large value) for the computational purposes. Therefore, the analysis results in a very small value for the volumetric strain, which allows the calculation of excess pore water pressure as described above.

In the centrifuge test 02, the measured excess pore water pressure at 62 mm depth below the base of the ice feature is 58 kPa. From the finite element analysis, the $\Delta\varepsilon_v$ is $6.5*10^{-4}$ at this position. K_u is 95.5 N/mm^2 when ν_u is 0.49. Therefore, the calculated value of the excess pore water pressure, Δp, is 62 kPa.

In real life, seabed soil could be sand, silt, or gravely sand. Once the average drift speed of ice feature is not enough to initiate the undrained deformation of soil, the drained condition should be considered.

5.2.4 Detailed Results of Numerical Analysis

a) Free field (no pipe in the seabed)

The results of the finite element analysis are compared with the Centrifuge Test 02 data in the steady state conditions.

Figure 5.8 shows the deformed mesh corresponding to a horizontal movement of 6.76 mm

of the model ice feature. A frontal soil mound is formed due to the forward and upward movement of the soil within the scour depth. This is consistent with the experimental evidence.

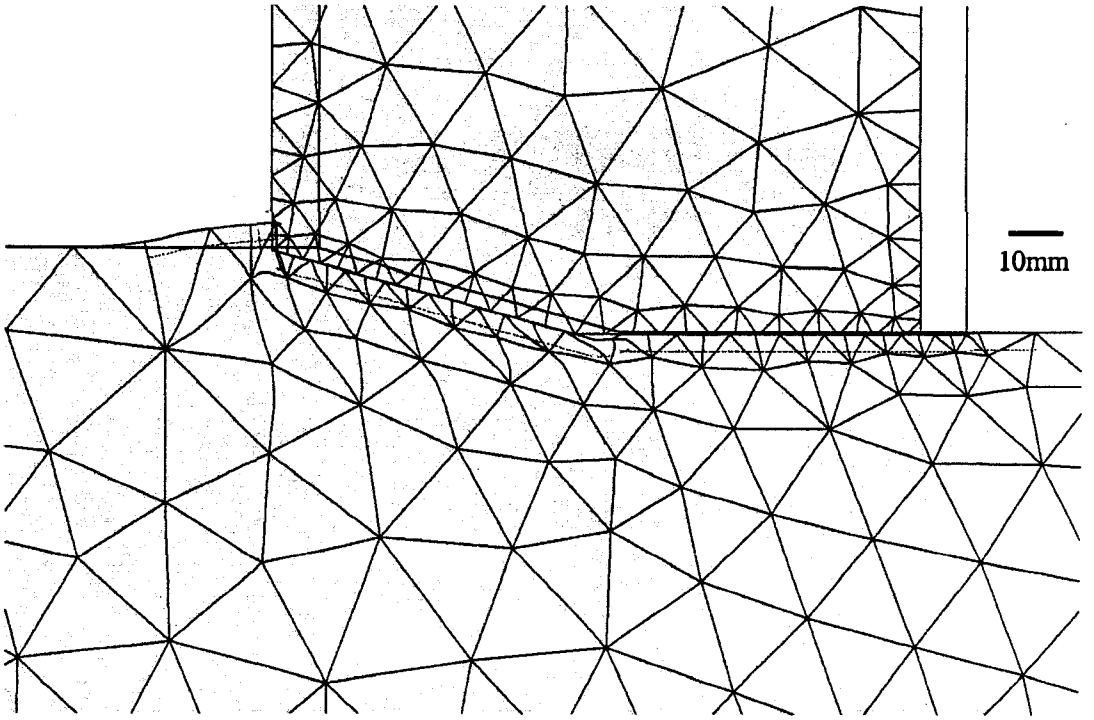

Figures 5.8 Deformed mesh at 6.76 mm horizontal movement of ice feature

In the finite element analysis, using the stress at stress points (Gauss points) along the interface between the ice feature and soil, the scour force is calculated at the inclined attack area (A-A section) and on the base (B-B section) of the ice feature. Figure 5.9 to Figure 5.12 show the stresses on the A-A section and B-B section for 6.76 mm horizontal movement of ice feature. Table 5.7 gives the scour force components calculated.

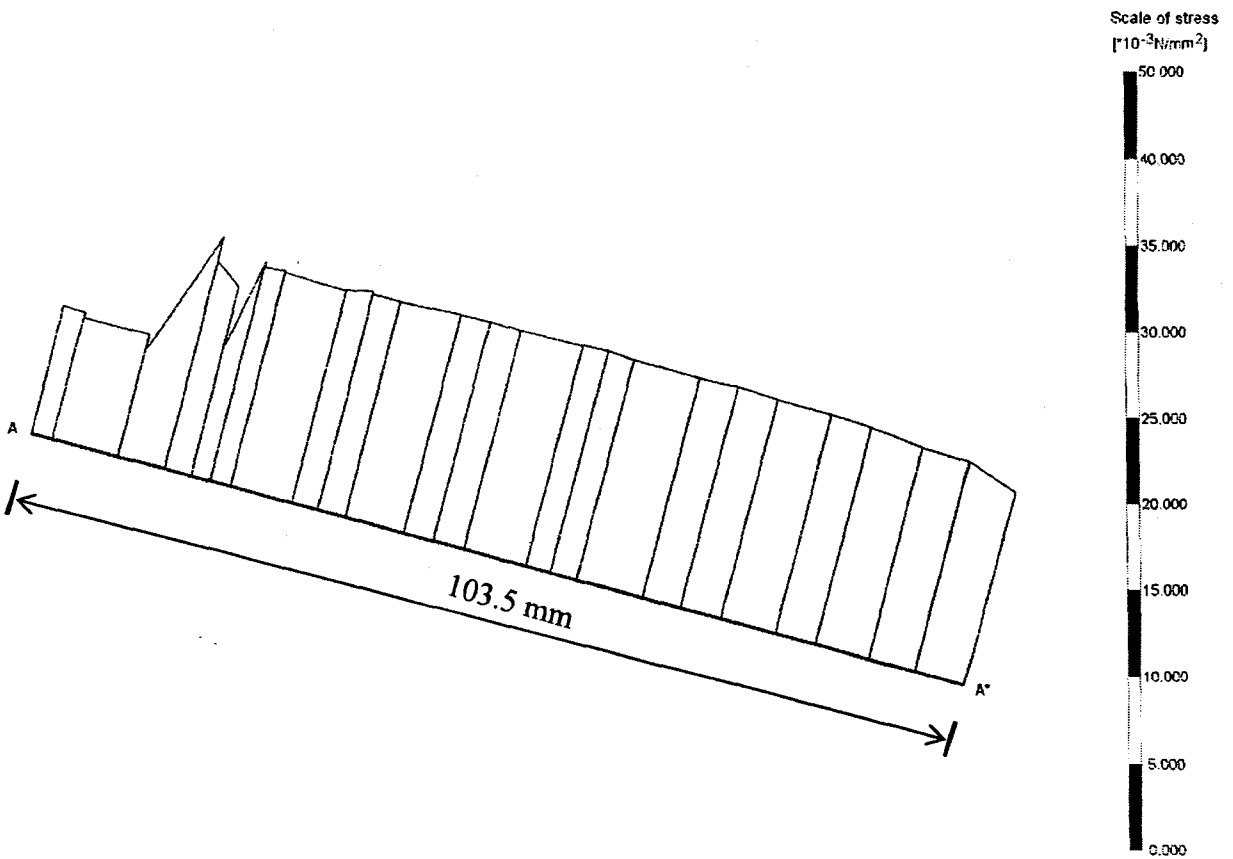

Equivalent force is 0.5 N/mm

Figure 5.9 Shear stress on the inclined surface of ice feature

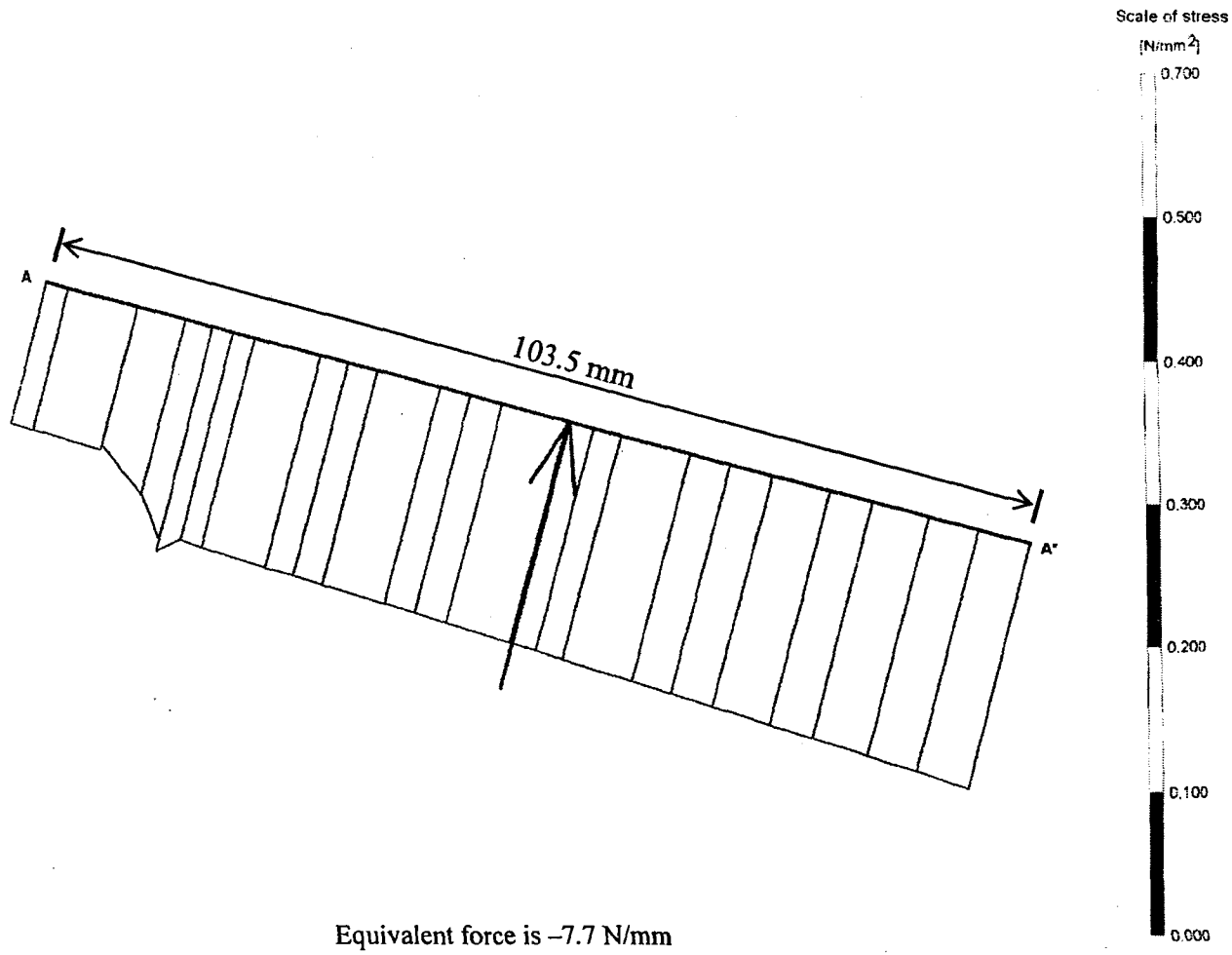

Equivalent force is –7.7 N/mm

Figure 5.10 Normal stress on the inclined surface of ice feature

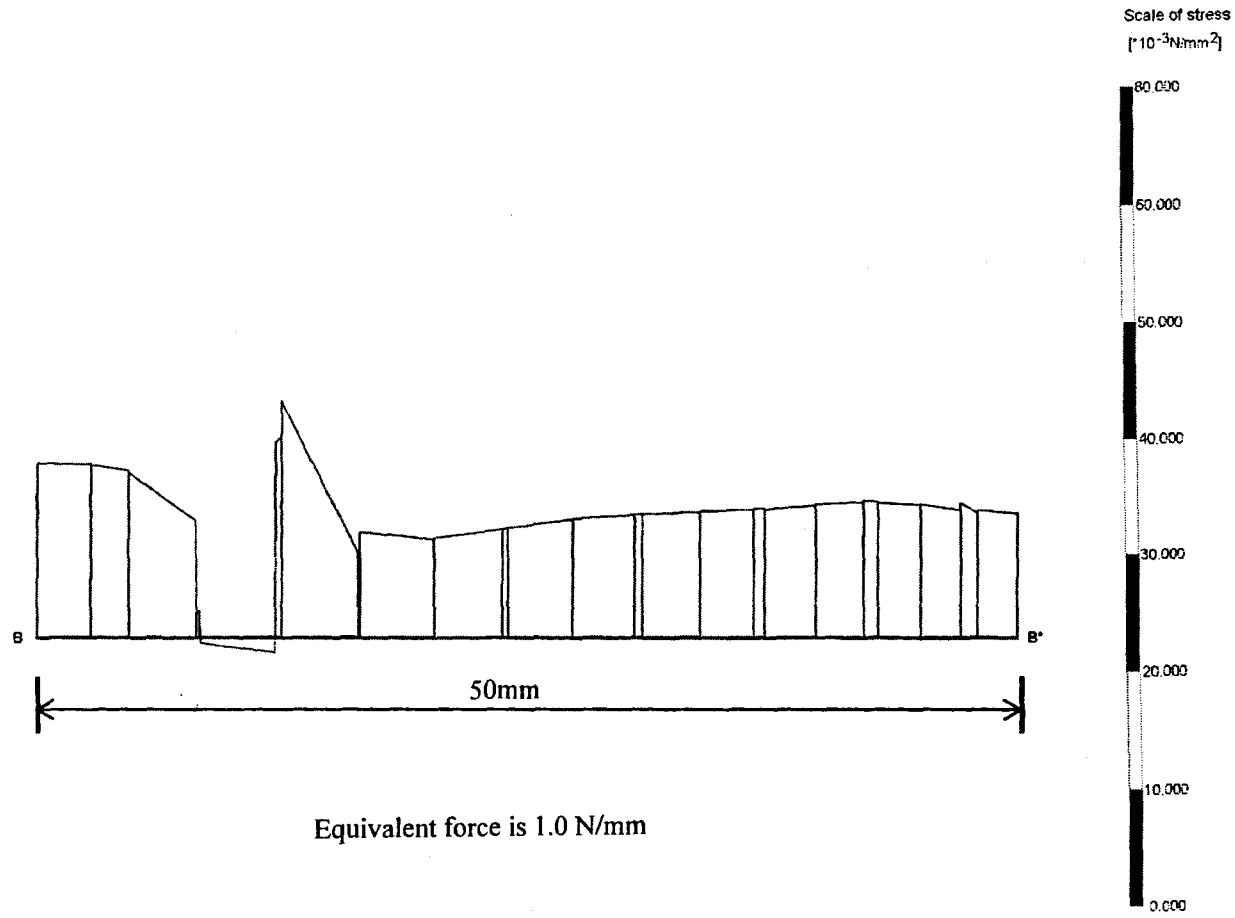

Figure 5.11 Shear stress on the base of ice feature

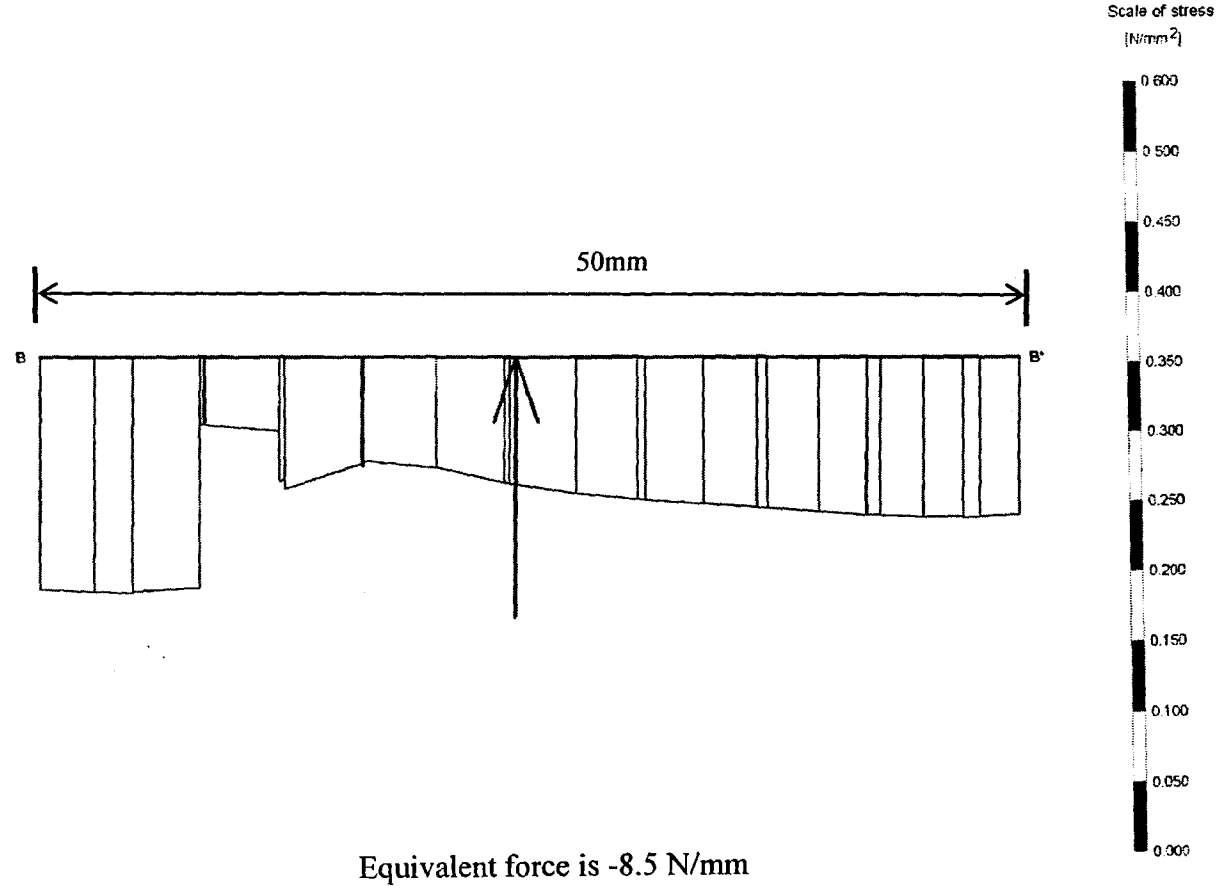

Equivalent force is -8.5 N/mm

Figure 5.12 Normal stress on the base of ice feature

Table 5.7 Scour force (N/mm) along the interface between the ice and seabed soil

	At the inclined attack area of ice feature	On the base of ice feature	Total scour force
F_x (N/mm)	7.7*sin15+0.5*cos15=2.5	1.0	3.5
F_y (N/mm)	7.7*cos15+0.5*sin15=7.6	8.5	16.1

Due to using total stresses at Gauss points, the vertical scour force includes the static water pressure that is 9.8 N/mm. The net vertical scour force is 6.3 N/mm. When the scour force components are adjusted for the actual width, 100 mm, of model iceberg, F_x, becomes 350 N and F_y becomes 630 N. The scour forces predicted by PLAXIS are close to the centrifuge test data (F_x = 328 N, F_y = 645 N). Figures 5.13 and 5.14 show a plot of the horizontal scour force F_x and the vertical scour force F_y developed during scouring. The steady state is achieved after the model iceberg moved horizontally about 6.76 mm.

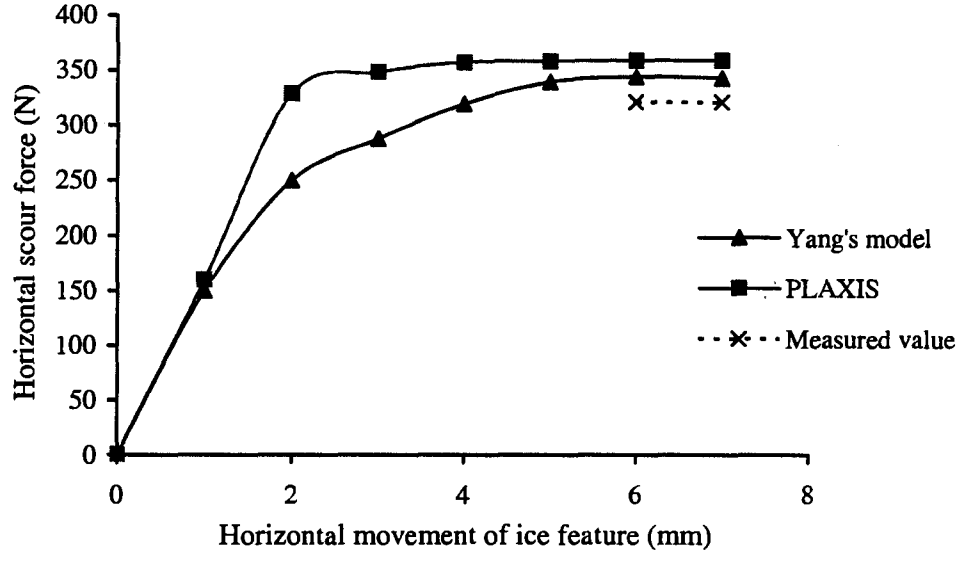

Figure 5.13 Horizontal component of scour force versus horizontal movement of ice feature

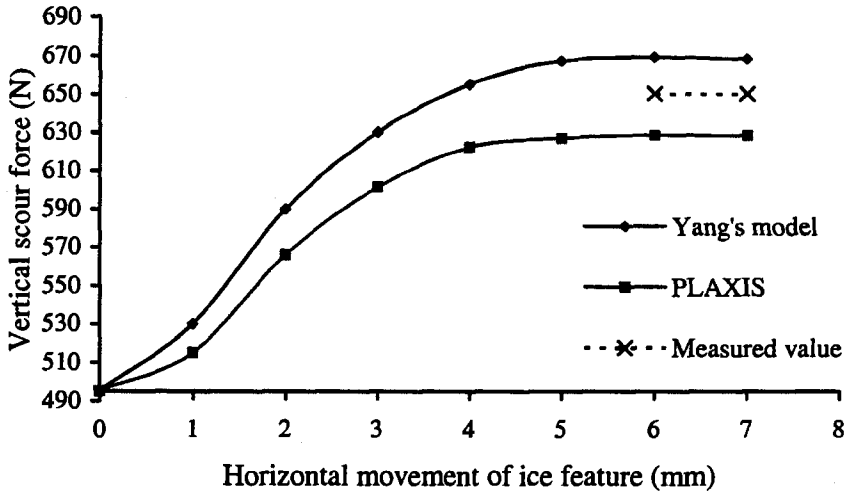

Figure 5.14 Vertical component of the scour force versus horizontal displacement of ice feature

According to the finite element analysis, the excess pore water pressure at 62 mm depth below the base of the ice feature is 61 kPa. This is close to the recorded value of 58 kPa in the Centrifuge Test 02.

Figure 5.15 shows the points where soil exhibited plastic behaviour during ice scouring. It is noticed that plastic zone develops between the seabed surface and a depth of about three times the scour depth.

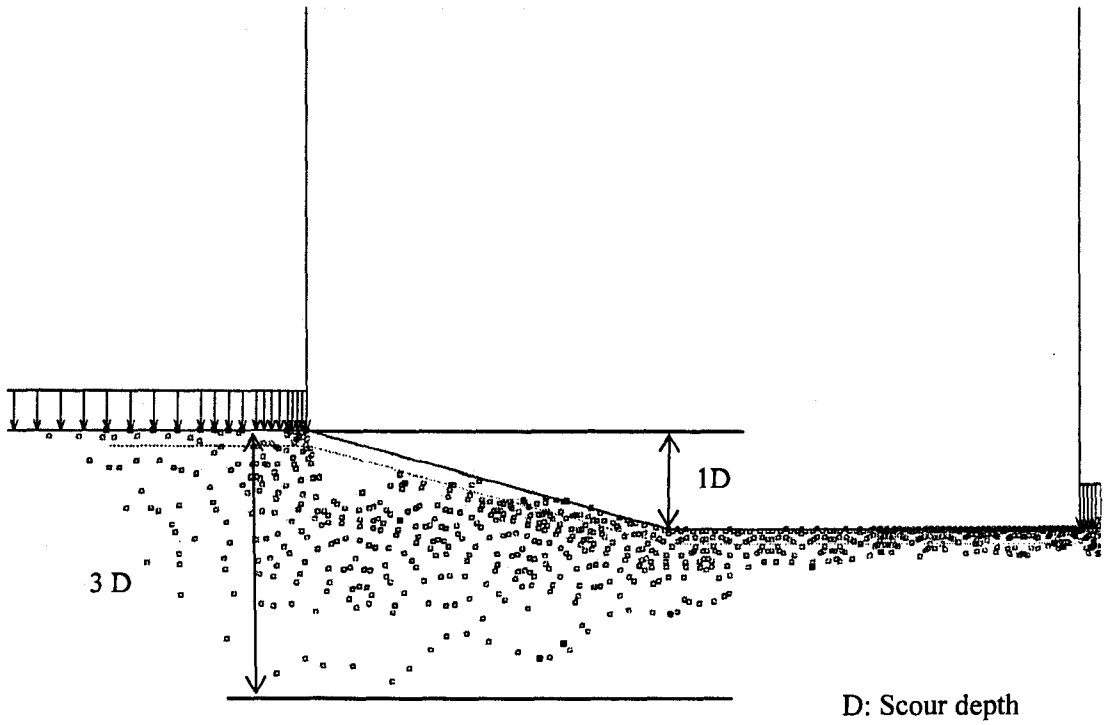

Figure 5.15 Plastic points in the seabed

b) Seabed with pipe

Stress and displacements around the pipe

In order to see the changes of stresses and displacements around the pipe during the ice scouring event, three different FE analyses are conducted. In the first analysis, there was no pipe at the proposed location for the pipeline. In the second analysis, the pipe was included in the simulation. In the last analysis, an anchor was attached to the pipe to reduce the displacements of the pipe to account for the three dimensional effects. These three different types of analyses will be referred to as Case 1, Case 2, and Case 3 in the following sections.

1) Stress distribution

Stresses acting on two vertical and two horizontal surfaces around the pipe are used to explore the changes of stresses in three cases described above. On the left side and bottom side, shown in Figure 5.16 and Figure 5.17, the normal stress in Case 3 is smaller than that of Case 1 and 2. This is because the anchor produces the resistant force during the ice-scouring. That shows the importance of three dimensional effects.

On the right side and the top of the pipe, the stresses are more concentrated around the pipe in Case 2 and 3 as shown in Figure 5.18 and Figure 5.19. The pipe with an anchor has a higher value of stress than the case with pipe only.

In these stress analyses, the intensity of stress acting on the pipe is larger on the surface of the pipe facing the ice scouring forces.

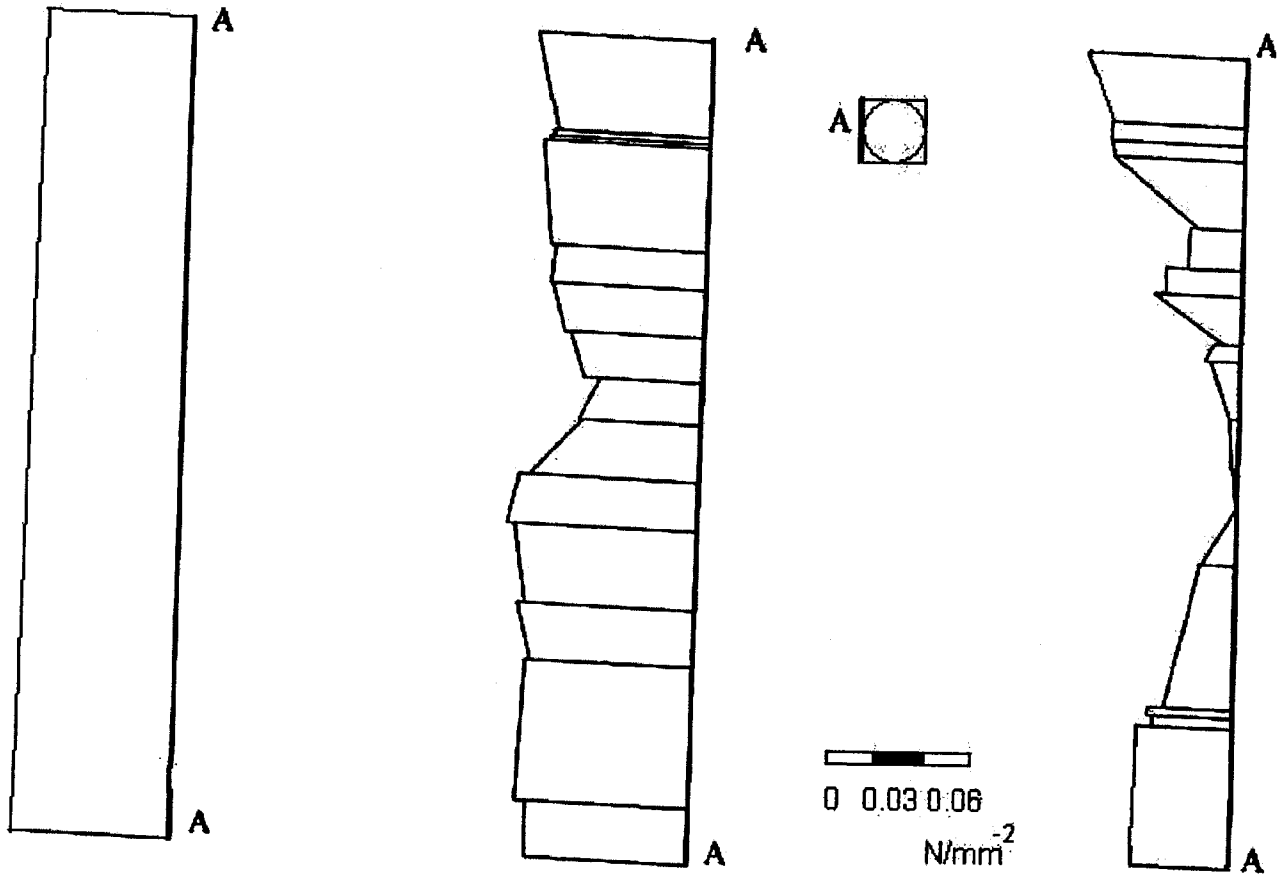

Figure 5.16 Normal stress on the left surface of pipe

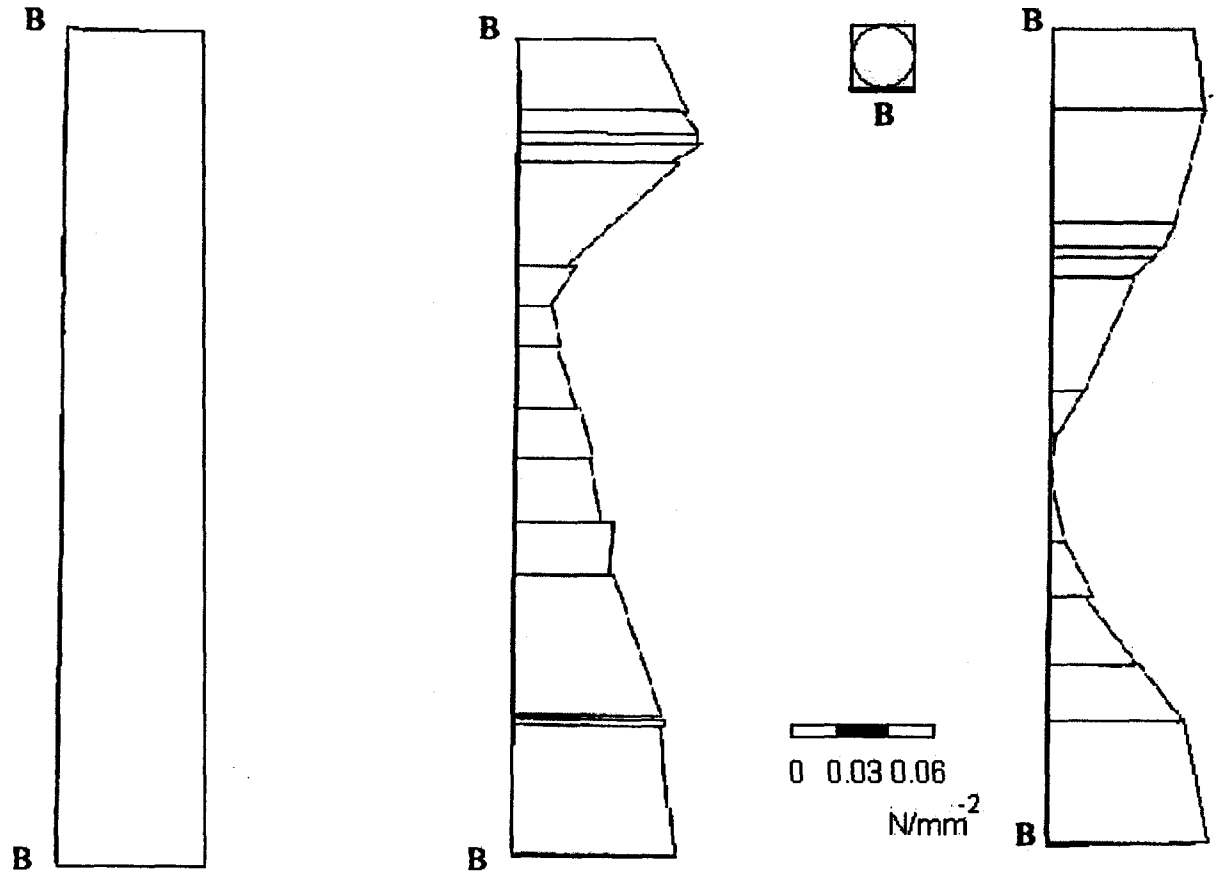

Figure 5.17 Normal stress on the bottom surface of pipe

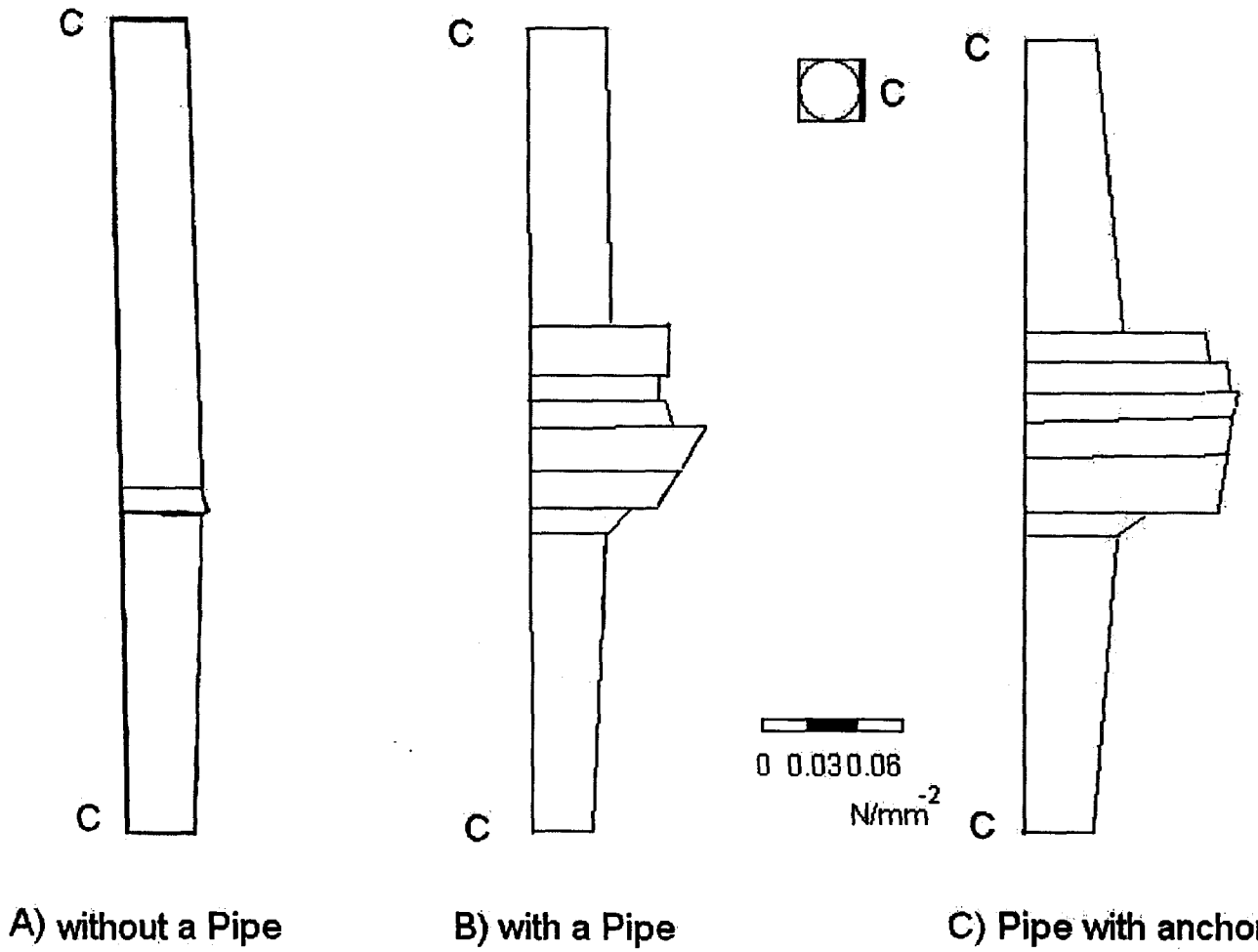

Figure 5.18 Normal stress on the right surface of pipe

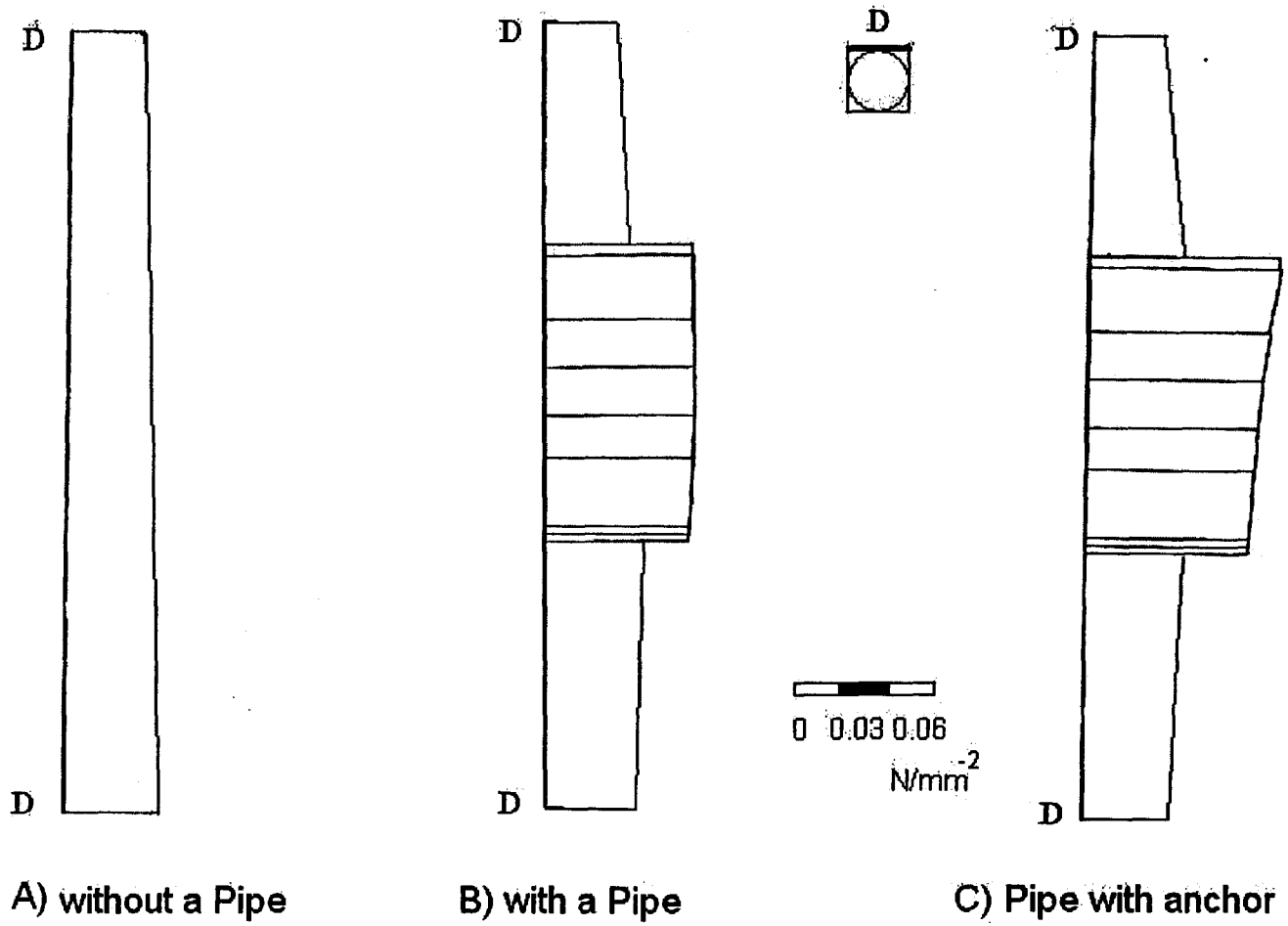

Figure 5.19 Normal stress on the top of pipe

2) **Displacements**

The displacements of the central point of the pipe indicate the differences among the three cases as shown in Table 5.8. It is noted that, for the pipe with an anchor (stiffness=1000kN/mm), the horizontal displacement, Δu, is 1.3 mm which is less than those predicted in the two other cases. As will be shown in the following sections, 3-D numerical analysis also gave 1.4 mm horizontal displacement of the pipe. In the present study, only a horizontal anchor is considered. In future studies, a vertical anchor should be added.

Table 5.8 Displacements of central point of pipe in three cases

Case	Central point		Δu(mm)	Δv(mm)
	X(mm)	Y(mm)		
Free field	106	148	-2.36	-3.56
With pipe	106	148	-2.32	-3.53
Pipe with anchor	106	148	-1.32	-3.45

(Note: u is the horizontal displacement and v is the vertical displacement.)

c) Scour force calculated by using Soft-Soil Model

Some of the parameters for the Soft-Soil Model were not available. A trial and error approach is taken to select parameters that will result in an agreement between the measured and calculated results for the stress strain relation. Using these parameters for the Soft-Soil model, PLAXIS produced displacements and scour forces which are quit close to those obtained by using the Mohr-Coulomb model as shown in Table 5.9.

Table 5.9 Scour force produced using the Soft-Soil model and Mohr-Coulomb model

	Scour force	
	F_x (N/mm)	F_y (N/mm)
Using Soft-Soil model	342	598
Using Mohr-Coulomb model	360	628

5.3 Two-Dimensional Finite Element Analysis Using ADINA

In order to compare with the results from PLAXIS in 2-D, the ice-scouring event is also simulated by using ADINA. Moreover, the 3-D simulation, which will be presented in the next chapter, makes use of the cross-section used in 2-D analysis.

5.3.1 Material Models

a) Soil model

The behaviour of soil is simulated by the Mohr-Coulomb Model. The basic parameters are the same as given in Table 5.1.

b) Model of ice feature

The ice feature is modeled as a linear elastic material with a high elastic modulus value. The parameters used for the ice feature are shown in Table 5.3.

c) Model of pipe

The pipe is assumed as a linear elastic material with a high elastic modulus value. The parameters used for the pipe are shown in Table 5.4.

5.3.2 Set-up of the 2-D Numerical Model

Similar to the analysis by PLAXIS, the pipe in the 2-D ADINA model is placed at the same location. A vertical cross-section along the scour axis is used for two-dimensional finite element model (1 mm of thickness), which is shown in Figure 5.20.

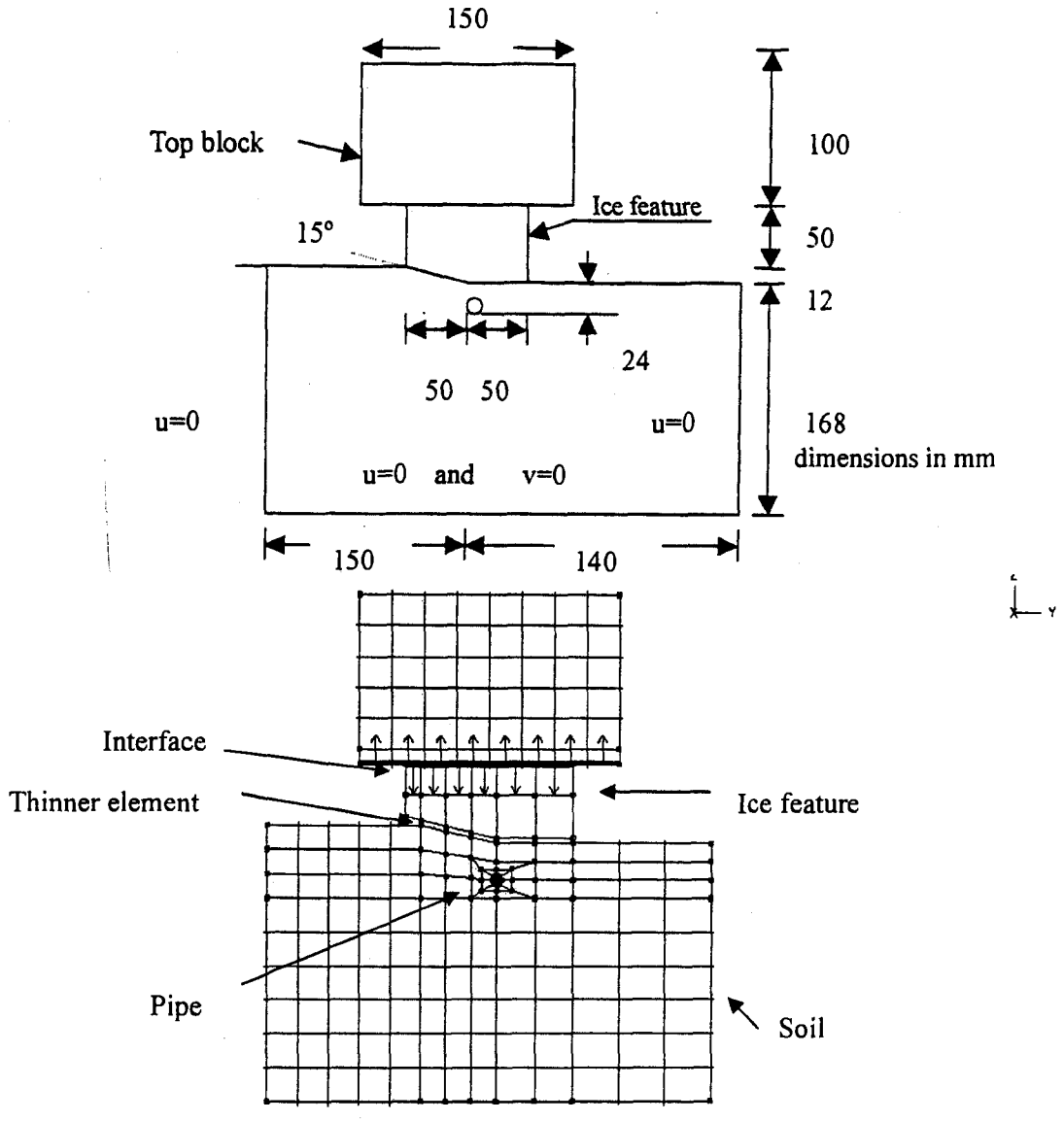

Figure 5.20 Schematics of solution region

u = horizontal displacement v = vertical displacement Length unit = millimetre

The top block is used to prevent tilting of the ice block during ice-scouring. The ice feature and the top block are made of a stiff material. Interface elements are used between the ice feature and the top block. Thin soil elements are placed between the ice feature and the soil mass. In this analysis, only the 4-node elements are employed in the mesh development process. The size of the solution region is 290 mm by 180 mm and the finite element mesh consists of 125 elements. The reasons for using such a coarse mesh are: (1) To use an identical mesh to Yang's 2-D model, (2) To save computational effort in running

3-D analysis, and (3) For making comparisons between the results of 2-D and 3-D analyses, it was decided that the cross-sections of 3-D model and 2-D model have the same mesh refinement.

First, 100 g is applied on the model, then the static water pressure 100 kPa is added on the surface of the soil mass (seabed surface). After that, 49.5 kPa is applied on top of the top block to represent the buoyant weight of the ice feature. Finally, 7 mm horizontal displacement is applied on the ice feature.

5.3.3 Deformation of the Seabed after Ice-scouring

1) Horizontal displacements of soil

Figure 5.21 shows that the maximum horizontal displacement which takes place in the soil occurs along the ice-soil interface. With increasing depth, the horizontal displacement of soil decreases.

2) Vertical Displacements of soil

It can be seen that the maximum vertical displacement occurs at a node under the inclined contact surface. Deformations in the seabed soils take place mainly in a region which is three times deeper than the ice-scouring depth.

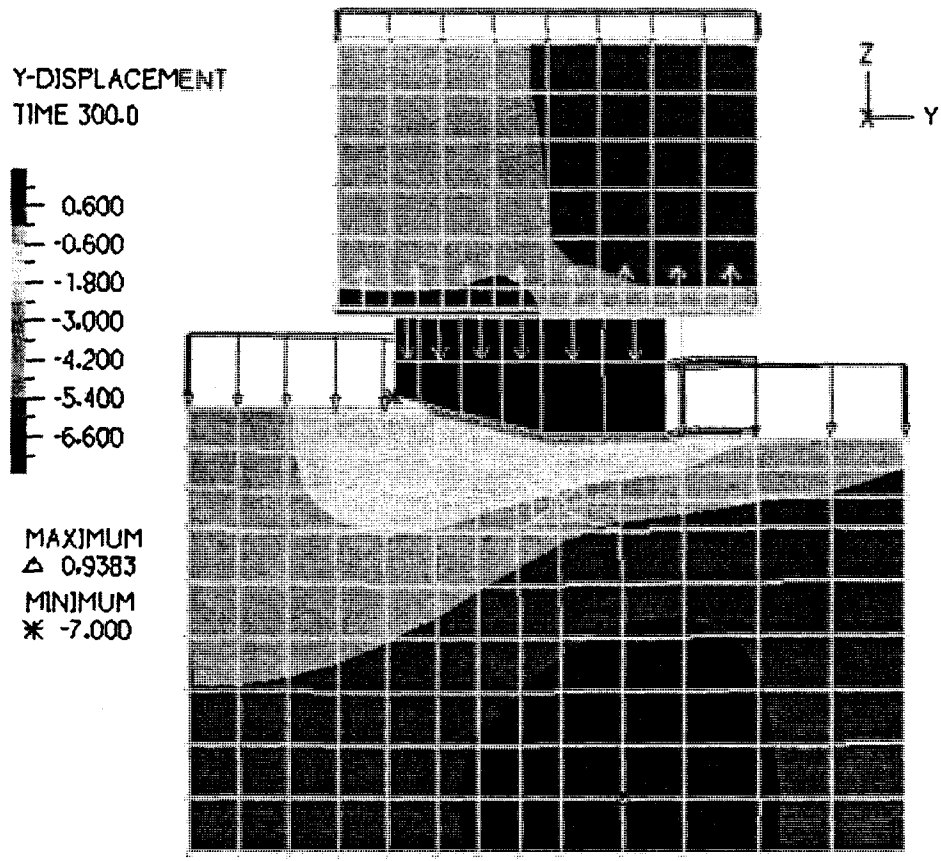

Figure 5.21 Horizontal displacements of the nodes in the seabed after 7mm horizontal movement of the ice-feature

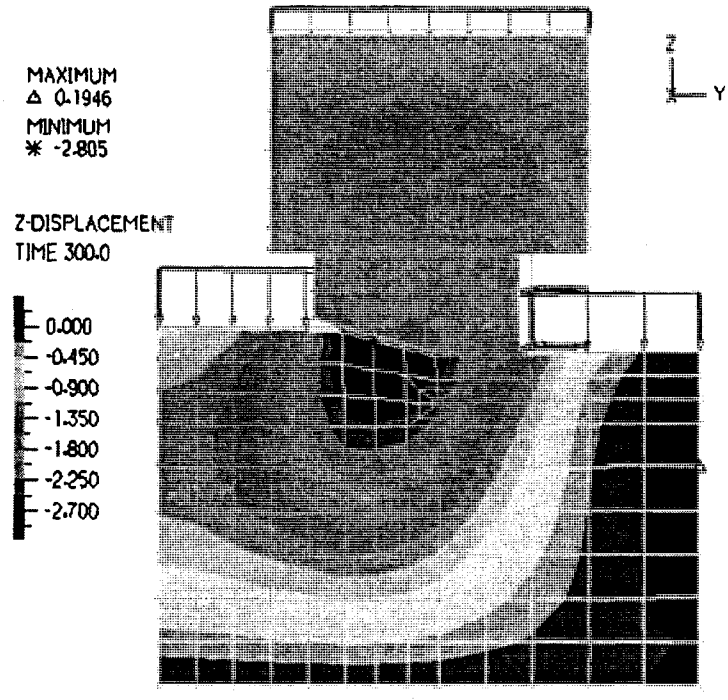

Figure 5.22 Vertical displacements of the nodes in the seabed after 7mm horizontal movement of the ice feature

5.3.4 Displacements of the Pipe

It can be seen that the pipe displaces both in the horizontal and vertical directions during the ice-scouring event. The node at the top of the pipe moves 3.2mm vertically and 2.1mm horizontally. The rotation of the pipe is 4.2°.

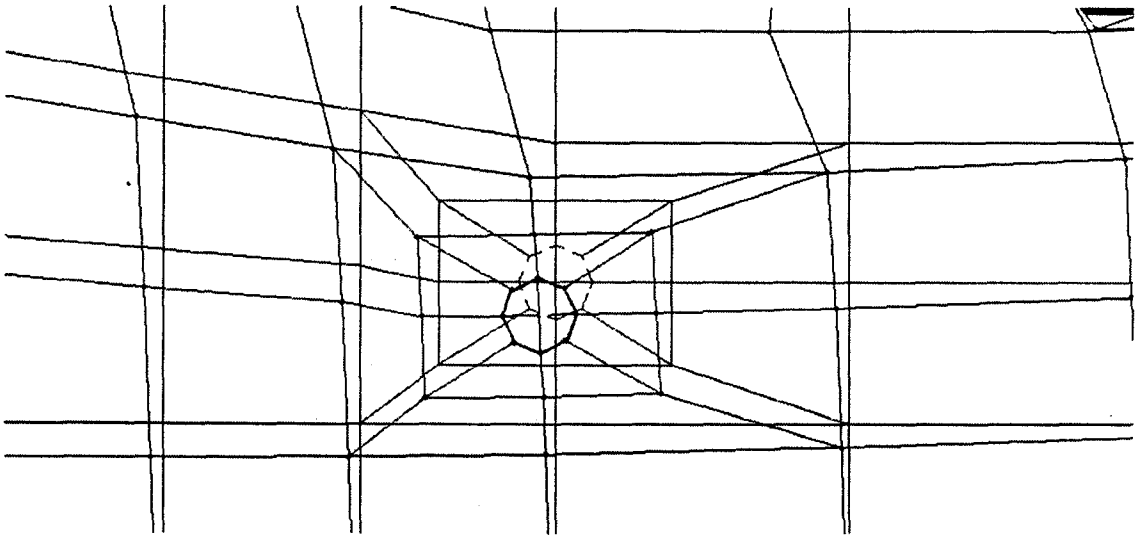

Figure 5.23 Displacement of the pipe after 7mm horizontal movement of the ice-feature

5.3.5 Calculation of Ice-scouring Force

Based on the stresses of elements along the ice-soil interface (element numbers: E124, E125, E128, E129, and E130) the components of the ice-scouring force are calculated at different time steps (that is corresponding to the horizontal movement of an ice feature). The details of the calculation steps are given in Appendix A.

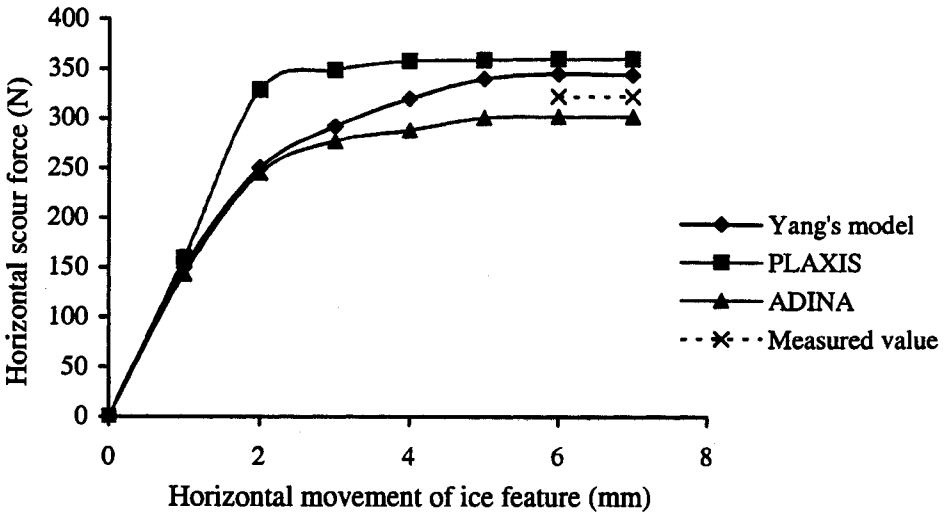

Figure 5.24 Horizontal scour force versus horizontal movement of the ice feature

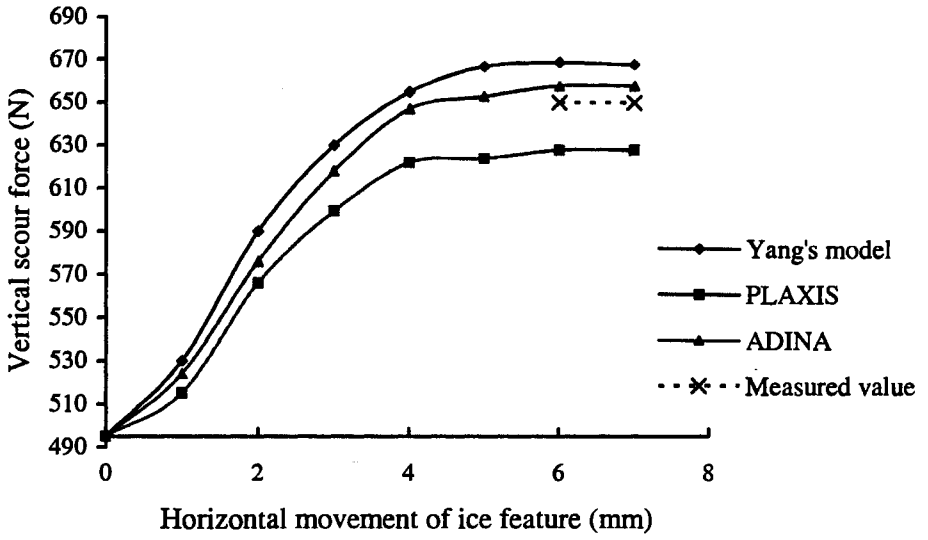

Figure 5.25 Vertical scour force versus horizontal movement of the ice feature

Figure 5.24 and Figure 5.25 show that after the ice feature moves 4.0 mm, the vertical component and horizontal component of scour force become constant. The ice-scouring reach the steady state.

CHAPTER 6
3-D FINITE ELEMENT MODEL USING ADINA

Lateral displacements of materials are not allowed in a 2-D plane strain numerical model. In addition, the movements of the pipeline perpendicular to its axis cannot be explored in a 2-D numerical analysis for the entire length of the pipe. It is necessary to simulate ice scouring event using a 3-D numerical model. This chapter describes 3-D simulations by ADINA.

6.1 Numerical Model

In this section, the geometry of the model, the types of material models, and the boundary conditions are described.

6.1.1 Geometry

Based on the geometry of 2-D model in ADINA, the 3-D domain is discretized as shown in Figure 6.1. The finite element mesh of 2-D model is extended 200 mm in X direction to obtain the 3-D mesh. Because of its symmetry, half the ice scour width is considered in the solution domain. The pipe is 6mm in diameter and is buried in the transient zone (Zone 2) under the keel of the ice feature (2 times the scouring depth). The material parameters are the same as in the 2-D analysis.

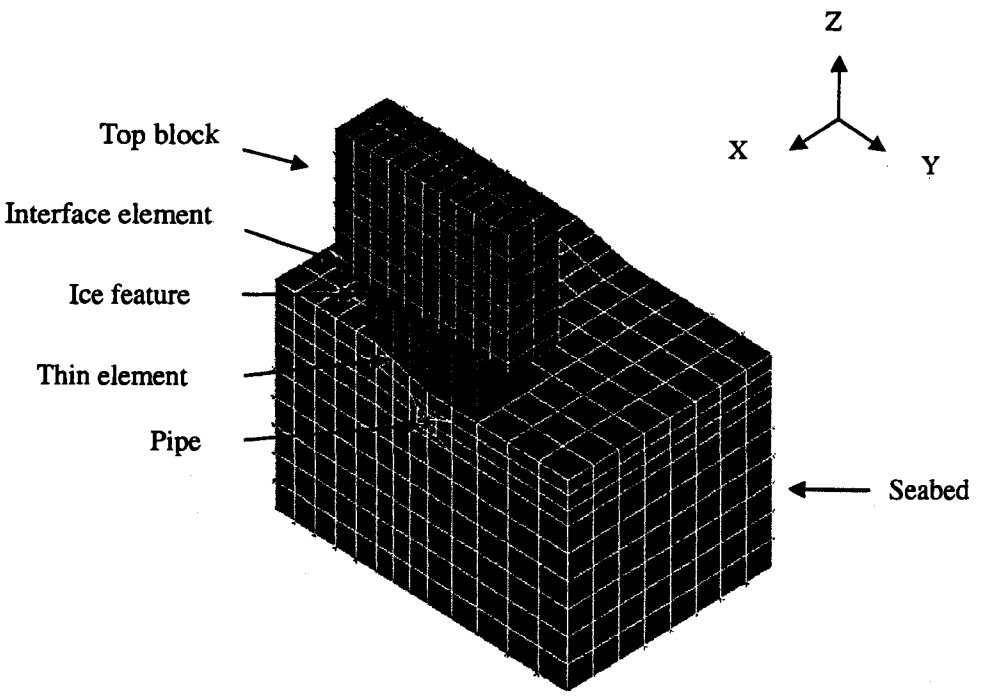

Figure 6.1 Schematics view of 3-D FE mesh

6.1.2 Element Type

The solution region for soil is 290 mm x 180 mm x 200mm. The eight node elements are used in the discretization and the finite element mesh consists of 1250 elements.

6.1.3 Boundary Conditions

Boundary conditions were assumed such that the bottom surface of the seabed is fixed in Z direction, two vertical side surfaces are fixed in the Y direction, while the front and the back of the seabed area are fixed in the X direction. For the ice block, the front and back surfaces are fixed in the X direction. Finally, the vertical side surfaces of the top block are fixed in Y direction. The top block is allowed to move freely in the Z direction.

6.1.4 Process of Solution

The large displacement option is adopted in the analysis. Time functions are used to control the application of loads. There are 5 time functions corresponding to the loading as shown in Table 6.1. Beyond the ice-scouring region, the soil is replaced by a distributed load which is equivalent to the weight of the soil.

Table 6.1 Loading controlled by the time functions

Time function	Loading
Time function 1 (time step 0 to 20)	100 times the acceleration of the earth's gravity.
Time function 2 (time step 20 to 40)	Soil weight
Time function 3 (time step 40 to 60)	Static water pressure 100kPa
Time function 4 (time step 60 to100)	Buoyant weight of ice feature applied on top of the top block as pressure, 49.5kPa
Time function 5 (time step100 to 500)	7mm horizontal displacement on the ice feature

6.2 Numerical Results

Deformation of the seabed after the movement of ice feature, displacement contours in the soil, stresses and displacements of the pipe are presented in this section.

6.2.1 Deformation of the Seabed after Ice-scouring

Figure 6.2 shows deformation of the seabed at the time step 403. It could be seen that the soil is lifted in a mound in front of the ice similar to the experimental phenomenon.

The horizontal and vertical displacement contours are presented in Figures 6.3 and 6.4. When the ice feature moves about 7 mm, the maximum horizontal displacement of soil is 4 mm along the interface between the soil and ice. Below the interface, the horizontal

displacement of soil is decreased with the depth. At the same time, the maximum vertical displacement of soil is 2.9 mm, which occurs below the base of the ice feature at a depth equal to two times the scour depth. The stress components in the soil element 112 versus time step curves indicate that the stress state reach failure at time step 170~180 (equivalent to about 4 mm) as shown in Figure 6.5 to Figure 6.7.

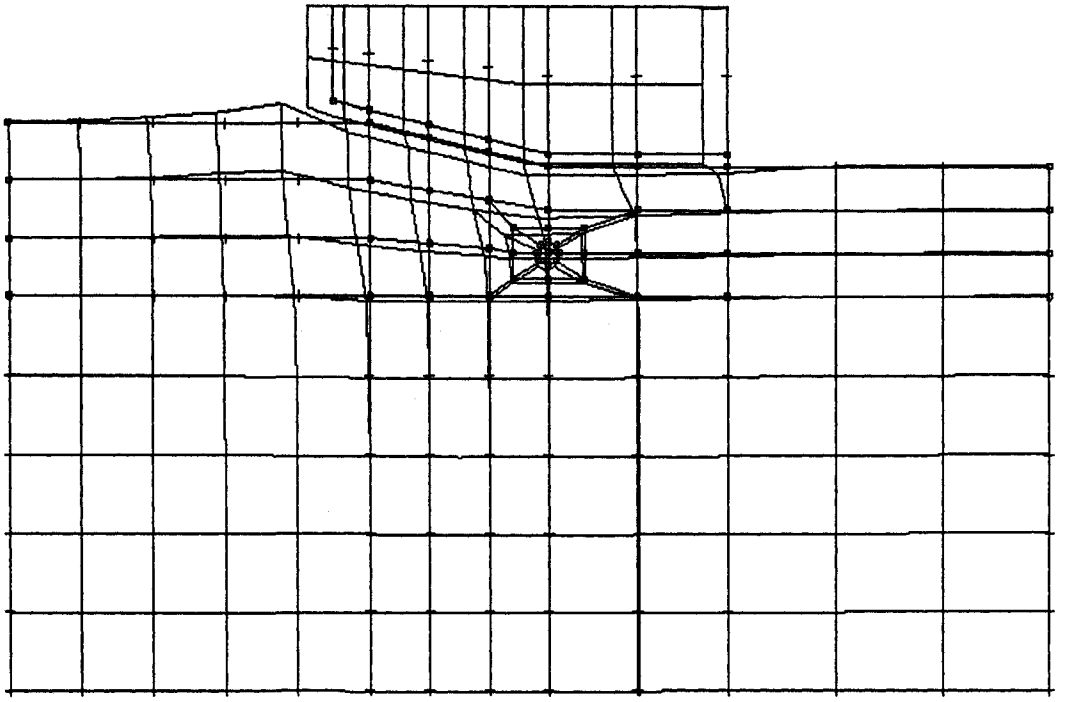

Figure 6.2 Deformation of soil after 7mm movement of ice feature

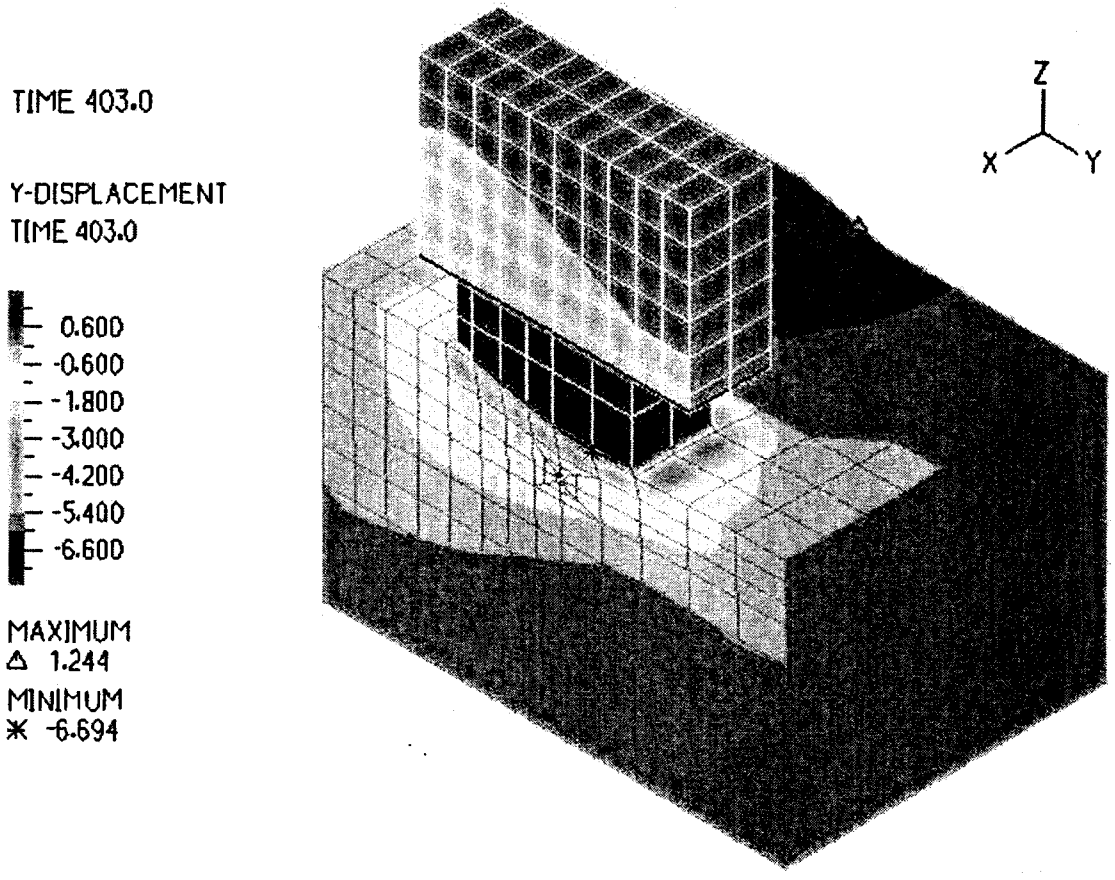

Figure 6.3 Horizontal displacement contours

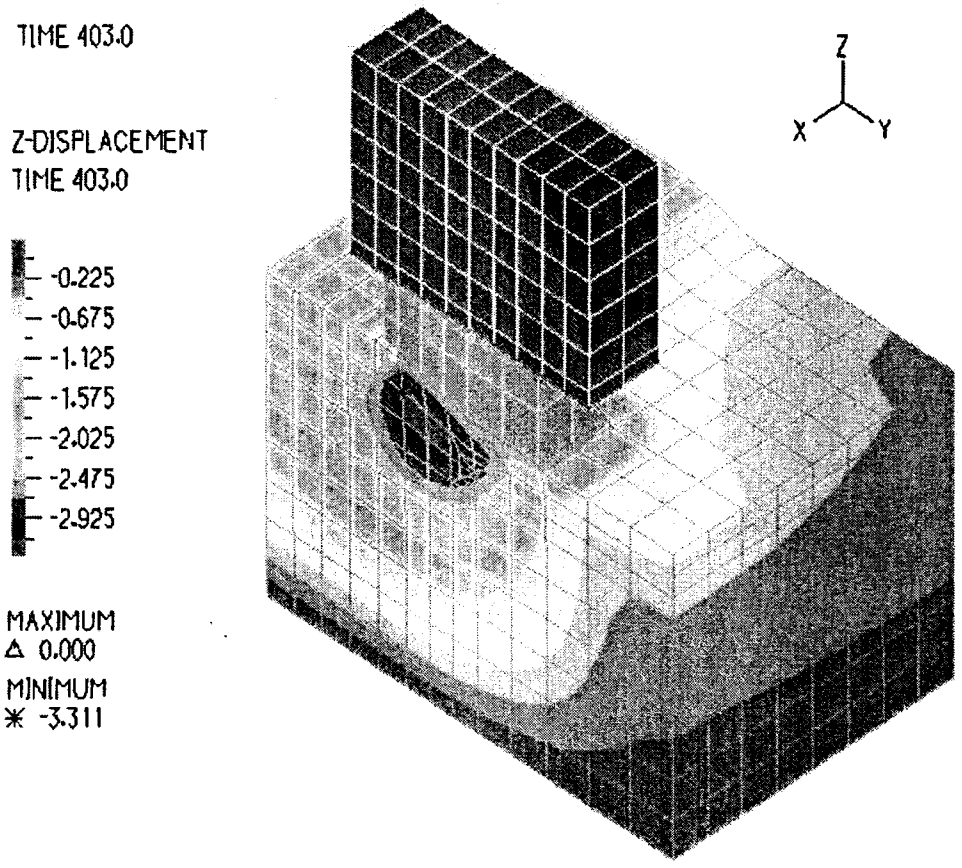

Figure 6.4 Vertical displacement contours

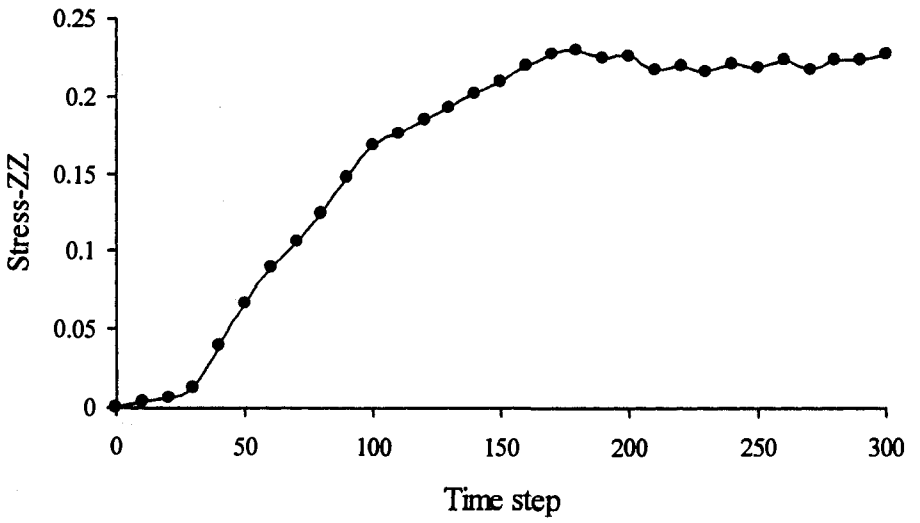

Figure 6.5 Stress-ZZ in soil element 112 (on inclined interface) versus time step

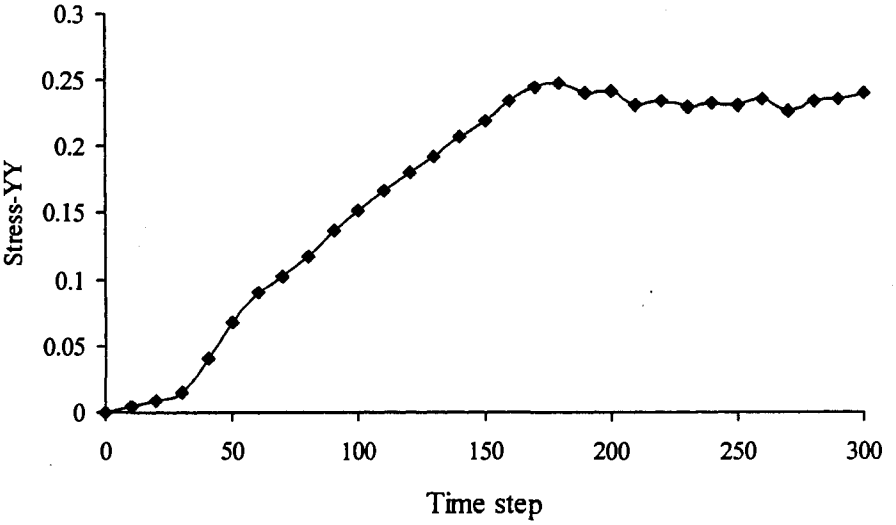

Figure 6.6 Stress-YY in soil element 112 (on inclined interface) versus time step

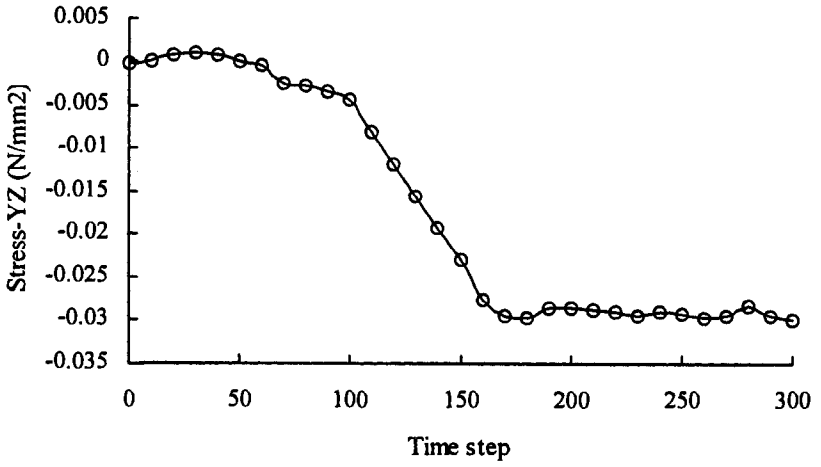

Figure 6.7 Stress-YZ in soil element 112 (on inclined interface) versus time step

6.2.2 Displacements of the Pipeline Resulting from the Movement of Ice Feature

Figure 6.8 and Figure 6.9 show the shape of the deflected pipeline at time step 403. The maximum horizontal deflection is about 1.4 mm and the maximum vertical deflection is 2.8 mm. The rotation of the pipe is 3.5° (see Figure 6.11). These values are less than those obtained from the 2-D analysis as shown in Table 6.2. If the maximum deflection of the pipe is required for design purposes, the results of the 2-D numerical model using plane strain analysis could be used; however, doing so might produce a too conservative design. It can be seen that the horizontal and vertical displacements of the pipe gradually decrease at pipe sections away from the symmetry plane in the X axis direction. Beyond 2 times the scour width, the direction of the horizontal displacements of the pipe is changed. These findings do not agree with Yang's results. One reason might be that the boundary of the soil region is chosen too close so that the soil moves backward to cause the pipe to deform. There are other reasons such as the boundary conditions at the end of the pipe and the type of elements used for the pipe. However, 3-D numerical model provides important information about the critical point on the deflected pipeline where large bending

moments might develop in the pipe. Furthermore, the pipe is subjected to torsional effects since the angle of twist is different at different cross-sections along the pipe as shown in Figure 6.6.

Table 6.2 Maximum displacements and rotation at 0-0 section by 2-D and by 3-D analysis

	2-D	3-D
Rotation(°)	4.2	3.5
Vertical displacement (mm)	3.2	2.8
Horizontal displacement (mm)	2.1	1.4

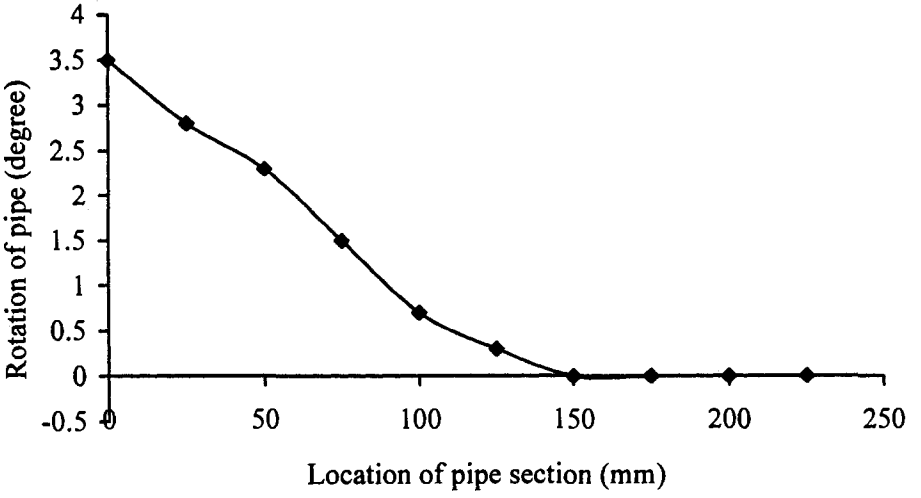

Figure 6.8 Rotation of pipe resulting from the movements of ice feature

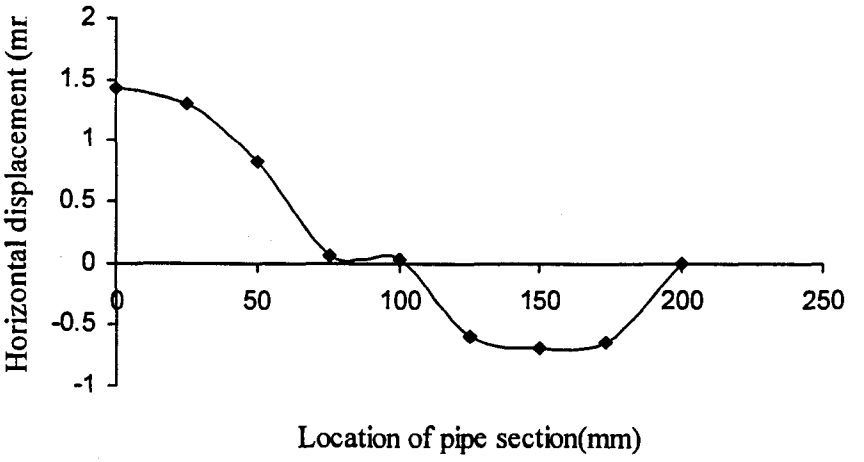

Figure 6.9 Horizontal displacement of pipe resulting from the movements of ice feature

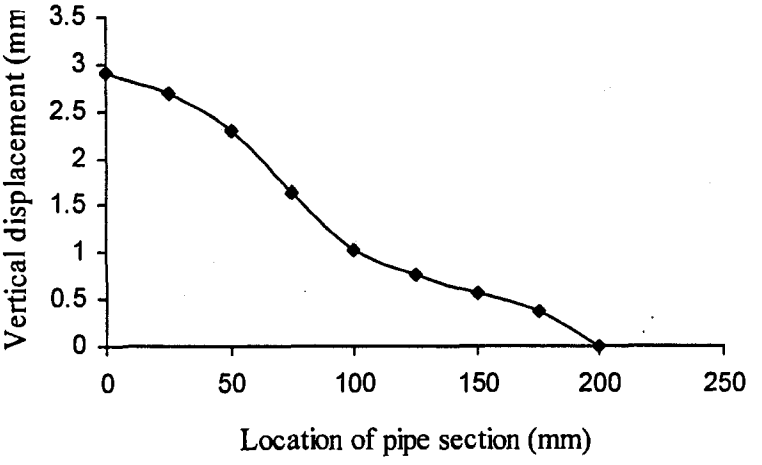

Figure 6.10 Vertical displacement of pipe resulting from the movements of ice feature

6.2.3 Stresses and Displacements of the Pipe

Figure 6.11 shows the deformation of the pipe at 0-0 section (symmetry plane). The stresses acting on the surface of the pipe and displacements at the nodes of the pipe are listed in Table 6.3 to 6.6. The maximum normal stress and shear stress take place at the

nodes 538 and 580 where the pipe faces the ice-scouring.

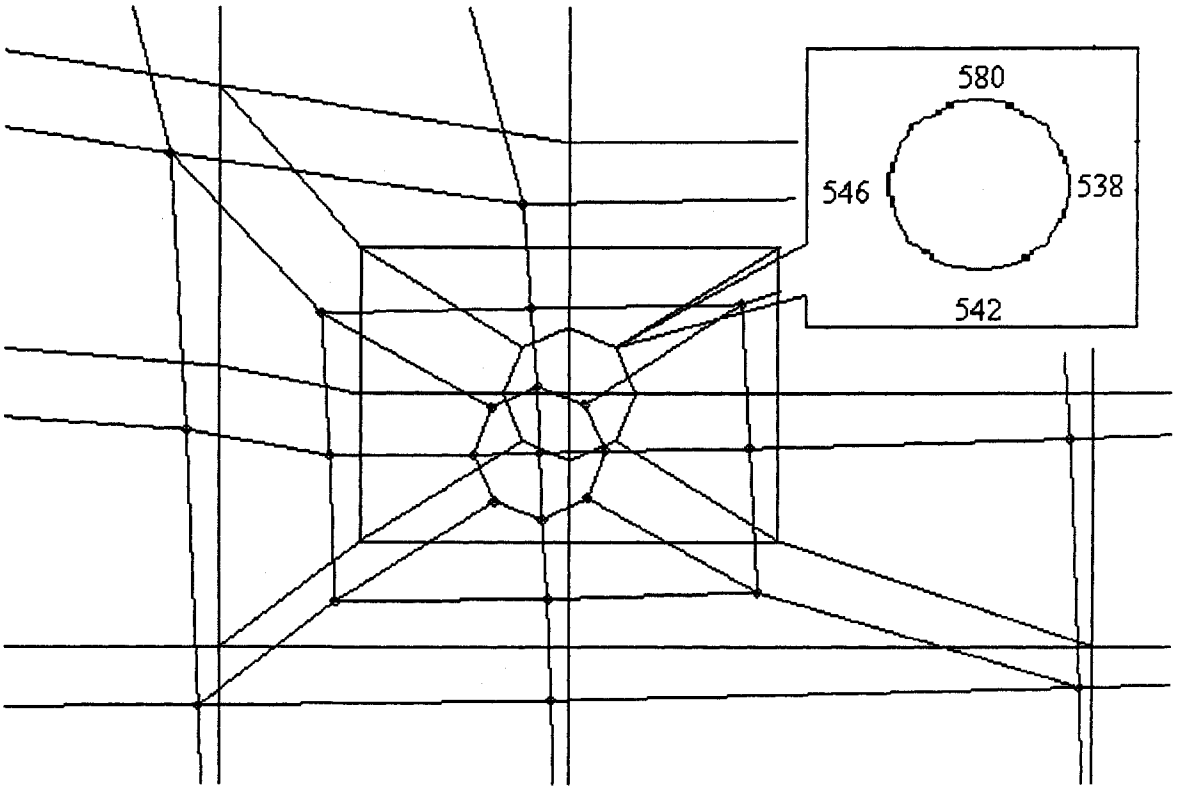

Figure 6.11 Deformation of the pipe at 0-0 section

Table 6.3 Stress components and displacement components of node 538 on the pipe at 0-0 section during the loading

Loading	σ_z (N/mm^2)	σ_y (N/mm^2)	σ_{yz} (N/mm^2)	Z Displacement (mm)	Y Displacement (mm)
100g	0.02	0.019	0.002	0.3	0.15
Static water pressure	0.03	0.025	0.003	0.45	0.2
Buoyant weight	0.05	0.041	0.008	0.65	0.35
7mm movement	0.22	0.18	0.035	2.6	1.4

Note:100 kPa static water pressure is applied on the surface of the seabed.

Table 6.4 Stress components and displacement components of node 542 on the pipe at 0-0 section during the loading

Loading	σ_z (N/mm^2)	σ_y (N/mm^2)	σ_{yz} (N/mm^2)	Z Displacement (mm)	Y Displacement (mm)
100g	0.025	0.015	0.005	0.3	0.15
Static water pressure	0.038	0.022	0.006	0.45	0.2
Buoyant weight	0.06	0.038	0.01	0.65	0.35
7mm movement	0.18	0.15	0.04	2.8	1.42

Note:100 kPa static water pressure is applied on the surface of the seabed.

Table 6.5 Stress components and displacement components of node 546 on the pipe at 0-0 section during the loading

Loading	σ_z (N/mm^2)	σ_y (N/mm^2)	σ_{yz} (N/mm^2)	Z Displacement (mm)	Y Displacement (mm)
100g	0.025	0.01	0.004	0.3	0.15
Static water pressure	0.03	0.025	0.0075	0.45	0.2
Buoyant weight	0.05	0.041	0.012	0.65	0.35
7mm movement	0.17	0.153	0.04	2.8	1.38

Note:100 kPa static water pressure is applied on the surface of the seabed.

Table 6.6 Stress components and displacement components of node 580 on the pipe at 0-0 section during the loading

Loading	σ_z (N/mm^2)	σ_y (N/mm^2)	σ_{yz} (N/mm^2)	Z Displacement (mm)	Y Displacement (mm)
100g	0.02	0.018	0.007	0.3	0.15
Static water pressure	0.031	0.023	0.009	0.45	0.2
Buoyant weight	0.048	0.038	0.014	0.65	0.35
7mm movement	0.18	0.15	0.058	2.7	1.5

Note:100 kPa static water pressure is applied on the surface of the seabed.

CHAPTER 7

SUMMARY, CONCLUSIONS, AND RECOMMENDATIONS FOR FUTURE RESEARCH

7.1 Summary

The ice-scouring is a common phenomenon in Arctic regions and the Canadian east coast where there are potential hydrocarbon production areas. Ice-scouring will lead to damage to offshore structures, in particular, marine pipelines. The main objective of this research is to explore numerically the influence of several important factors on the determination of a safe and cost effective burial depth of a pipeline in ice-scouring regions.

In order to achieve the above objective, the deformation of seabed soil, the magnitude of the scour force, and displacements of a pipe are calculated by the finite element method.

Based on centrifuge test data of Lach and Yang's numerical analysis, the 2-D and 3-D numerical models are built using PLAXIS and ADINA.

7.2 Conclusions

Based on the numerical modeling of ice-scouring event, the following conclusions are drawn:

1) The soil deformed plastically within 3 times of ice-scouring depth. This behaviour is consistent with the finding of other researchers. This information can be used to determine the boundary between Zone 2 and Zone 3.

2) The displacements of the pipe in 3-D model are smaller than those predicted by 2-D model due to the three dimensional effects. Bending and torsion of the pipe along its long axis can only be calculated in 3-D FE analysis. Torsion of the pipe has not been mentioned in the literature previously. The integrity of the pipe should be evaluated by taking into account the effects of bending and torsion in addition to axial deformations and the internal pressure.

3) The FE method is used successfully to simulate an ice-scouring event in a centrifuge test. The components of the scour force, deformations of soil, and displacements of the pipeline are calculated. The FE predictions are reasonably close to the centrifuge test data. This conclusion, however, is subject to the use of a representative soil model in the analysis.

4) FE model provides the distribution of stresses imposed on the pipe by the surrounding soil. These stresses can be used to find the deformed shape of the pipe.

5) Using the interface elements in the numerical analysis helps to obtain a better agreement between the calculated and measured values. In addition, convergence problems are reduced.

7.3 Recommendations for Future Research

Based on the literature review and present study, the following recommendations are

suggested for future research.

1) The present numerical analyses were undertaken to simulate ice-scouring event from a small-scale centrifuge test. Further analyses of other scouring events would be necessary to validate FE models.

2) More elaborate analysis should be carried out to fully account for large displacements including a complete scouring of soil for large distances. Present analysis show only a small portion of the complete process of ice scouring.

3) The pipeline should be represented by beam or shell elements.

4) More sophisticated soil models should be used in the simulation of the behaviour of seabed soils.

REFERENCES

ADINA 8.3, R& D Inc. (2005). AD INA theory manual.

Arunchalam, V.M., Bobby, W., Muggeridge, D.B. and Stacey, R.A. (1985). A review of interaction of icebergs with offshore structure. The 4th International Conference on Behaviour of Offshore Structures (BOSS'85) Delft, The Netherlands July 1-5,1985. pp.693-704.

Barker, A. and Timco, G.. (2002a). Laboratory experiments of ice scour processes: rigid ice indentor. Cold Regions Science and Technology 35 (3), pp.195-206.

Barker, A. and Timco, G.. (2003). Laboratory experiments of ice scour processes: buoyant ice model. Cold Regions Science and Technology 36 (3), 103-114.

Blasco, S., Shearer J.M., and Myers, R. (1998). Seabed scouring by sea-ice:scouring process and impact rates: Canadian Beaufort shelf. Proceedings of Ice Scour and Arctic Marine Pipelines Workshop, 13th International Symposium on Okhotsk Sea and Sea Ice, Mombetsu, Hokkaido, Japan, 1-4 February 1998. pp.53-57.

Chari, T.R. and Prasad, K.S.R. (1986). Analytical and experimental modeling of iceberg scours and pits. 3rd Canadian Conference on Marine Geotechnical Engineering, St. John's Newfoundland, Vol.2 .pp 457-468.

Clark, J.I., Landva, J., Collins, W.t. and Barrie, J.V. (1986). The geotechnical aspects of seabed pits in the Grand Banks area. 3rd Canadian Conference on Marine Geotechnical Engineering, St. John's Newfoundland, Vol.2 .pp 431-455.

Clark, J.I., Phillips, R. and Paulin, M.J. (1998). Ice scour research for safe design of pipelines: 1978-1998. 13th International Symposium on Okhotsk Sea and Sea Ice, Mombetsu, Hokkaido,Japan, 1-4 February 1998. pp.1-8.

Croasdale, K., Brown, R., Campbell, P., Crocker, G.., Jordaan, I., King, T., McKenna, R. and Myers, R. (2001). Iceberg risk to seabed installations on the Grand Banks.

Proceedings of the 16th International Conference on Port and Ocean Engineering under Arctic Conditions. POAC'01, Ottawa, Canada, August 12-17, 2001. pp. 1019-1028.

Croasdale, K.R.(1985). Recent developments in ice mechanics and ice loads. The 4th International Conference on Behaviour of Offshore Structures (BOSS'85) Delft, The Netherlands July 1-5,1985. 53-74.

Crooks, J.H.A., Jefferies, M.G., Becker, D.E. and Been, K.(1986). Geotechnical properties of Beaufort sea clays. 3rd Canadian Conference on Marine Geotechnical Engineering, St. John's Newfoundland, Vol.1 pp.329-343.

Ebbesmeyer, C.C., Okubu, A. and Helseth, J.M. (1980). Description of iceberg probability between Baffin Bay and Grand Banks using a Stochastic model. Deep Sea Research, Vol. 27 A, pp. 975-986.

Eden, D.J. and Eyles, N. (2002). Case study of a relict iceberg scour exposed at Scarborough Bluffs, Toronto, Ontario: implications for pipeline engineering. Can. Geotech J.39: pp.519-534 (2002)

International Ice Patrol. (1980). "Report of the International Ice Patrol Service in the North Atlantic Ocean", U.S. Coast Guard Bulletin, No: 66, 68 p.

Kenny, S., Phillips, R., Mckenna, R.F. and Clark, J.I. (2000). Response of buried arctic marine pipelines to ice gouge events. Proceedings of 2nd Ice Scour and Arctic Marine Pipelines Workshop, Mombest, Japan, February 6- 9, 2000. pp. 217-220.

Konuk, I., Yu, S. and Gracie, R. (2005). A 3-dimensional continuum ALE model for ice scour study of trench effects. 24th International Conference on Offshore Mechanics and Arctic Engineering, Proceedings of OMAE'05.

Konuk, I., Yu, S. and Gracie, R. (2005). An ALE FEM model of ice scour. The 11th International Conference of International Association of computer Methods and Advances in Geomechanics, Turin, Italy, June 19-21, 2005.

Konuk, I. and Fredj, A. (2004). FEM model for pipeline analysis of ice scour – a critical review. 23rd International Conference on Offshore Mechanics and Arctic Engineering, Proceedings of OMAE'04.

Kovacs, A. and Mellor, M. (1974). Sea ice morphology and ice as a geologic agent in the southern Beaufort Sea, Reprint from The Coast and the Shelf of the Beaufort Sea. The Arctic Institute of North America, Arlington, VA, 1974, pp.113-164.

Lach, P.R. (1996). Centrifuge modeling of large soil deformation due to ice scour. Ph.D.Thesis. Memorial University of Newfoundland, St. John's, Newfoundland, 685p.

Lach, P.R. and Clark, J.K. (1996). Numerical simulation of large soil deformation due to ice scour. The 49th Canadian Geotechnical Conference of the Canadian Geotechnical Society, Vol.1 pp. 189-198.

Lach, P.R., Clark, J.K., and Poorooshasb, F. (1993). Centrifuge modeling of ice scour. 4th Canadian Conference on Marine Geotechnical Engineering, St. John's Nwefoundland, pp.356-374.

Lewis, C.F.M. and Barrie, J.V. (1981). Geological evidence of iceberg grounding and related seafloor processes in the Hibernia discovery area of Grand Bank, Newfoundland. Proceedings, Symposium on Production and Transportation Systems for the Hibernia Discovery, Newfoundland Petroleum Directorate. St.John's. Newfoundland, pp.146-177.

Lewis, C.F.M. and Blasco, S.M. (1990). Character and Distribution of Sea-Ice and Iceberg Scours. Proceedings of the Workshop on Ice Scouring and the Design of Offshore Pipelines, Calgary, Alberta, pp. 57-101

Mobil Oil Canada Ltd. (1985). Hibernia Development Project, Environmental Impact Statement, Vol.IIIa, Biophysical Assessment, 258p.

Nixon, J.F., Palmer, A., and Phillips, R. (1996). Simulations for buried pipeline deformations beneath ice scour. Offshore Marine and Arctic Engineering, Florence, Italy. 10p.

Nordco Limited. (1984). A review of ice information for offshore Eastern Canada. Report submitted to Royal Commission on the Ocean Ranger Marine Disaster.

Palmer, A., Konuk, I., Niedoroda, A.W., Been, K., and Croasdale, K.R. (2005). Arctic

seabed ice gouging and large subgouge deformations. The International Symposium on Frontiers in Offshore Geotechnics, Perth, Western Australia, September 19-21, 2005.

Palmer, A. (2000). Gouging in the context of critical issues of Arctic offshore pipeline development. Proceedings of 2nd Ice Scour and Arctic Marine Pipelines Workshop, Mombest, Japan, February 6-9, 2000. pp. 5-10.

Palmer, A. (1998). Alternative paths for determination of minimum burial depth to safeguard pipelines against ice scouring. 13th International Symposium on Okhotsk Sea and Sea Ice, Mombetsu, Hokkaido,Japan, 1-4 February 1998. pp.9-16.

Palmer, A. (1997). Geotechnical evidence of ice scour as a guide to pipeline burial depth. Canadian Geotechnical Journal, 34: 1002-1003.

Palmer, A. (1990). Design of Marine pipelines in seabed vulnerable to ice scour. Workshop on Ice Scouring and the Design of offshore pipelines, Calgary, Canada, pp.167-178.

Palmer, A., Konuk I., Love J., Been K. and Comfort, G. (1989). Ice scour mechanisms. Proceedings, 10th International Conference on Port and Ocean Engineering under Arctic Conditions, Lulea, pp.123-132.

Paulin, M.J. (1997). Safety and Integrity of Arctic Marine Pipelines, Progress Report #1: Results of Field Study, C CORE, St. John's, Newfoundland, Publication 97 C 30, July, 1997.

PLAXIS V8.3 (2006). PLAXIS 8.3 Manual.

Potts, D.M. and Zdravkovic, L. (1999). Finite Element Analysis in Geotechnical Engineering: Theory. Published by Thomas Telford publishing, Thomas Telford Ltd, 1 Heron Quay, London.

Poorooshasb, F. and Clark, J.I. (1990). On small scale ice scour modeling. Proceedings on Ice Scouring and Design of Offshore Pipelines, Calgary, Canada, pp.193-235.

Schofield, A.N. (1980). Cambridge Geotechnical Centrifuge Operations. Geotechnique,

30, No.3, pp.227-268.

Shinji Kiokal, Yoshikathu Yasunaga, Hideyuki Nishimaki and Hiroshi Saeki. (2000). Behavior of ridge ice at a time of ice scouring. Proceedings of 2nd Ice Scour and Arctic Marine Pipelines Workshop, Mombest, Japan, February 6-9, 2000.pp. 163-171.

Simo, J.C., Ju, J.W., Pister, R.L., and Taylor, R.L. (1988). Assessment of Cap Model: Consistent return algorithms and rate-dependent extension, Journal of Engineering Mechanics, Volume114. pp. 191-218.

Sonnichsen, G. and King, E. (2001). Surficial sediments, Grand Bank, Offshore Newfoundland. PERD/CHC Report. 31-37. Geological Survey of Canada, Dartmouth, Canada.

Stepanov, I.V., Timofeyev, O.Y., Klepikov, A.V. and Malek, V.N. (1998). An approach to optimization of the burial depth of underwater pipelines on the Arctic offshore.13th International Symposium on Okhotsk Sea and Sea Ice, Mombetsu, Hokkaido, Japan, 1-4 February, 1998. pp.59 - 70.

Surkov G.A., Truskov P.A., Zemluk S.V., Polomoshnov A.M., and Astafyev S.V. (2000). Choosing optimum underwater pipeline burial profile on Northeast Sakhalin Shelf. Proceedings of 2nd Ice Scour and Arctic Marine Pipelines Workshop, Mombetsu, Japan, February 6-9, 2000. pp. 207-216.

Woodworth-Lynas, C.M.L. (1998). Sub-scour soil deformations and development of ideas from field work in the last decade. 13th International Symposium on Okhotsk Sea and Sea Ice, Mombetsu, Hokkaido, Japan, 1-4 February, 1998. pp. 33-42

Woodworth-Lynas, C.M.L., Nixon, J. D., Phillips, R. and Palmer, A. (1996). Subgouge deformations and the security of Arctic marine pipelines. Proceedings, 28th Annual Offshore Technology Conference, Houston, pp. 657-664 (1996)

Woodworth-Lynas, C.M.L. (1996). Verification of centrifuge model results against field data: results from the Pressure Ridge Ice Scour Experiment (PRISE). 13th International Symposium on Okhotsk Sea and Sea Ice, Mombetsu, Hokkaido, Japan, 1-4 February 1998. pp.123-138.

Yang, Q.S., Poorooshasb, F. and Poorooshasb, H.B.(1993). Analysis of subscour deformation by finite element method. 4th Canadian Conference on Marine Geotechnical Engineering. Vol.2, pp. 739-754.

Yang, Q.S. and Poorooshasb, H.B. (1997). Numerical modeling of seabed ice scour. Computers and Geotechnics, Vol.21, No. 1, pp. 1-20.

APPENDIX A
CALCULATION OF ICE- SCOURING FORCES

Scour forces calculated using ADINA

This appendix describes the calculation of ice- scouring forces acting on the seabed in 2-D numerical analysis by ADINA. The soil below the inclined surface of the ice feature consists of three elements (E124, E125, E128), the soil below the base of the ice feature consists of 2 elements (E 129, E130) as shown in Figure A1.The numerical analysis provides the stresses in the middle of each element. Therefore, the increase of stress due to the movement of ice-feature can be obtained. It is noted that the vertical stresses on the bottom seabed soil do not change during ice scouring. To simplify the calculation, the constant shearing resistance force (c_f x base area=20 kPa x base area) provided by the seabed soil is assumed to act at the base of the ice feature. The effect of this force is gradually added to the horizontal component of the ice force until the ice scouring process reaches the steady state. The increments of vertical and horizontal components of scour force due to ice feature movements are calculated as follows.

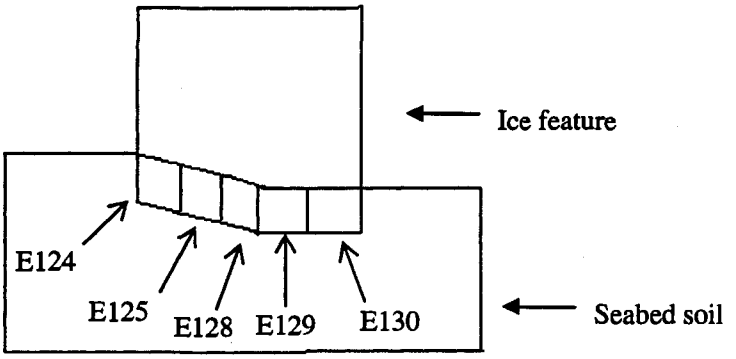

Figure A1 Elements along the interface between the seabed soil and ice feature

The increment of normal stress ($\Delta\sigma_\alpha$) and the increment of shear stress ($\Delta\tau_\alpha$) acting on the soil under the inclined surface of ice feature can be calculated using Eqns. A1 and A2.

$$\Delta(\sigma)_\alpha = \frac{\Delta\sigma_{zz} + \Delta\sigma_{yy}}{2} + \frac{\Delta\sigma_{zz} - \Delta\sigma_{yy}}{2}\cos 2\theta + \Delta\tau_{yz}\sin 2\theta \qquad \text{A1}$$

$$\Delta(\tau)_\alpha = -\frac{\Delta\sigma_{zz} - \Delta\sigma_{yy}}{2}\sin 2\theta + \Delta\tau_{yz}\cos 2\theta \qquad \text{A2}$$

where: α is the angle between the inclined surface and the horizontal plane.

θ is the angle between the inclined surface and the vertical plane.

Calculation of Scouring Force at time=140 (without pipe)

From the stress components at the middle of each element, the increments of stress components are calculated during the ice scouring as shown in the following tables.

Table A.1 Increase in stress components in element 124 (time step =140)

E124	σ_{zz} (N/mm^2)	σ_{yy} (N/mm^2)	τ_{yz} (N/mm^2)
Time step=100	-1.69E-01	-1.53E-01	-4.32E-03
Time step =141	-2.03E-01	-2.07E-01	-1.91E-02
$\Delta\sigma_{zz}$(N/mm^2)	-3.42E-02	--	--
$\Delta\sigma_{yy}$(N/mm^2)	--	-5.44E-02	--
$\Delta\sigma_{yz}$(N/mm^2)	--	--	-1.48E-02

Table A.2 Increase in stress components in element 125 (time step =140)

E125	σ_{zz} (N/mm^2)	σ_{yy} (N/mm^2)	τ_{yz} (N/mm^2)
Time step=100	-1.27E-01	-1.18E-01	-1.54E-03
Time step =141	-1.37E-01	-1.42E-01	-1.54E-02
$\Delta\sigma_{zz}$(N/mm^2)	-9.69E-03	--	--
$\Delta\sigma_{yy}$(N/mm^2)	--	-2.45E-02	--
$\Delta\sigma_{yz}$(N/mm^2)	--	--	-1.39E-02

Table A.3 Increase in stress components in element 128 (time step =140)

E128	σ_{zz} (N/mm^2)	σ_{yy} (N/mm^2)	τ_{yz} (N/mm^2)
Time step=100	-1.37E-01	-1.31E-01	-8.26E-04
Time step =141	-1.38E-01	-1.40E-01	-1.61E-02
$\Delta\sigma_{zz}$(N/mm^2)	-6.57E-04	--	--
$\Delta\sigma_{yy}$(N/mm^2)	--	-8.91E-03	--
$\Delta\sigma_{yz}$(N/mm^2)	--	--	-1.53E-02

The stress components acting on the inclined surface (α=15°, θ=75°) are calculated according to Eqns. A1 and A2 as shown in the following table.

Table A.4 Increments of stress components acting on the inclined surface (α =15°, θ=75°) (time step =140)

	$\Delta\sigma_{zz}$ (N/mm^2)	$\Delta\sigma_{yy}$ (N/mm^2)	$\Delta\sigma_{yz}$ (N/mm^2)	$\Delta\sigma_{\alpha=15°}$ (N/mm^2)	$\Delta\tau_{\alpha=15°}$ (N/mm^2)
E124	-0.0342	-0.0544	-0.0148	-0.04298	0.017869
E125	-0.00969	-0.0245	-0.0139	-0.01765	0.01574
E128	-0.00066	-0.0089	-0.0153	-0.00888	0.015305
Total stress	--	--	--	-0.06951	0.048913
Average stress	--	--	--	-0.023	0.016

The normal force (F_n) and the shear force (F_t) are calculated as follows.

$F_n=\Delta\sigma_\alpha$ x Area=-0.023 x 5200=-120 (N)

$F_t=\Delta\tau_\alpha$ x Area=0.016 x 5200=-85 (N)

F_n is resolved in the vertical direction

120 x cos15° =116 (N)

and in the horizontal direction

120 x sin15° =31 (N)

F_t is resolved in the vertical direction

85 x sin15° =21.9 (N)

and in the horizontal direction

85 x cos15° =81.7 (N)

Assuming 30% of the constant shearing resistance force F_{rs} is already acting at time step 140

F_{rs}=0.02 x 50 x100 x 0.3 =30 (N)

Total force in the vertical direction

F_v=-116.17+21.89=-94.28 (N)

Total force in the horizontal direction

F_h=-31.11-81.74-30= -142.85 (N)

Calculation of Scouring Force at time=180 (without pipe)

From the stress components at the middle of each element, the increments of stress components are calculated during the ice scouring as shown in the following tables.

Table A.5 Increase in stress components in element 124 (time step =180)

E124	σ_{zz} (N/mm^2)	σ_{yy}(N/mm^2)	τ_{yz}(N/mm^2)
Time step=100	-1.69E-01	-1.53E-01	-4.32E-03
Time step =181	-2.30E-01	-2.48E-01	-2.96E-02
$\Delta\sigma_{zz}$(N/mm^2)	-6.15E-02	--	--
$\Delta\sigma_{yy}$(N/mm^2)	--	-9.52E-02	--
$\Delta\sigma_{yz}$(N/mm^2)	--	--	-2.53E-02

Table A.6 Increase in stress components in element 125 (time step =180)

E125	σ_{zz} (N/mm^2)	σ_{yy}(N/mm^2)	τ_{yz}(N/mm^2)
Time step=100	-1.27E-01	-1.18E-01	-1.54E-03
Time step =181	-1.43E-01	-1.60E-01	-2.70E-02
$\Delta\sigma_{zz}$(N/mm^2)	-1.62E-02	--	--
$\Delta\sigma_{yy}$(N/mm^2)	--	-4.22E-02	--
$\Delta\sigma_{yz}$(N/mm^2)	--	--	-2.54E-02

Table A.7 Increase in stress components in element 128 (time step =180)

E128	σ_{zz} (N/mm^2)	σ_{yy}(N/mm^2)	τ_{yz}(N/mm^2)
Time step=100	-1.37E-01	-1.31E-01	-8.26E-04
Time step =181	-1.44E-01	-1.53E-01	-2.94E-02
$\Delta\sigma_{zz}$(N/mm^2)	-6.74E-03	--	--
$\Delta\sigma_{yy}$(N/mm^2)	--	-2.21E-02	--
$\Delta\sigma_{yz}$(N/mm^2)	--	--	-2.86E-02

The stress components acting on the inclined surface (α=15°, θ=75°) are calculated according to Eqns. A1 and A2 as shown in the following table.

Table A.8 Increments of stress components acting on the inclined surface (α=15°, θ=75°) (time step =180)

	$\Delta\sigma_{zz}$ (N/mm^2)	$\Delta\sigma_{yy}$ (N/mm^2)	$\Delta\sigma_{yz}$ (N/mm^2)	$\Delta\sigma_{\alpha=15°}$ (N/mm^2)	$\Delta\tau_{\alpha=15°}$ (N/mm^2)
E124	-0.0615	-0.0952	-0.0253	-0.07645	0.030338
E125	-0.0162	-0.0422	-0.0254	-0.03068	0.028495
E128	-0.0067	-0.0212	-0.0286	-0.02201	0.028383
Total stress	--	--	--	-0.12914	0.087216
Average stress	--	--	--	-0.043	-0.029

The normal force (F_n) and the shear force (F_t) are calculated as following.

$F_n = \Delta\sigma_\alpha$ x Area=-0.043 x 5200=-223.6 (N)

$F_t = \Delta\tau_\alpha$ x Area=0.029 x 5200=-150.8 (N)

F_n is resolved in the vertical direction

223.6 x cos15° =215.8 (N)

and in the horizontal direction

223.6 x sin15° =57.8 (N)

F_t is resolved in the vertical direction

150.8 x sin15° =39 (N)

and in the horizontal direction

150.8 x cos15° =145.7 (N)

Assuming 60% constant shearing resistance force (F_{rs}) is expected at time step 180.

F_{rs}=0.02 x 50 x100 x 0.6 =60 (N)

Total force in the vertical direction

F_v=-215.8+39 =-176.8 (N)

Total force in the horizontal direction

F_h=-57.79-145.7-60= -263.49 (N)

Calculation of Scouring Force at time=220 (without pipe)

From the stress components at the middle of each element, the increments of stress components are calculated during the ice scouring as shown in the following tables.

Table A.9 Increase in stress components in element 124 (time step =220)

E124	σ_{zz} (N/mm^2)	σ_{yy}(N/mm^2)	τ_{yz}(N/mm^2)
Time step=100	-1.69E-01	-1.53E-01	-4.32E-03
Time step =221	-2.20E-01	-2.35E-01	-2.90E-02
$\Delta\sigma_{zz}$(N/mm^2)	-5.19E-02	--	--
$\Delta\sigma_{yy}$(N/mm^2)	--	-8.16E-02	--
$\Delta\sigma_{yz}$(N/mm^2)	--	--	-2.47E-02

Table A.10 Increase in stress components in element 125 (time step =220)

E125	σ_{zz} (N/mm^2)	σ_{yy}(N/mm^2)	τ_{yz}(N/mm^2)
Time step=100	-1.27E-01	-1.18E-01	-1.54E-03
Time step =221	-1.34E-01	-1.45E-01	-2.61E-02
$\Delta\sigma_{zz}$(N/mm^2)	-6.96E-03	--	--
$\Delta\sigma_{yy}$(N/mm^2)	--	-2.72E-02	--
$\Delta\sigma_{yz}$(N/mm^2)	--	--	-2.46E-02

Table A.11 Increase in stress components in element 128 (time step =220)

E128	σ_{zz} (N/mm^2)	σ_{yy}(N/mm^2)	τ_{yz}(N/mm^2)
Time step=100	-1.37E-01	-1.31E-01	-8.26E-04
Time step =221	-1.38E-01	-1.40E-01	-1.61E-02
$\Delta\sigma_{zz}$(N/mm^2)	-6.57E-04	--	--
$\Delta\sigma_{yy}$(N/mm^2)	--	-8.91E-03	--
$\Delta\sigma_{yz}$(N/mm^2)	--	--	-1.53E-02

The stress components acting on the inclined surface (α=15°, θ=75°) are calculated according to Eqns. A1 and A2 as shown in the following table.

Table A.12 Increments of stress components acting on the inclined surface (α=15°, θ=75°) (time step =220)

	$\Delta\sigma_{zz}$ (N/mm^2)	$\Delta\sigma_{yy}$ (N/mm^2)	$\Delta\sigma_{yz}$ (N/mm^2)	$\Delta\sigma_{\alpha=15°}$ (N/mm^2)	$\Delta\tau_{\alpha=15°}$ (N/mm^2)
E124	-0.0519	-0.0816	-0.0247	-0.06628	0.028816
E125	-0.007	-0.0272	-0.0246	-0.02069	0.026349
E128	-0.0275	-0.0239	-0.0218	-0.03818	0.017963
Total stress	--	--	--	-0.12515	0.073129
Average stress	--	--	--	-0.042	0.024

The normal force (F_n) and the shear force (F_t) are calculated as following.

$F_n = \Delta\sigma_\alpha$ x Area=-0.042 x 5200=-216.5 (N)

$F_t = \Delta\tau_\alpha$ x Area=0.024 x 5200=-126.5 (N)

F_n is resolved in the vertical direction

216.5 x cos15° =209(N)

and in the horizontal direction

216.5 x sin15° =56 (N)

F_t is resolved in the vertical direction

126.5 x sin15° =32.7 (N)

and in the horizontal direction

126.5 x cos15° =122.2 (N)

Assuming 90% constant shearing resistance force (F_{rs}) is expected at time step 220

F_{rs}=0.02x 50 x100 x 0.9 =90 (N)

Total force in the vertical direction

F_v=-209+32.7=-176.3 (N)

Total force in the horizontal direction

F_h=-56-122.2-90= -268.2 (N)

Calculation of Scouring Force at time=260 (without pipe)

From the stress components at the middle of each element, the increments of stress components are calculated during the ice scouring as shown in the following tables.

Table A.13 Increase in stress components in element 124 (time step =260)

E124	σ_{zz} (N/mm^2)	σ_{yy}(N/mm^2)	τ_{yz}(N/mm^2)
Time step=100	-1.69E-01	-1.53E-01	-4.32E-03
Time step =261	-2.24E-01	-2.37E-01	-2.97E-02
$\Delta\sigma_{zz}$(N/mm^2)	-5.59E-02	--	--
$\Delta\sigma_{yy}$(N/mm^2)	--	-8.36E-02	--
$\Delta\sigma_{yz}$(N/mm^2)	--	--	-2.54E-02

Table A.14 Increase in stress components in element 125 (time step =260)

E125	σ_{zz} (N/mm^2)	σ_{yy}(N/mm^2)	τ_{yz}(N/mm^2)
Time step=100	-1.27E-01	-1.18E-01	-1.54E-03
Time step =261	-1.35E-01	-1.44E-01	-2.66E-02
$\Delta\sigma_{zz}$(N/mm^2)	-7.70E-03	--	--
$\Delta\sigma_{yy}$(N/mm^2)	--	-2.60E-02	--
$\Delta\sigma_{yz}$(N/mm^2)	--	--	-2.50E-02

Table A.15 Increase in stress components in element 128 (time step =260)

E128	σ_{zz} (N/mm^2)	σ_{yy}(N/mm^2)	τ_{yz}(N/mm^2)
Time step=100	-1.37E-01	-1.31E-01	-8.26E-04
Time step =261	-1.66E-01	-1.67E-01	-2.19E-02
$\Delta\sigma_{zz}$(N/mm^2)	-2.86E-02	--	--
$\Delta\sigma_{yy}$(N/mm^2)	--	-3.51E-02	--
$\Delta\sigma_{yz}$(N/mm^2)	--	--	-2.10E-02

The stress components acting on the inclined surface (α=15°, θ=75°) are calculated according to Eqns. A1 and A2 as shown in the following table.

Table A.16 Increments of stress components acting on the inclined surface (α=15°, θ=75°) (time step =260)

	$\Delta\sigma_{zz}$ (N/mm^2)	$\Delta\sigma_{yy}$ (N/mm^2)	$\Delta\sigma_{yz}$ (N/mm^2)	$\Delta\sigma_{\alpha=15°}$ (N/mm^2)	$\Delta\tau_{\alpha=15°}$ (N/mm^2)
E124	-0.0559	-0.0836	-0.0254	-0.07049	0.028921
E125	-0.0077	-0.026	-0.025	-0.02146	0.02622
E128	-0.0286	-0.0351	-0.021	-0.03956	0.019801
Total stress	--	--	--	-0.13152	0.074942
Average stress	--	--	--	-0.044	0.025

The normal force (F_n) and shear force (F_t) are calculated as following.

$F_n = \Delta\sigma_\alpha$ x Area=-0.044 x 5200=-227.5 (N)

$F_t = \Delta\tau_\alpha$ x Area=0.025 x 5200=-129.6 (N)

F_n is resolved in the vertical direction

227.5 x cos15° =219.8(N)

and in the horizontal direction

227.5 x sin15° =58.9 (N)

F_t is resolved in the vertical direction

129.6 x sin15° =33.5 (N)

and in the horizontal direction

129.6 x cos15° =125.2 (N)

Assuming 100% constant shearing resistance force (F_{rs}) is expected at time step 260

F_{rs}=0.02x 50 x100 x 1.0 =100 (N)

Total force in the vertical direction

F_v= -219.8+33.5=-186.3 (N)

Total force in the horizontal direction

F_h=-58.9-125.2-100= -284.1 (N)

Calculation of Scouring Force at time step =300 (without pipe)

From the stress components at the middle of each element, the increments of stress components are calculated during the ice scouring as shown in the following tables.

Table A.17 Increase in stress components in element 124 (time step =300)

E124	σ_{zz} (N/mm^2)	σ_{yy}(N/mm^2)	τ_{yz}(N/mm^2)
Time step=100	-1.69E-01	-1.53E-01	-4.32E-03
Time step =300	-2.28E-01	-2.41E-01	-3.00E-02
$\Delta\sigma_{zz}$(N/mm^2)	-5.91E-02	--	--
$\Delta\sigma_{yy}$(N/mm^2)	--	-8.76E-02	--
$\Delta\sigma_{yz}$(N/mm^2)	--	--	-2.57E-02

Table A.18 Increase in stress components in element 125 (time step =300)

E125	σ_{zz} (N/mm^2)	σ_{yy}(N/mm^2)	τ_{yz}(N/mm^2)
Time step=100	-1.27E-01	-1.18E-01	-1.54E-03
Time step =300	-1.37E-01	-1.45E-01	-2.73E-02
$\Delta\sigma_{zz}$(N/mm^2)	-9.51E-03	--	--
$\Delta\sigma_{yy}$(N/mm^2)	--	-2.69E-02	--
$\Delta\sigma_{yz}$(N/mm^2)	--	--	-2.57E-02

Table A.19 Increase in stress components in element 128 (time step =300)

E128	σ_{zz} (N/mm^2)	σ_{yy}(N/mm^2)	τ_{yz}(N/mm^2)
Time step=100	-1.37E-01	-1.31E-01	-8.26E-04
Time step =300	-1.62E-01	-1.73E-01	-2.18E-02
$\Delta\sigma_{zz}$(N/mm^2)	2.49E-02	--	--
$\Delta\sigma_{yy}$(N/mm^2)	--	-4.15E-02	--
$\Delta\sigma_{yz}$(N/mm^2)	--	--	-2.10E-02

The stress components acting on the inclined surface (α=15°, θ=75°) are calculated according to Eqns. A1 and A2 as shown in the following table.

Table A.20 Increments of stress components acting on the inclined surface (α=15°, θ=75°) (time step =300)

	$\Delta\sigma_{zz}$ (N/mm^2)	$\Delta\sigma_{yy}$ (N/mm^2)	$\Delta\sigma_{yz}$ (N/mm^2)	$\Delta\sigma_{\alpha=15°}$ (N/mm^2)	$\Delta\tau_{\alpha=15°}$ (N/mm^2)
E124	-0.059	-0.0876	-0.0257	-0.0738	0.029406
E125	-0.0095	-0.0269	-0.0257	-0.02355	0.0266
E128	-0.025	-0.042	-0.021	-0.03667	0.022432
Total stress	--	--	--	-0.13402	0.078438
Average stress	--	--	--	-0.045	0.026

The normal force (F_n) and the shear force (F_t) are calculated as following.

$F_n = \Delta\sigma_\alpha$ x Area=-0.045 x 5200=-234(N)

$F_t = \Delta\tau_\alpha$ x Area=0.026 x 5200=-135.2 (N)

F_n is resolved in the vertical direction

234 x cos15° =226(N)

and in the horizontal direction

234 x sin15° =60.6 (N)

F_t is resolved in the vertical direction

135.2 x sin15° =35 (N)

and in the horizontal direction

135.2 x cos15° =130.6 (N)

Assuming 100% constant shearing resistance force (F_{rs}) is expected at time step 300

F_{rs}=0.02x 50 x100 x 1.0 =100 (N)

Total force in the vertical direction

F_v= -226+35=-191 (N)

Total force in the horizontal direction

F_h= -60.6-130.6-100= -291.2 (N)